POLITECNICO di TORINO

I Facoltà di Ingegneria
Dipartimento Energia

DISSERTATION FOR THE
DEGREE OF DOCTOR OF SCIENCE

**A COMPREHENSIVE METHODOLOGY for the OPTIMIZATION of
the OPERATING STRATEGY of HYBRID ELECTRIC VEHICLES**

Ing. Edoardo Pietro Morra

Tutors: *Prof. Ezio Spessa (Politecnico di Torino)*
PhD. Ing. Alberto Vassallo (GMPT-E)

April 2012

To my family, the support without which I could have never succeeded

SUMMARY

The sustainable exploitation of energy and reduction of pollutant emissions are main concerns in our society. Driven by more stringent international standards, automobile manufacturers are developing new technologies such as the Hybrid Electric Vehicles (HEVs). These innovative systems combine the main benefits of traditional Internal Combustion Engines (ICEs) with those of Battery Electric Vehicles (BEVs), while overcoming their main drawbacks.

HEVs can offer significant improvements in the efficiency of the propulsion system, but they also lead to higher complexities in the design and in the control. In order to exploit all the expected advantages, a dedicated optimization of the Hybrid Operating Strategy (HOS) is required. In this framework, simulation plays a key role in identifying the optimal HOS, where the primary design targets are the fuel economy, emission reduction and improvement in the vehicle performance (including acceleration, driving range, operational flexibility and noise).

With such a perspective, a simulation study was performed involving the implementation, in Matlab environment, of zero-dimensional models of a Series Hybrid Electric Vehicle (SHEV) and a Parallel Hybrid Electric Vehicle (PHEV). As far as the hybrid operating strategy is concerned, three different approaches were investigated:

➢ A *novel Benchmark Optimizer (BO)*, that determines the best possible operating strategy for the selected target, mission profile and powertrain design. The single solution is characterized by a vector, in which every scalar independently defines the mechanical power of the electric machine, for the PHEV, or the engine speed, for the SHEV, at each time step of the selected driving cycle

➢ A *real-time optimizer* based on the *Minimization of the Total system Losses (TLM)*. It involves a vector-approach, in order to select, at each time step, the power split that guarantees the minimum system losses. It requires a reduced number of calibration parameters and, therefore, is computationally fast and adequate to work in real-world applications. Based on this technique, two different methodologies concerning the engine component are considered: the *Total engine losses* (*TLM TOT*) and the *Recoverable* (with respect to the optimal operating point) *engine losses* (*TLM REC*)

➢ A *real-time optimizer* based on the *Total Load Switch Thresholds*. It switches the operating mode depending on the load and speed signals. It involves a scalar-approach and requires a reduced

number of calibration parameters. It is by far the method that requires the least computational effort

In all the three cases, the numerical optimizer is based on Genetic Algorithm (GA) techniques. GAs are inspired by the mechanism of natural selection, in which better individuals are likely to be the winners in a competing environment. It is a statistical approach able to solve optimization problems whose objective function is non-continuous, non-differentiable, stochastic and highly non-linear.

The study analyses the optimization of the well-to-wheel CO_2 emissions of a Parallel and a Series Hybrid Electric Vehicles along the New European Driving Cycle (NEDC) and the Artemis Driving Cycles within the following case setup:

Hybrid Architecture	Engine	Plug-In Feature
Parallel	Compression Ignition	with
		without
	Spark Ignition	with
		without
Series	Compression Ignition	with
		without
	Spark Ignition	with
		without

In the case of the only compression ignition engine, also NO_x emissions were considered as optimization criteria along the NEDC.

After a short introduction related to the automotive industry environmental impact (Chapter 1) and a overview of the Hybrid Electric Vehicle technology (Chapter 2), Chapter 3.1 deals with a detailed description of the methodology regarding the hybrid powertrain modelling in Matlab environment (Chapter 3.1). Afterwards, Chapter 3.2 shows a comprehensive overview of the Genetic Algorithm based methods and three adopted Hybrid Operating Strategies.

Chapter 4.1 and Chapter 4.2 present the main results achieved respectively with the parallel and the series hybrid architectures. First, the benchmark optimization results are shown in order to define the potentiality of the considered powertrain. Both the time histories of the main controlled parameters and the overall target performance are analyzed. Afterwards, the study focuses on the comparison between the real time optimizers and the benchmark, analysing the potentialities of the Total Losses Minimization and the Total Load Switch Threshold techniques, by means of a "system overview". Once more, both time histories and global parameters are provided as main indicators of the HOS performance.

Chapter 4.3 shows a case study of a parallel-hybrid diesel powertrain featuring a high-voltage Belt Alternator Starter (BAS), that was realized within a research project in collaboration with GMPT-E (Torino). As a distinguish feature of this application, also the combustion noise of the engine has been optimized with respect to the requirements of GMPT-E. This is a noteworthy feature of the Minimization of Total Losses algorithm that shows its potentiality in optimizing not-global targets.

Finally, Chapter 4 draws the main conclusions of this study, showing the novelties of the proposed methodology and suggesting further improvements.

OUTLINE

9

1. INTRODUCTION

The development of road transportation vehicles, featured by Internal Combustion Engines (ICEs), represents one of the greatest success of the modern engineering. At present, there are over 600 million passenger cars worldwide and their number is continuing to grow (Fig. 1.1) ([1, 2]).
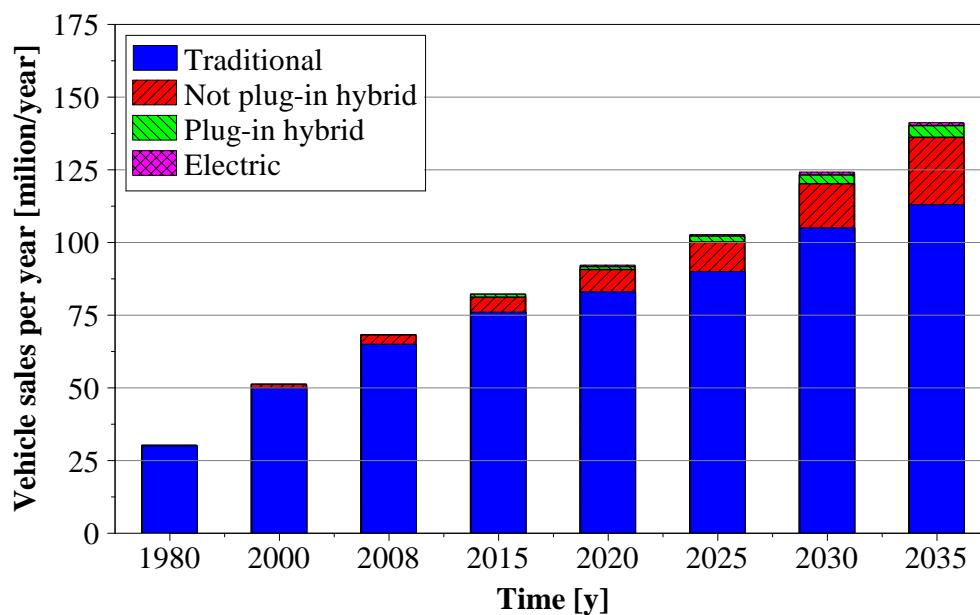
Figure 1.1 - Passenger light-duty vehicle sales by type ([1])

However, the deterioration of the air quality, global warming and depletion of petroleum resources are becoming severe threats for the road transportation. In the meanwhile, more rigorous emissions standards and higher oil prices are stimulating the development of cleaner and more efficient vehicles.

Hybrid Electric Vehicles (HEV) and Electric Vehicles (EV - that do not directly consume oil), represent most solutions for the foreseeable future. In the so called New Policies Scenario prospected by the International Energy Agency ([1]), electrified vehicles (i.e. HEVs and EVs) collectively account for 6% of new passenger vehicle sales by 2020 and 19% by 2035 (Fig. 1.1).

1.1   The environmental impact of the transportation sector

In the last decades, research and development activities have driven the transportation sector to high-efficiency and clean technologies. Three are the main environment concerns associated to the traditional road transportation:

1. exploitation of <u>not renewable energies</u>
2. production and release of <u>greenhouse gases</u>
3. production and release of <u>emissions</u>

Petroleum and its derivates represent the major <u>energy source</u> of today society. They result from the long-term decomposition of living matters imprisoned in geologically stable layers, therefore they are not-renewable. Their availability depends on the discovery of new reserves and the cumulative consumption: maintaining current trends, the world oil reserve will be exhausted by 2040 ([3]). Regarding the transportation sector, it is the primary sector in the petroleum consumption and, in the next future, it will continue to drive the growth in global oil demand.
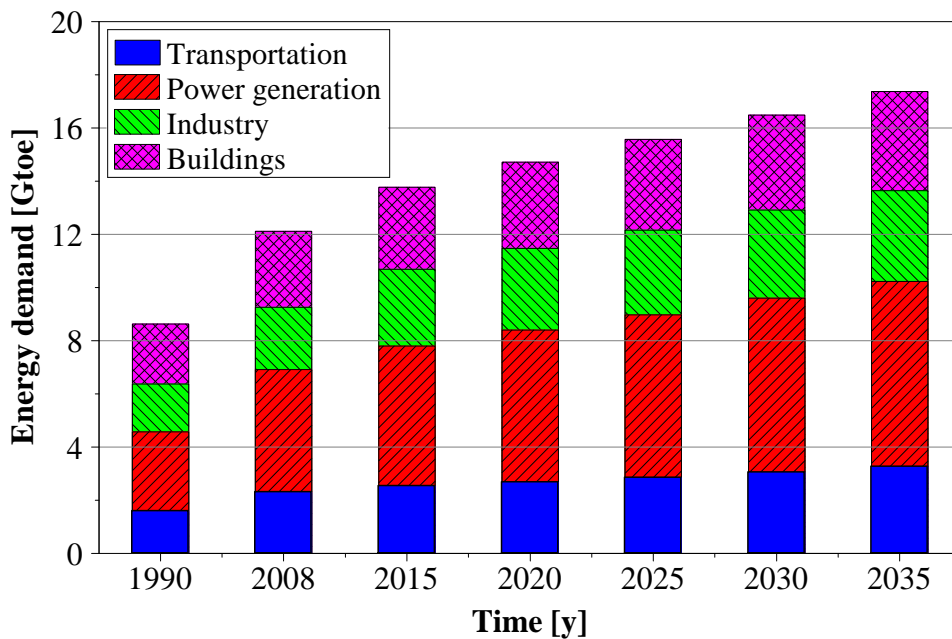

Figure 1.2 – Global energy demand by sector ([2])

Primary oil consumption share of the automobile sector will rise from the current 54 % up to about 60 % in 2035 ([2]), increasing of 1.3 % per year in 2008-2035 (Fig. 1.2) ([1]). This trend is a sharp decline in the rate of growth and is a consequence of the adopted measures for the improving the vehicle fuel economy. The growth in the oil consumption will come from the non-OECD regions and inter-regional bunkers, while transport energy demand will decline slightly in the OECD. It should be underlined that, given the limitations on further improving the efficiency of conventional vehicles, the rate by which new vehicle technologies penetrate the car market will have a major impact on the oil demand. The main factor that will affect this change are the pump price of oil-based fuels and technological advances in alternative vehicle technologies to lower their cost and improve their operational performance.

Concerning global warming, it is a result of the "greenhouse effect" induced by the presence of carbon dioxide and other greenhouse gases in the atmosphere. An increased earth temperature results in major ecological damages to its ecosystems. The International Energy Agency estimates that 22 % of all CO_2 emissions stem from the transport sector, and, in particular, 16 % from the road transport ([1]). Figure 1.3 shows the likely increase of the transport sector's share from 21 % to 24 % in 1990-2035. The main reason for this increase is the higher cost of reducing green-house gas emissions than in most other sectors.
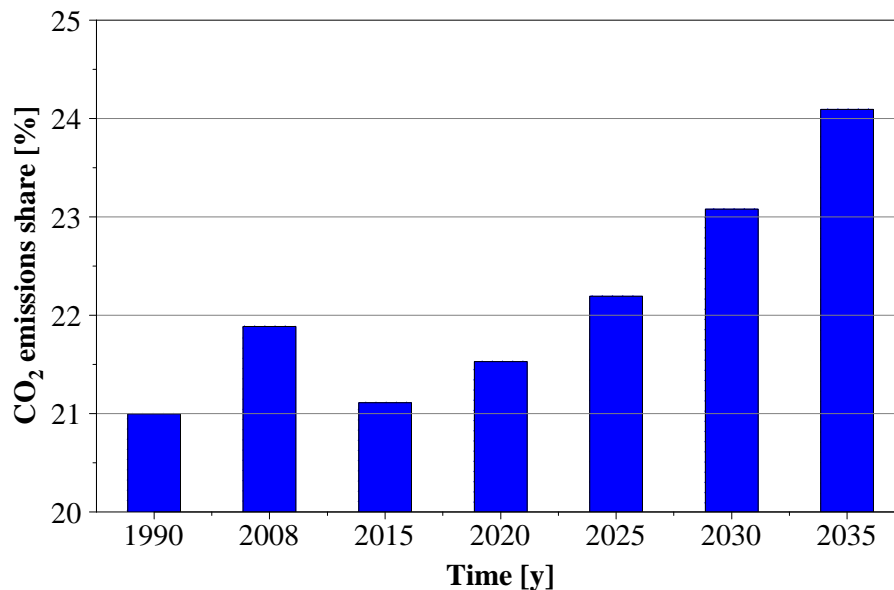
Figure 1.3 – CO_2 emissions share of the transport sector ([2])

In addition to carbon dioxide, other emissions (CO, CH_4, NO_x, N_2O, heavy metals, particulate matter, etc) of the transport sector affects air, water and soil quality. At present, the majority of the vehicles relies on the combustion of hydrocarbon fuels. Their ideal combustion yields only to carbon dioxide and water, not directly dangerous to the environment. However, in a real reaction, the gaseous products also consist of nitrogen oxides (NO_x), carbon monoxides (CO), unburned HCs and particulate matter, all of which are toxic to the human health ([4,5]).

1.2   The EU legislation framework for passenger cars

In almost all countries with high motorization levels, the motor vehicle pollutant emission are restricted by legislation limits. Starting in 1992, the New European Driving Cycle (NEDC) was adopted in the European Union regulation to capture the transient operation of motor vehicles during the testing of exhaust gas emission ([6]). The New European Driving Cycle (NEDC) is applied in laboratory chassis dynamometers, is based on traffic data from European capitals (Paris and Rome) and tries to characterize typical driving conditions that consist of complex series of accelerations, decelerations and vehicle stops. It is characterized by a cold-start procedure: before the test, the vehicle is soak for at least 6 hours at a test temperature of 20-30°C. Then, test procedure is started and the emission evaluation begins at the same time.

Beginning with the cold start, the first urban part (ECE – European Test Cycle) is run four times; afterwards, an extra-urban section (EUDC – Extra Urban Driving Cycle) is carried out once (Fig. 1.4). During the NEDC, the exhaust gases of the vehicle are diluted and a sample is collected in a bag ([7]).
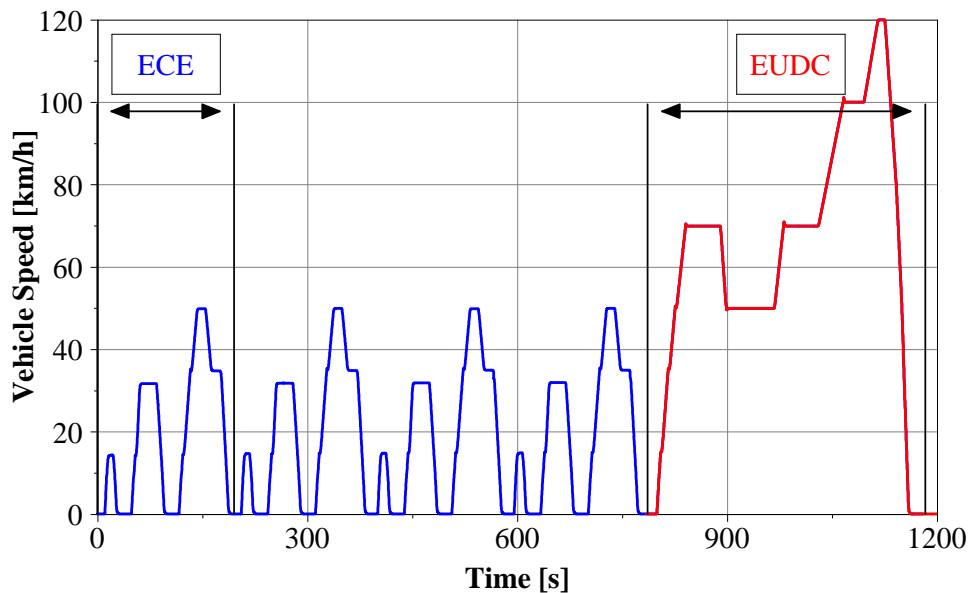

Figure 1.4 – New European Driving Cycle (NEDC)

Regarding the greenhouse gases (GHG), the European Commission has signed voluntary agreements (1998-1999) with the automotive industry for their reduction. These agreements define the fleet-average CO_2 emission targets for new cars sold in the European Union, to be reached collectively by the association members. In particular, the new legislation will set binding emissions targets to ensure an average of 130 [g_{CO2}/km] from the new passenger car fleet. A further emission reduction of 10 [g_{CO2}/km], will be provided by complimentary measures, such as biofuels, tire pressure monitoring, gear shift indication and active actions that enable the driver to optimize the fuel economy. Manufacturers who miss the average CO_2 targets will be subject to fines.

Concerning the control of pollutant emissions, the European Union has introduced common requirements for motor vehicles (the so-called "Euro" standards). These emission limits have been defined through a series of directives staging increasingly stringent requirements. Currently,

emissions of nitrogen oxides (NO_x), total hydrocarbon (THC), non-methane hydrocarbons (NMHC), carbon monoxide (CO) and particulate matter (PM) are regulated for most vehicle types. Their compliance is determined by running the engine along the New European Driving Cycle and is a necessary condition for the EU market. The emissions standards for the only M1 category are briefly summarized in Tab. 1.1 (i.e. vehicles for the carriage of passengers and with no more than eight seats in addition to the driver).

Table 1.1 – EU emission standards for passenger cars (category M1) [g/km] ([6])

	Date	CO	HC	HC+NO_x	NO_x	PM
Diesel						
Euro 1	1992.07	2.72	-	0.97	-	0.14
Euro 2, IDI	1996.01	1	-	0.7	-	0.08
Euro 2 DI	1996.01	130	-	0.9	-	0.1
Euro 3	2000.01	0.64	-	0.56	0.5	0.05
Euro 4	2005.01	0.5	-	0.3	0.25	0.025
Euro 5	2009.09	0.5	-	0.23	0.18	0.05
Euro 6	2014.09	0.5	-	0.17	0.08	0.005
Gasoline						
Euro 1	1992.07	2.72	-	0.97	-	-
Euro 2	1996.01	2.2	-	0.5	-	-
Euro 3	2000.01	2.3	0.2	-	0.15	-
Euro 4	2005.01	1	0.1	-	0.08	-
Euro 5	2009.09	1	0.1	-	0.06	0.005
Euro 6	2014.09	1	0.1	-	0.06	0.005

2. TECHNOLOGICAL BACKGROUND

The concept of Hybrid Electric Vehicles dates back to the last years of the XIX century. At that time, the engineering of Internal Combustion Engines was less advanced than that of electric motors. Therefore, electric components were required in order to assist the ICE and to provide the vehicles acceptable performance ([8]).

Today, <u>conventional vehicles</u> (featured by ICEs) provide good performance and long operating range. The energy source is petroleum fuel, characterized by high energy density. Their drawbacks are the environmental pollution and poor fuel economy. This last is mainly due to ([8]):

- ➢ the mismatch of engine efficiency characteristics with the real life operating requirements
- ➢ the dissipation of vehicle kinetic energy during braking
- ➢ the inadequacy in stop-and-go driving patterns

<u>Battery Electric Vehicles (BEVs)</u> are characterized by higher powertrain efficiency and zero local environmental pollution. As drawback, their operating range is far less competitive then traditional vehicle one, due to the low energy density of the electro-energy storage systems.

<u>Hybrid Electric Vehicles (HEVs)</u> combine the advantages of both traditional and electric vehicles. They usually couple an ICE with one or more Electric Machines. The resulting overall efficiency is improved with respect to conventional vehicles by some main features ([9]):

1. engine downsizing and downspeeding
2. recuperation of the kinetic and potential energy during braking phases (regenerative braking)
3. ICE switch-off during standstill, to avoid idling fuel consumption (Stop & Start strategy)
4. load point shift of the ICE operation to higher torques or shut-off of the engine and only electric mode driving, to avoid the engine part-load operation

Due to the presence of a multiple power source, many are the possible working configurations (Fig. 2.1) ([8]):

1. ICE alone propelling (conventional vehicle mode, red arrow)

2. EM alone propelling (only electric mode, blue arrow)
3. ICE and EM propelling (electric boost, violet arrow)
4. regenerative braking (green arrow)
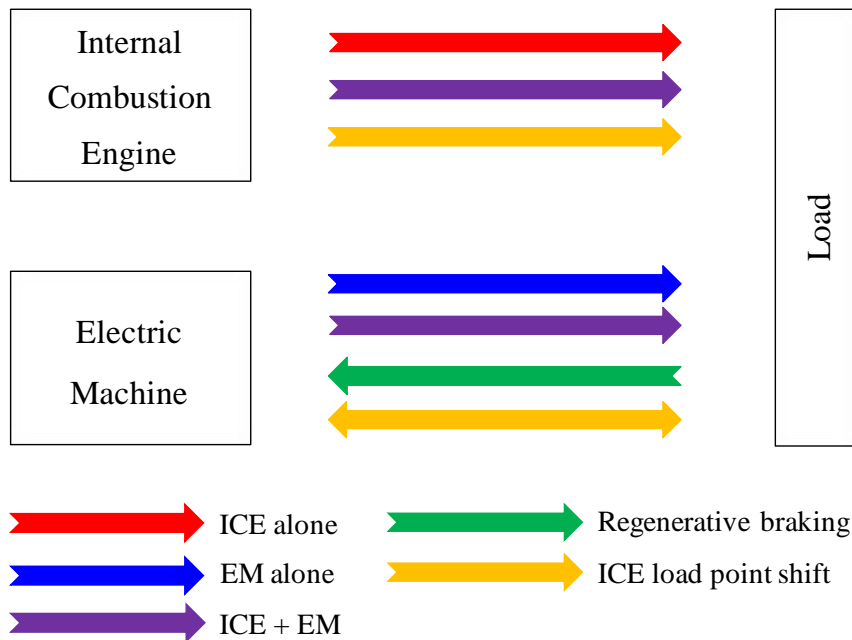5. ICE (positive or negative) load point shift (yellow arrow)

Figure 2.1 – Conceptual illustration of the working patterns of hybrid electric drivetrains

With a proper design and control, the overall performance, efficiency and emissions can be highly optimized. However, deciding the operating mode depends on many factors, such as the physical configuration of the drivetrain, powertrain efficiency characteristics, load characteristics, driver behavior, etc. *In order to reach the expected advantages of the vehicle hybridization, it is essential to employ each powertrain component through the best possible approach. Within this framework, computational modeling is an important tool to optimize the operating strategy of hybrid electric vehicles.*

2.1 Classification of the Hybrid Electric Vehicles

The architecture of a hybrid vehicle is defined as the connection of the components that characterize the energy chain and the control interface. Traditionally, HEVs are classified into three main categories (Fig. 2.2) ([6, 10]):

1. **Series Hybrid Electric Vehicles (SHEVs)**: two Electrical Machines (EMs) are connected through a power converter. This component is an electric power coupler that controls the power flows from the batteries and generator (EM2) to the electric motor (EM1) or vice versa. Typically, EM2 features as generator, in order to convert the mechanical power of the ICE into electrical power to be supplied to the battery or to the traction electric machine. The generator, in case of no dedicated starter, works as motor during the engine launch. Both the load and the speed of the ICE are decoupled from the driving conditions

2. **Parallel Hybrid Electric Vehicles (PHEVs)**: two mechanical power sources (an Internal Combustion Engine and an Electric Machine) are linked through a mechanical coupler. They can both supply traction power to the wheel shaft. The only load of both the ICE and the EM is decoupled from the driving pattern, instead their speed is function of the vehicle velocity and gear shift strategy

3. **Series/Parallel Hybrid Electric Vehicles (SPHEVs)**: two power couplers are employed: one mechanical and the other one electrical. This configuration is the combination of series and parallel structures, possessing the major features of the both. Typical example are the Mixed Hybrid Electric Vehicle and the Power Split Hybrid Electric Vehicle ([10, 11]).
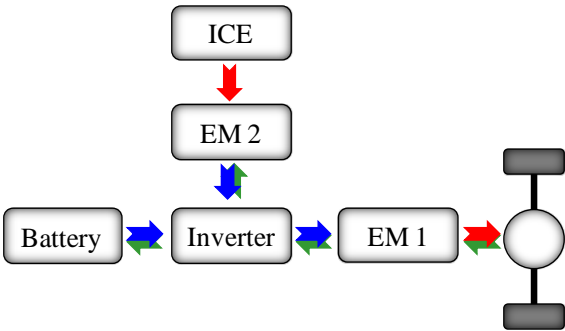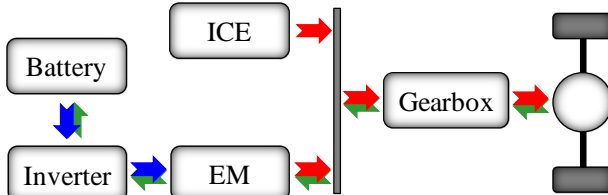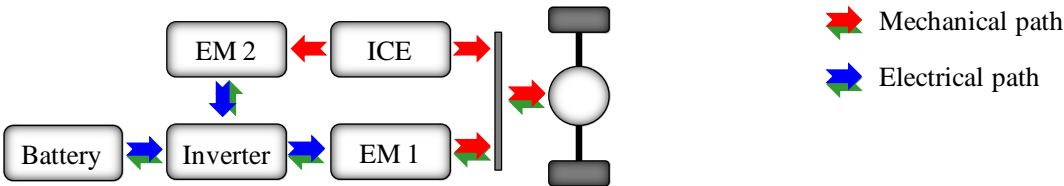
Figure 2.2 – Classification of the Hybrid Electric Vehicles

Two are the major advantages of the PHEV over the SHEV. Both the power sources directly supply torque to the driven wheels without any energy conversion. Moreover, there is no additional generator and the EM is smaller than in the series configuration (EM1) because it is not sized for the maximum required traction power. Regarding the SHEVs, two are the major advantages over the PHEVs. First, the electrical coupling between the engine and the wheel shaft allows a complete independent operation (both at the speed and at the load level) from the driving pattern. Second, the structure and control of the ICE are usually less complex. In general, *hybrid vehicles present at least two degrees of freedom in the power generation. Their optimization, with respect to selected target(s) and boundary conditions, is the main focus of this study.*

2.2   Main components of the hybrid electric vehicles

2.2.1 Internal Combustion Engine (ICE)

The Internal Combustion Engine is the most widespread power source for road transportation vehicles and, in the foreseeable future, it will still be the dominant vehicular power source ([12]). In HEVs, its operation differs significantly from that of a conventional motor vehicle due to the available degrees of freedom in the power generation. In the framework of this study, two different engine types are considered:

1. Continuous Variable Valve Timing (CVVT) Spark Ignition (SI) engine
2. Direct Injection Turbo Compression Ignition (CI) engine

Spark-Ignition (SI) engines

They are characterized by a combustion process of the air-fuel mixture ignited by a spark of a spark plug. In particular, SI **Continuous Variable Valve Timing (CVVT)** engines (Fig. 2.3) offers the ability of independently controlling the intake and the exhaust valves. These variations are defined on a spectrum that optimize engine performance and efficiency under all operating conditions.

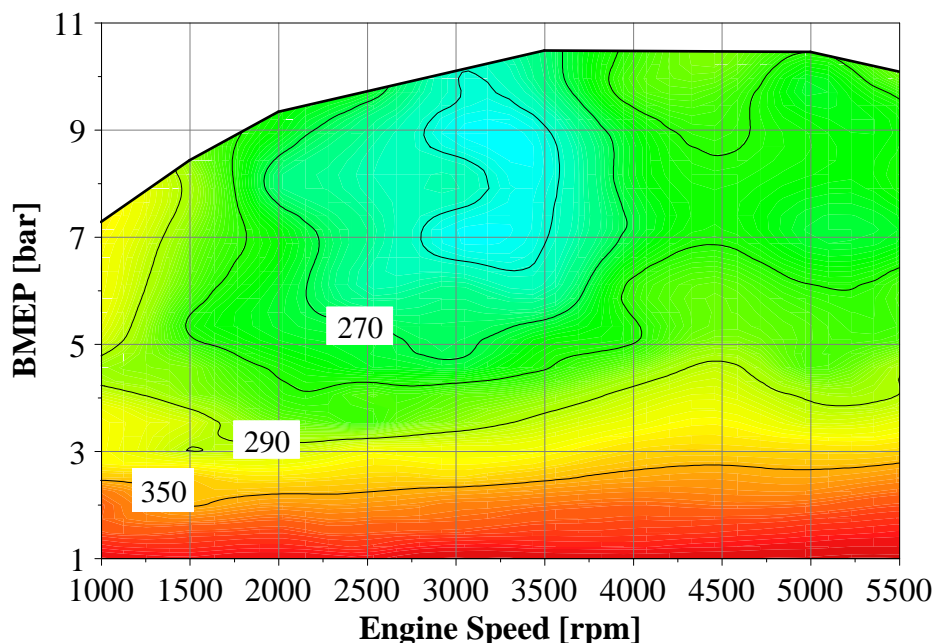**Figure 2.3 – BSFC map of the considered CCVT Spark Ignition ICE [g/kWh]**

Main variation criteria with respect to a conventional SI engine are ([13]):

➢ **Late intake valve closing**: during the compression stroke, the piston pushes air out of the cylinder and guarantees a higher inlet pressure for the next intake cycle. Pumping losses are reduced up to 40% and NO_x emissions are decreased during partial load conditions

➢ **Early intake valve closing**: pumping losses at low engine speeds are reduced up to 40% (with a fuel economy improvement of up to 7%). NOx emissions can also be reduced

➢ **Early intake valve opening**: exhaust gases partially flow out of the cylinder, via the intake valve. The Exhaust Gas Recirculation grade can be highly improved assisting the control of the NOx emission production. Volumetric efficiency is improved

➢ **Early/late exhaust valve closing**: by holding the exhaust valve, the cylinder is more deeply emptied. By closing the valve slightly early, more exhaust gas remains in the cylinder: fuel efficiency is improved and NOx emissions are reduced

In the past, this technology has been prevented to become widespread by engineering difficulties such as dynamic performance at high engine speed, power consumption, long term durability and repeatability ([14]).

Spark Ignition engines do not require demanding after-treatment systems: due to the stochiometric combustion, the well known three-way catalytic converter can be adopted. Accordingly, *within the boundary conditions of this study, the only target of the hybridization of the powertrain featuring the SI engine is the optimization of the fuel economy.*

Compression-Ignition (CI) engines

They are characterized by the self-ignition of the air-fuel mixture in the final phases of the compression stroke. At a given engine speed, airflow is essentially unchanged and load control is achieved by varying the amount of fuel that is injected. Moreover the compression ratio is not depending of the ignition-limit of the fuel and it can be increased with respect to SI engines.
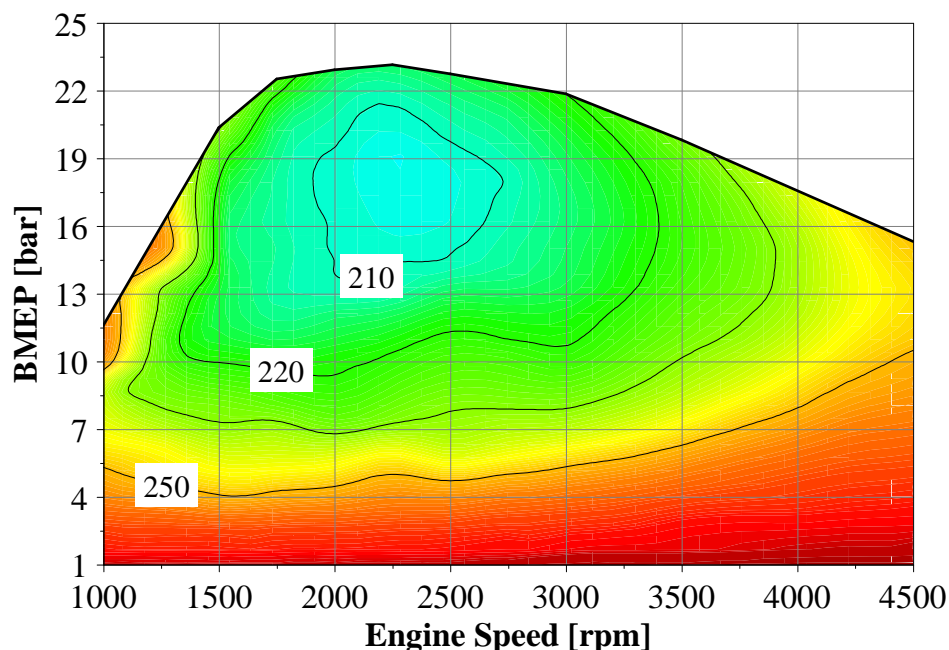

Figure 2.4 – BSFC map of the considered Turbo Compression Ignition ICE [g/kWh]

The above mentioned features result in a better fuel economy than in SI engines. The resulting BSFC map (Fig. 2.4) is characterized by an minimum BSFC about 20% lower than that of the CVVT SI engine. As drawback, due to the lean combustion, pollutant emissions represent an main concern for this engine typology. As far as the NO_x are concerned, they can mainly be reduced by controlling the duration of the diffusion combustion (increasing the rate of injection) and by reducing the combustion temperature (retarding the injection timing and increasing the rate of the Exhaust Gas Recirculation). However, these methods reduce the fuel efficiency and performance of the engine. Figure 2.5 reports the $BSNO_x$ emission map for the considered CI engine.
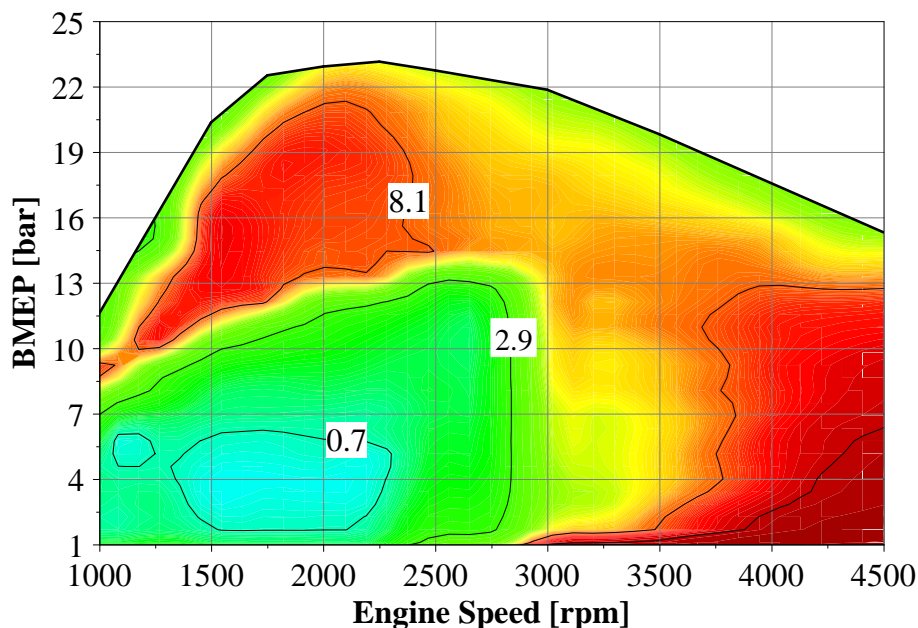
Figure 2.5 – BSNO$_x$ map of the considered Turbo Compression Ignition ICE [g/kWh]

The electrification of vehicles featuring CI engines can be an important tool in order to reach the required emissions standard and to maintain high vehicle performance and fuel economy. W*ithin the boundary conditions of this study, the target of the powertrain hybridization featuring the CI engine is both the optimization of the fuel economy and the reduction of the NO$_x$ emissions.*

2.2.2 Motor Generator Unit (MGU)

The electric propulsion system (the so called Motor Generator Unit - MGU) consist of electric motors, power converters and electronic controllers. The electric motor converts electric into mechanical energy in order to propel the vehicle or, vice versa, mechanical into electric energy to recharge the energy storage. The power converter supplies the electric motor with the proper voltage and current levels.

The choice of electric propulsion systems for EVs and HEVs depends on a number of factors, including driver's expectations, vehicle constraints and energy source. The road transportation requires frequent starts and stops, high powers and torques and a very wide speed range.

Nowadays, hybrid electric vehicles are equipped almost exclusively with three-phase machines: the majority of them is Asynchronous (ASM) or Permanent Magnet Synchronous (PSM) ([10]). While the rotating magnetic field and the rotor are synchronous in PSMs, in ASMs, there is a slip between the rotor speed and phase rotation speed. PSMs guarantee higher full and partial load efficiencies, instead ASMs show a better overload capacity (i.e. the ability of the electric motor to supply, for a short time, a higher torque than the permanently accessible maximum one) ([15]).
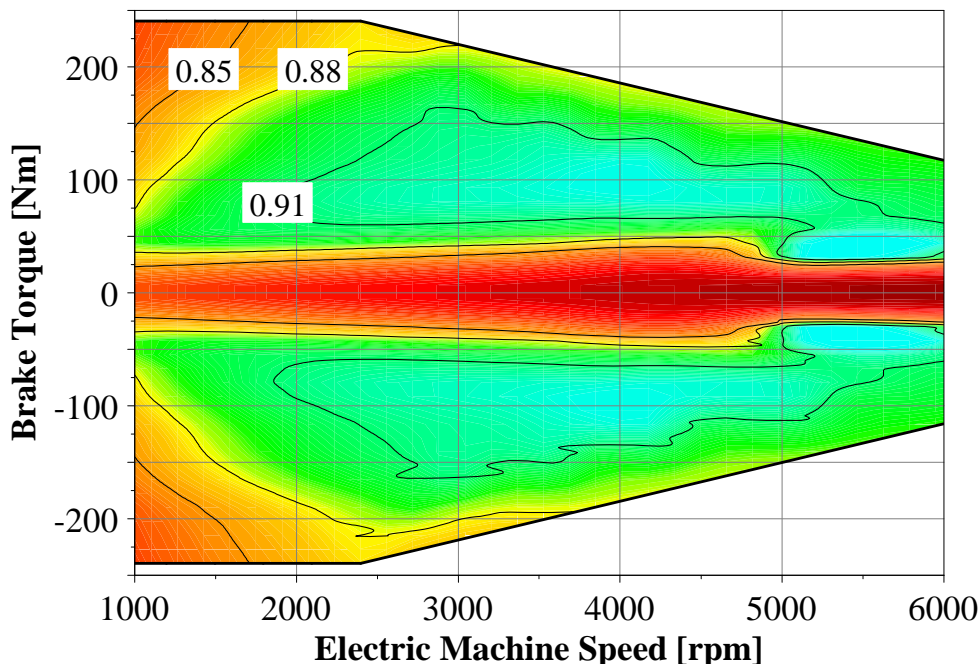
Figure 2.6 – Efficiency map of the selected PSM Electric Machine [-]

The project under discussion takes into consideration a <u>Brushless Permanent Magnet (PSM) Electric Machine</u> ([8,15]). These systems, by using high-energy permanent magnets as field excitation mechanism, can be designed with high power density, high speed, and high operation efficiency. Their main advantages are:

➢ High efficiency: due to the use of permanent magnets for the excitation (which consume no power) and to the absence of a mechanical commutator and brushes (low mechanical friction losses), they are the most efficient electric motors (Fig. 2.6)

➢ Compactness: very high flux densities in the motor are achievable due to the current introduction of high-energy density magnets (rare-earth magnets). This allows high torques with a resulting reduction in the size and in the weight

➢ Simple control and cooling (no current circulation in the rotor)

➢ Low maintenance and great reliability (no brushes and mechanical commutators)

However, brushless Permanent Magnet Electric Motors present some technical and economical disadvantages:

➢ High cost: due to the expensive rare-earth magnets

➢ Limited constant power range

➢ Limited maximum speed

2.2.3 Electric energy storage: the electrochemical battery

"Energy storages" are devices that accumulate energy, deliver energy (discharging phase) and accept energy (charging phase). Several types of energy storages have been proposed for the automotive industry: chemical batteries, supercapacitors, high-speed flywheels, etc. For road transportation applications, their main requirements are: high specific energy, high specific power, high efficiency, low maintenance and management requirements, low cost and safety during the utilization ([8]).

Electrochemical batteries (Fig. 2.7) are devices that convert electrical energy into chemical energy during the charging phase, and vice versa during the discharging phase. They are arranged by several cells stacked together in series ($N_{cells,series}$) and in parallel ($N_{cells,parallel}$). A cell is an independent and complete unit that possesses all the basic electrochemical properties ([16,17]).
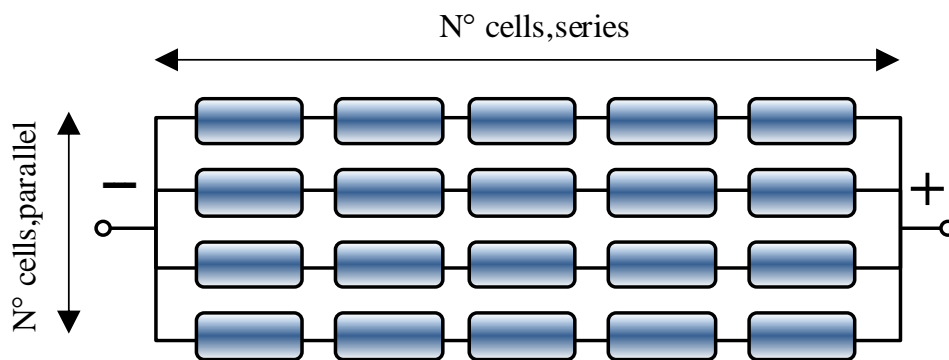
Figure 2.7 – General scheme of an electro-chemical battery [-]

Some main features characterizes the behavior of the electrochemical batteries:

➢ **Capacity [Ah]**: the ampere-hours obtained by a complete discharge (from a fully charged state until the terminal voltage drops to its cut-off voltage)

➢ **State Of Charge (SOC) [-]**: the SOC is defined as the ratio of the remaining capacity over the fully charged capacity. A complete charge or discharge of the battery is not allowed for commercial batteries to improve their durability and stability of performance

➢ **Specific energy [Wh/kg]**: the maximum energy that can be generated/accumulated per unit of battery mass

➢ **Specific power [W/kg]:** the maximum power per unit of battery mass that can released or absorbed in a short period. It is an important feature in order to reduce the battery weight, especially in high-power demand applications, such as HEVs

In this study, Lithium-Ion battery cells are considered. This technology adopts lithiated carbon material as negative electrode, lithiated transition metal oxide as positive electrode and liquid

organic solution or solid polymer as electrolyte. Lithium ions move through the electrolyte between the positive and negative electrodes and accomplish the chemical energy transfer. They allow a very high nominal voltage, resulting in excellent specific energy and specific power (see the Ragone Diagram in Fig. 2.8) ([10]).
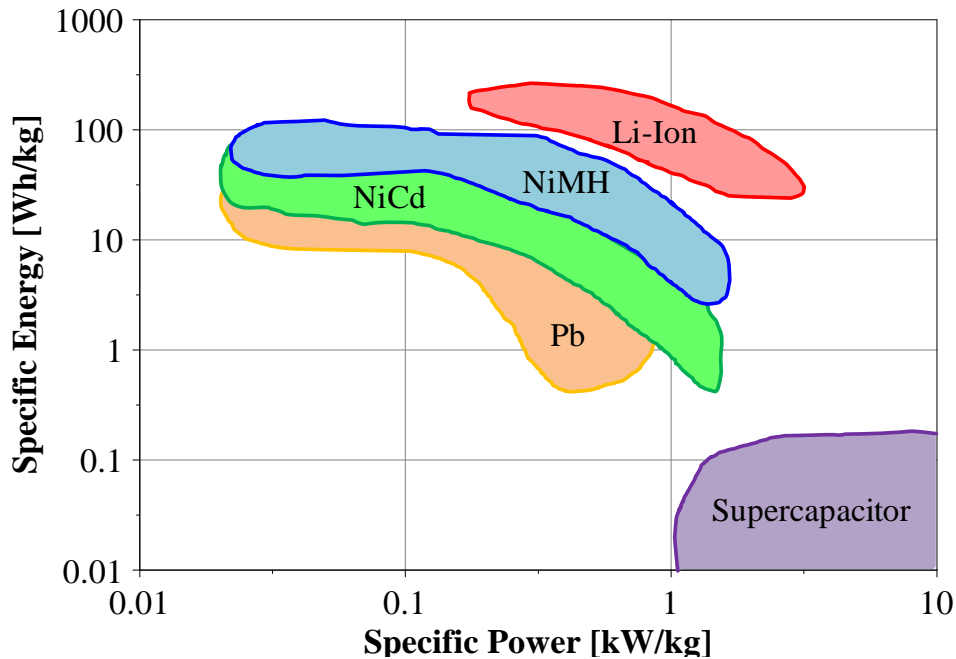
Figure 2.8 – Electric energy storage systems: ranges of specific energy vs. specific power (Ragone Diagram) [-]

Table 2.1 reports the data sheet of the selected Lithium-Ion cell. In particular, the capacity [Ah], nominal voltage [V], specific energy [Wh/kg], specific power [W/kg] and available operating range are reported.

Table 2.1 – Cell data sheet of the selected Li-Ion battery

Electrical specification	
Capacity	4.5 Ah
Nominal voltage	3.6 V
Specific Energy	75 Wh/kg
Specific power	2300 W/kg
SOC working range	0.2 – 0.8

The global performance of the battery are a straightforward combination of the cell structure in Fig. 2.7. As far as the battery capacity is concerned, this equal to the cell capacity multiplied by the number of strings:

$$C_{batt}=C_{cell} \cdot n_{cell,parallel} \qquad (2.1)$$

Concerning the battery nominal voltage, this is equal to the cell nominal voltage multiplied by the number of the cells per string:

$$V_{N,batt}=V_{N,cell} \cdot n_{cell,series} \qquad (2.2)$$

3. METHODOLOGY

3.1   Zero dimensional simulation of hybrid electric powertrains

This study deals with the zero-dimensional simulation, in Matlab environment, of the drivetrain of two hybrid electric vehicle architectures: a Series Hybrid Electric Vehicle (SHEV) and a Parallel Hybrid Electric Vehicle (PHEV).

SERIES HYBRID ELECTRIC VEHICLES   PARALLEL HYBRID ELECTRIC VEHICLES

Mechanical path   Electrical path
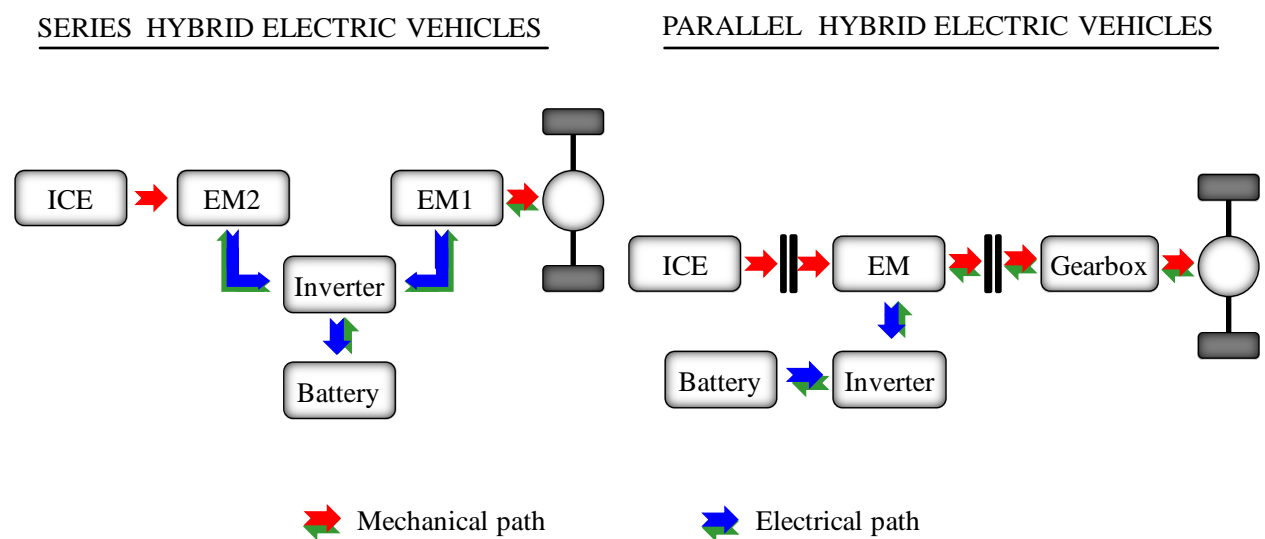
Figure 3.1 – Layout of the considered hybrid electric drivetrains

Figure 3.1 shows the main components of the analyzed drivetrains: a single shaft PHEV with two clutches and gearbox and the SHEV without gearbox. In the PHEV, the EM is powered by the battery through the inverter and is mechanically linked to the engine crankshaft. ICE and EM directly supply torque to the wheels via the gearbox, according to the torque split determined by the control logic unit. Two clutches are installed: one between the EM and the gearbox (as in traditional vehicles) and one between the ICE and EM in order to allow deep regenerative braking and pure electric mode. In the SHEV, the electric machine EM1 supplies the required traction power

to the wheels. The electric power needed by EM1 is provided by the battery and generator (EM2, mechanically connected to the ICE). The operation of the engine is independent on both the speed and the load of the driving pattern. Nor clutches neither gearbox are installed.

Tables 3.1 and 3.2 report respectively the main features of the considered hybrid electric vehicles and their case setup in the framework of this study.

Table 3.1 – Main features of the considered hybrid electric vehicles

	PARALLEL HYBRID ELECTRIC VEHICLE				SERIES HYBRID ELECTRIC VEHICLE			
	Gasoline		Diesel		Gasoline		Diesel	
	Not Plug-In	Plug-In	Not Plug-In	Plug-In	Not Plug-In	Plug-In	Not Plug-In	Plug-In
ICE	1.8 l CVVT SI 92.6 kW		1.7 l Turbo CI 95.5 kW		1.8 l CVVT SI 92.6 kW		1.7 l Turbo CI 95.5 kW	
EM or EM1	PSM - 30 kW - 124.1 Nm				PSM - 90 kW - 528.0 Nm			
EM2	-				PSM - 100 kW - 333.1 Nm			
Battery	110x1 cells 1.8 kWh 55.2 kW	110x2 cells 3.6 kWh 110.4 kW	110x1 cells 1.8 kWh 55.2 kW	110x2 cells 3.6 kWh 110.4 kW	110x1 cells 1.8 kWh 55.2 kW	110x2 cells 3.6 kWh 110.4 kW	110x1 cells 1.8 kWh 55.2 kW	110x2 cells 3.6 kWh 110.4 kW
Gearbox	6 gear manual transmission				-			
Vehicle	1600 kg	1700 kg	1600 kg	1640 kg	1685 kg	1720 kg	1645 kg	1680 kg
	$c_W \cdot A$=0.65 m^2 - k_R=0.009 - Wheels: 205/55/R16				$c_W \cdot A$=0.65 m^2 - k_R=0.009 - Wheels: 205/55/R16			

(*) the mass here displayed refers to the base vehicle mass, considering 75 kg for the load of the driver

As mentioned, two internal combustion engines are considered: a 1.8 l (93 kW peak power) Spark Ignition engine with Continuous Variable Valve Timing feature and a 1.7 l (96 kW peak power) Turbo Compression Ignition engine (please, refer to Chapter 2.2.1 for further details). As far as the electric machines are concerned, three Permanent Magnet Synchronous machines are employed (Chapter 2.2.2).

The parallel architecture features a 30 kW peak power PMS; instead, a 90 kW peak power high-torque traction motor and a 100 kW peak power generator are adopted in the case of the series architecture. Regarding the energy storage, two battery packs with Lithium-Ion battery cells are considered (Chapter 2.2.3): a 1x110 cells (1.8 kWh energy content and 55.2 kW peak power) in the case of the not plug-in HEVs and a 2x110 cells (3.6 kWh energy content and 110.4 kW peak power) in the case of the plug-in HEVs. A 6-gear manual transmission is implemented in the only case of the parallel hybrid vehicles, whereas the electric motor of the SHEV is featured by a direct mechanical connection to the wheel shaft.

Table 3.2 – Considered Hybrid Electric Vehicles

Hybrid Architecture	Engine	Plug-In Feature
Parallel	Compression Ignition	with
		without
	Spark Ignition	with
		without
Series	Compression Ignition	with
		without
	Spark Ignition	with
		without

Table 3.2 reviews the considered case setup: four Parallel and four Series Hybrid Electric Vehicles. For each architecture the both engines (CVVT-SI and Turbo-CI) as well as the plug-in or not plug-in features are evaluated (with a total number of 8 combinations).

3.1.1 Internal Combustion Engine

The ICE is modeled through experimentally derived look-up tables, from which fuel consumption and emissions are mapped as functions of the engine speed and Brake Mean Effective Pressure (BMEP - see the BSFC map in Fig. 2.3, Fig. 2.4 and the $BSNO_x$ map in Fig. 2.5).
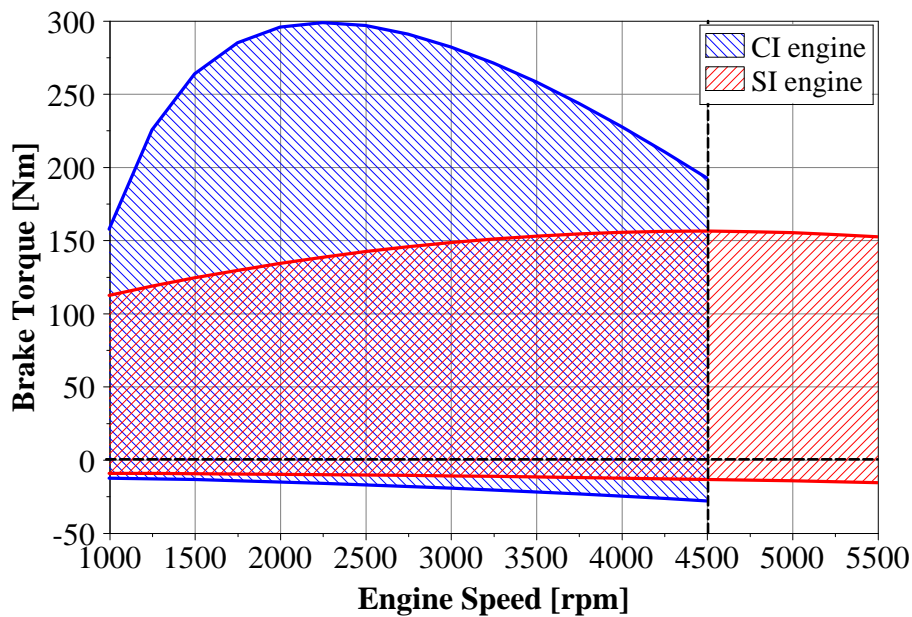

Figure 3.2 - ICEs: operating range

The ICE operating range (Fig. 3.2) is between the full load curve (Accelerator Pedal Position - APP set to 100%) and the motored condition (APP set to 0%). The accelerator and engine speed are determined by the virtual driver (please, refer to Chapter 3.2 for further details) depending on the load request of the mission driving profile.

A semi-empirical correlation was introduced to reproduce the engine warm-up ([18, 19]). This is required in order to correctly account for the changes in friction losses during the thermal transients and to simulate the ICE cold start.

3.1.2 Motor Generator Unit

The selected electric machines are Brushless Permanent Magnet Electric motors/generators: can either deliver load to the driveline/engine or recover energy to be stored in the battery or to be supplied at the electric transmission ([20, 21]).

The mechanical power supplied in motor mode (Eq. (3.1)) and the electric power supplied to the battery in generator mode (Eq. (3.2)) are determined as follows:

Motor: $\qquad P_{EM}=\varepsilon_{el,mec}P_{batt}-T_{EM,fr}\omega_{EM}=\varepsilon_{EM}P_{batt}$ $\qquad\qquad$ (3.1)

Generator: $\qquad P_{batt}=\varepsilon_{el,mec}(P_{EM}-T_{EM,fr}\omega_{EM})=\varepsilon_{EM}P_{EM}$ $\qquad\qquad$ (3.2)

The total efficiency ε_{EM} includes the electro-mechanical conversion efficiency and the friction losses of the electric machine. ε_{EM} is obtained from experimentally-derived look-up tables as a function of the electric machine speed and torque (see Fig. 2.5).

3.1.3 Battery

The electric energy storage system is a forced air cooled Lithium-Ions battery pack. It is described by means of the equivalent circuit shown in Fig. 3.3 ([22, 23]). This circuit defines the battery current i as a function of two electric resistances (the so-called Ohmic R_{ohm} and charge transfer R_{ct}) and a capacitance (diffusion layer capacitance C_{dl}).

The battery current (Eq. (3.3)) and the State Of Charge (SOC – i.e. the ratio of the instantaneous capacity over the total capacity, Eq. (3.4)) are evaluated as follows:

$$\frac{di}{dt}=\frac{C_{dl}\dot{V}_{oc}-i-C_{dl}i\dot{R}_{ohm}+\frac{V_{oc}}{R_{ct}}-\frac{P_{EM}}{R_{ct}i}-\frac{R_{ohm}}{R_{ct}}i-\frac{C_{dl}}{i}\dot{P}_{EM}}{C_{dl}R_{ohm}-\frac{C_{dl}P_{EM}}{i^2}}$$
$\qquad\qquad$ (3.3)

$$SOC(t)=\frac{Q_0-\int_{t_0}^{t}i\,dt}{Q}$$
$\qquad\qquad$ (3.4)

where the current is positive when supplied by the battery to the electric machine and negative when the battery is recharged.
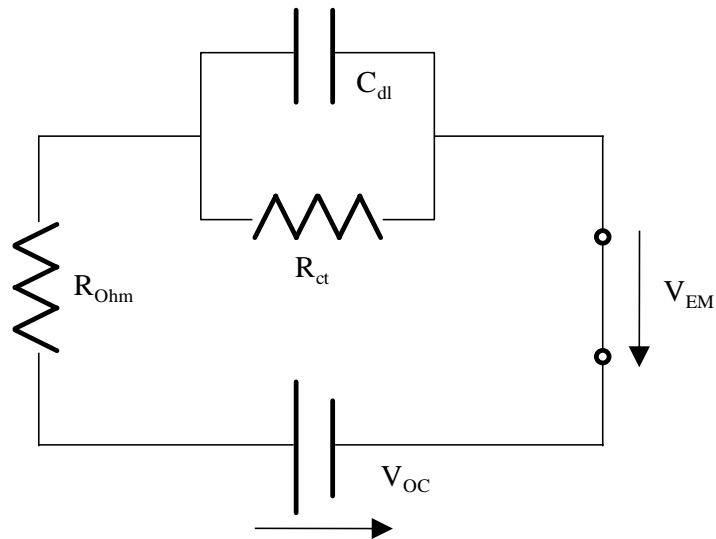
Figure 3.3 - Battery: equivalent electric circuit

The resulting battery efficiency during successive step charge and discharge phases is displayed in Fig. 3.4 for four power levels (respectively ±5 kW, ±10 kW, ±15 kW, ±20 kW). The figure refers to the battery of the plug-in configurations: 110 battery cells per string and 2 cell stings (see Tab. 3.1).
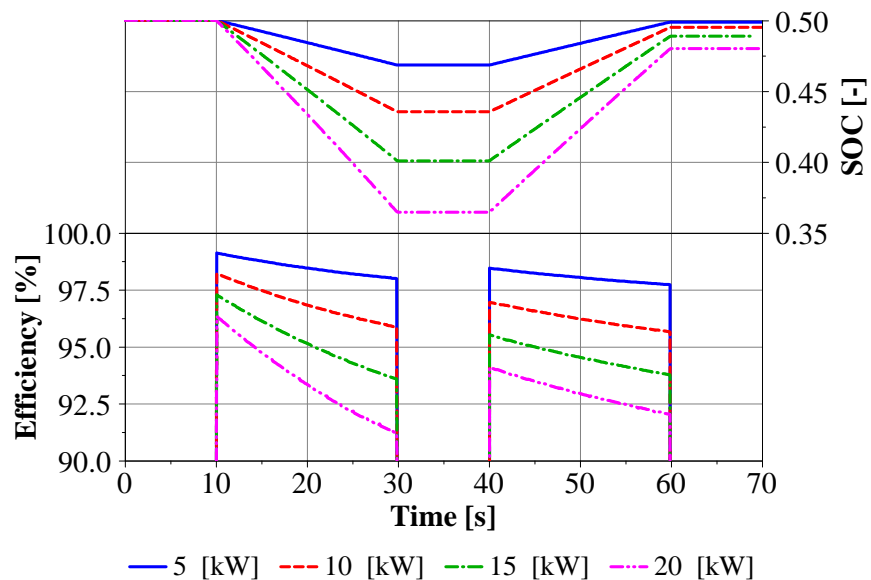
Figure 3.4 – Battery: SOC and efficiency during step power requests and supplies

As regards the battery temperature θ_{batt}, it is estimated from the energy balance of:

➢ the Joule heat losses (+)

> in case of fan-on, the heat rejected through the pack cooling system, based on forced-air convection (H_{batt}) (-)

The resulting governing equations of the battery temperature are:

Fan ON: $$\dot{\theta}_{batt} = \frac{(R_{ohm}i^2 + R_{ct}i_{ct}^2) - H_{batt}(\theta_{batt} - \theta_{air})}{c_{p,batt}M_{batt}}$$ (3.5)

Fan OFF: $$\dot{\theta}_{batt} = \frac{(R_{ohm}i^2 + R_{ct}i_{ct}^2)}{c_{p,batt}M_{batt}}$$ (3.6)

The SOC and the battery equivalent temperature are used in order to define the operating constraints. These are taken into consideration in order to improve the component durability and stability of performance.
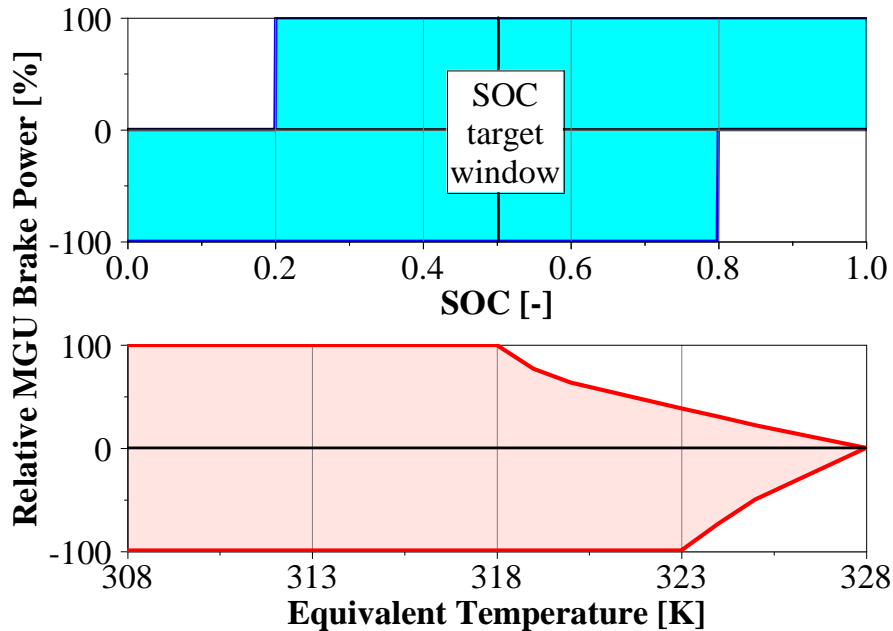
Figure 3.5 – Battery: SOC and temperature derating

In particular the SOC is bounded the operative interval [0.2 - 0.8] (see Tab. 2.1), and the temperature cannot exceed 328 K.

3.1.4 Driveline

The driveline is strictly function of the considered hybrid architecture. Its main components are the clutche(s) (no in the case of the SHEV), gearbox (for the only PHEV), driveshaft, differential and the half shafts. All these components are modeled according to their inertia, efficiency and speed ratio.

Regarding the gearbox, it plays a key role in the global driveline efficiency ([23, 24]). Its transmitted traction power ($P_{gb,out}$) is calculated through the following equation:

$$P_{gb,out}=\omega_{gb,out}\left[\varepsilon_{gb}r_{gb}\left(T_{gb,in}-I_{gb,in}\dot{\omega}_{gb,in}\right)-I_{gb,out}\dot{\omega}_{gb,out}\right] \qquad (3.7)$$

with: $\quad r_{gb}=\dfrac{\omega_{gb,in}}{\omega_{gb,out}}$ $\qquad\qquad\qquad\qquad\qquad\qquad\qquad$ (3.8)

where the transmission efficiency ε, angular speed ω, inertia I, and speed ratio r are considered. The transmission efficiency is modeled as a function of the gear number, input torque, input speed and oil temperature. In order to properly describe the change in the oil temperature θ_{gb}, a zero-dimensional thermal model of this component has been implemented according to Fig. 3.6:

$$P_{in} = k_1 \cdot (\theta_{ICE} - \theta_{gb}) + k_2 \cdot P_{gb,l}$$

$$P_{out} = k_3 \cdot (\theta_{gb} - \theta_{air}) + k_4 \cdot (\theta_{gb} - \theta_{air}) \cdot v_{car}$$
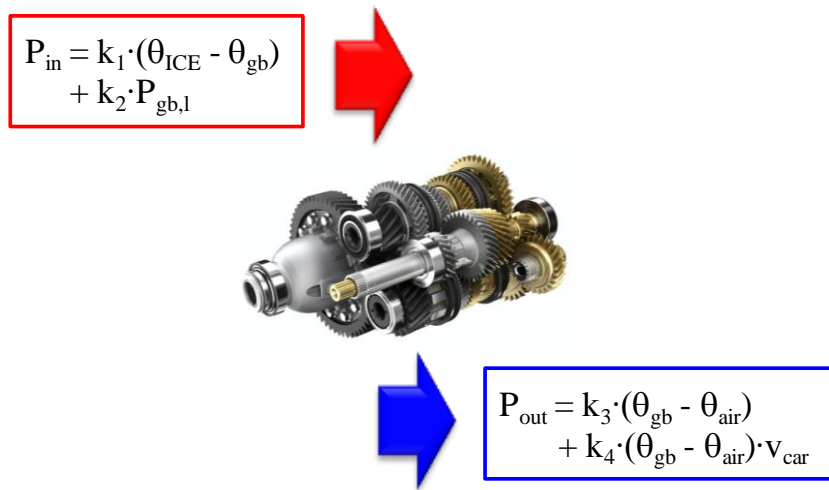
Figure 3.6 – Gearbox: zero-dimensional thermal model

Four terms are considered in the zero-dimension thermal model of the gearbox:

1. the heat conduction from the engine (+)

2. the internal losses of the gearbox (+)

3. the heat conduction to other vehicle components via case supports and output propeller shafts (-)

4. the convection heat loss towards the ambient air (-)

The calibration coefficients k_1 to k_4 were determined on the basis of available experimental gearbox temperature profiles, via least-square fits optimization. The gearbox transmission efficiency ε_{gr} is then estimated by means of the equivalent temperature of the gearbox and of the experimental transmission efficiency maps. These maps are defined as a function of the input torque and input speed for each gear number at $\theta_{gb,1}$ = 313.15 K and at $\theta_{gb,2}$ = 353.15 K (Fig. 3.7). Due to intellectual property reasons the transmission efficiency was normalized with respect to its maximum value.
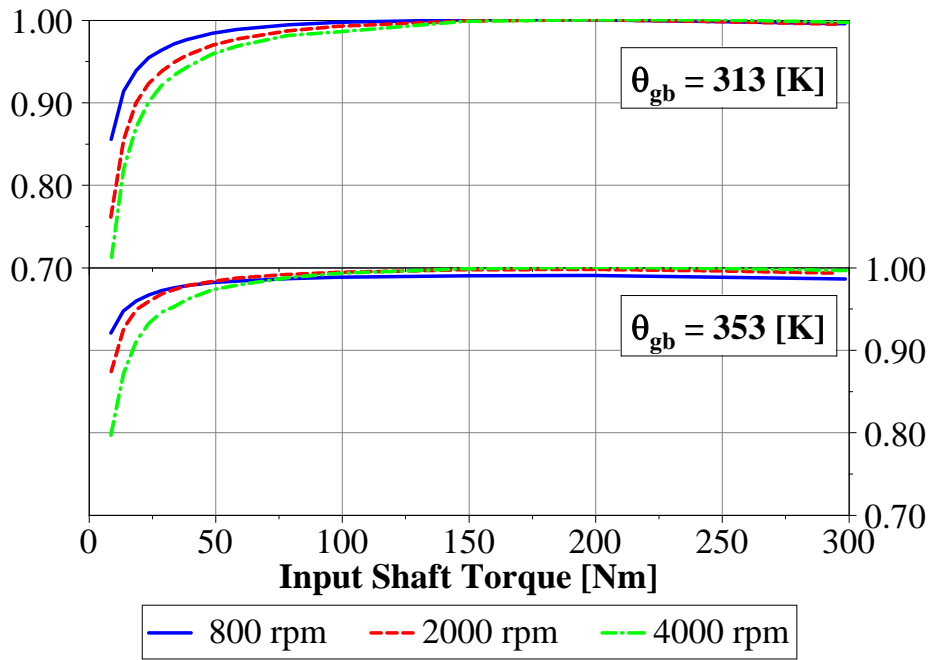
Figure 3.7 - Gearbox: relative transmission efficiency (gear number 1)

The resulting transmission efficiency is defined as logarithmic interpolation and extrapolation of the efficiency at the actual gearbox equivalent temperature:

$$\varepsilon_{gb} = \left(\varepsilon_{gb,\theta2} - \varepsilon_{gb,\theta1}\right) \cdot \frac{\ln\left(\frac{\theta}{\theta1}\right)}{\ln\left(\frac{\theta2}{\theta1}\right)} + \varepsilon_{gb,\theta1} \tag{3.9}$$

The drop in transmission efficiency due to spin and contact losses are dominated by oil viscosity for low input torques, typical of urban driving.

3.1.5 Vehicle

The traction power P_{req} at the vehicle wheels depends, in case of flat route, on the tire rolling resistance (dominant at low vehicle speed), aerodynamic drag resistance (prevailing at high speeds) and inertial resistance (active during speed transients). The resulting required traction power can be expressed as:

$$P_{req} = \left(r_{roll} \cdot v_{car} \cdot M_{car} + \frac{1}{2} \cdot C_{drag} \cdot \rho_{air} \cdot A_{car} \cdot v_{car}^2 + M_{car} \dot{v}_{car}\right) \cdot v_{car} \tag{3.10}$$

where r_{roll} is the rolling resistance coefficient, C_{drag} is the drag coefficient, ρ_{air} is the external air density, A_{car} the frontal area and M_{car} is the mass of the vehicle.

The last line of Tab. 3.1 resumes the main parameters of the selected medium class vehicle, required to apply Eq. 3.10.

3.1.6 Driving Cycles

Driving cycles are test cycles used to standardize the evaluation of vehicles fuel economy and emissions. They are speed–time sequences that represent the traffic conditions and driving behavior in a specific condition. For each powertrain configuration, the following driving cycles were considered (Fig. 3.8):

➢ New European Driving Cycle (NEDC)

➢ Artemis Urban Cycle (AUC)

➢ Artemis Road Cycle (ARC)

➢ Artemis Motorway Cycle (AMC)
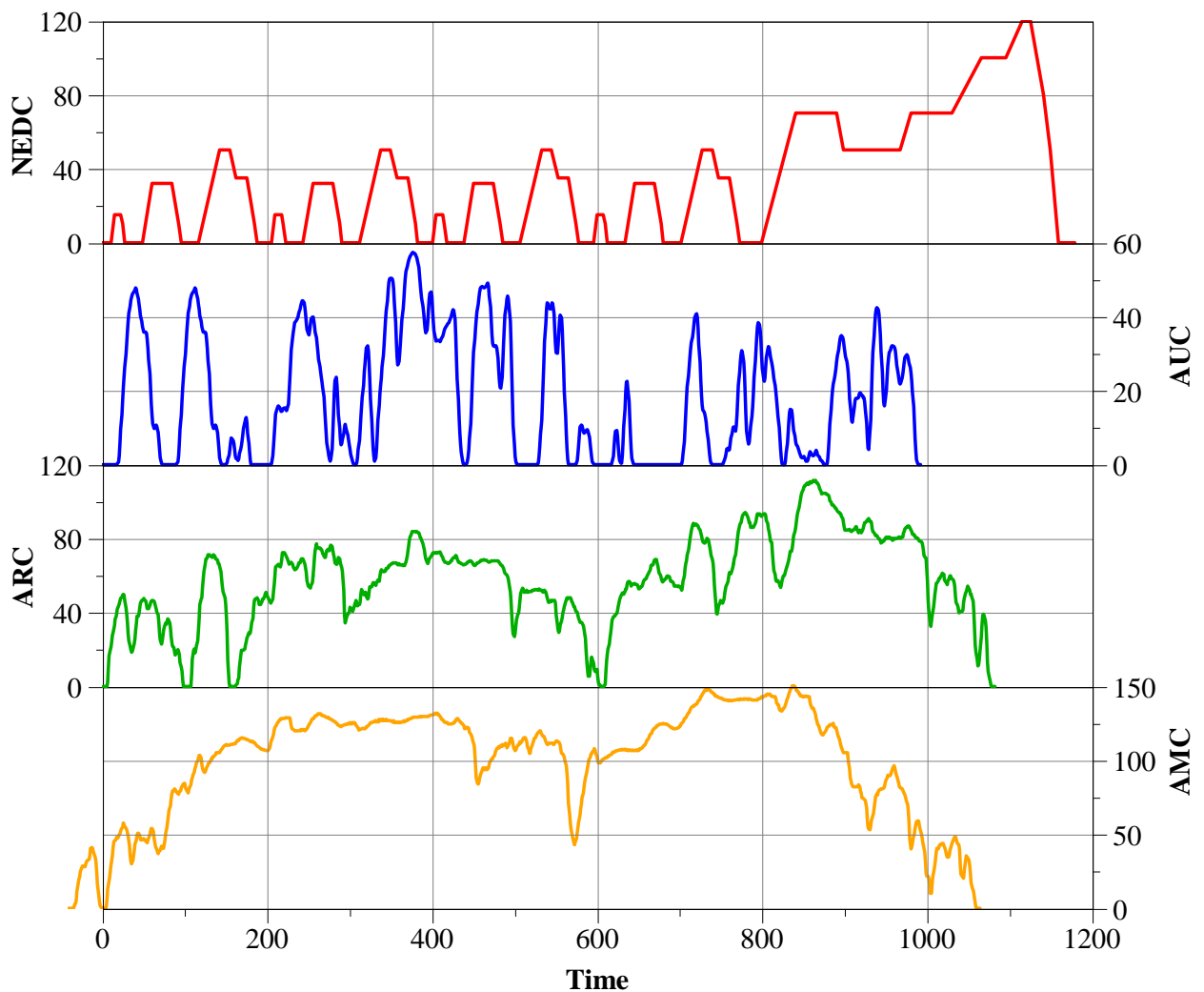
Figure 3.8 – Considered driving cycles

A driving cycle consists of a combination of driving modes including idle, cruise, acceleration and deceleration. Also the maximum, minimum and average speeds are main characteristics of the cycle. Table 3.3 compares the main parameters of the adopted driving cycles.

Table 3.3 - Driving cycle characteristic parameters

	NEDC	AUC	ARC	AMC
Time [s]	1180	993	1082	1068
Distance [km]	11.01	4.87	17.27	29.54
V-max [km/h]	120	57.5	111.1	150.4
V-avg [km/h]	44.1	23.4	58.8	100.7
Acc-max [m/s^2]	1.04	2.33	2	1.72
Acc-avg [m/s^2]	0.56	0.61	0.4	0.31
Dec-max [m/s^2]	-1.39	-2.81	-3.67	-2.92
Dec-avg [m/s^2]	-0.76	-0.65	-0.42	-0.39
Idle time [%]	23.8	24.4	2.3	1.1

For instance, the noteworthy difference in the idle time share and the average speed between the Artemis Urban Cycle (respectively 24.4 % and 23.4 km/h) and the Artemis Motorway Cycle (respectively 1.1 % and 100.7 km/h) will have a major impact on the hybridization outcomes.

3.2 Implementation of the Hybrid Operating Strategy

The control logic of the hybrid electric powertrains, in the framework of the Matlab ([25]) model, is responsible for the definition of the following main parameters ([23]):

➢ Accelerator Pedal Position (APP)

➢ Brake Pedal Position (BPP)

➢ Clutch Pedal Position (CPP)

➢ gear number and gear shift event

➢ traction power split between ICE and EM in the case of positive traction power

➢ braking power split between brakes and EM in the case of negative traction power

Their main structure is resumed in Fig. 3.9, where it is underlined the difference between the conventional vehicle and dedicated hybrid powertrain information.

CONTROL LOGIC

TRADITIONAL POWERTRAIN				HYBRID POWERTRAIN	
ACCELER. PEDAL POSITION	BRAKE PEDAL POSITION	CLUTCH PEDAL POSITION	GEAR NUMBER or GEAR SHIFT	SPLIT ICE-Battery (pos. traction)	SPLIT Brakes-EM (neg.traction)
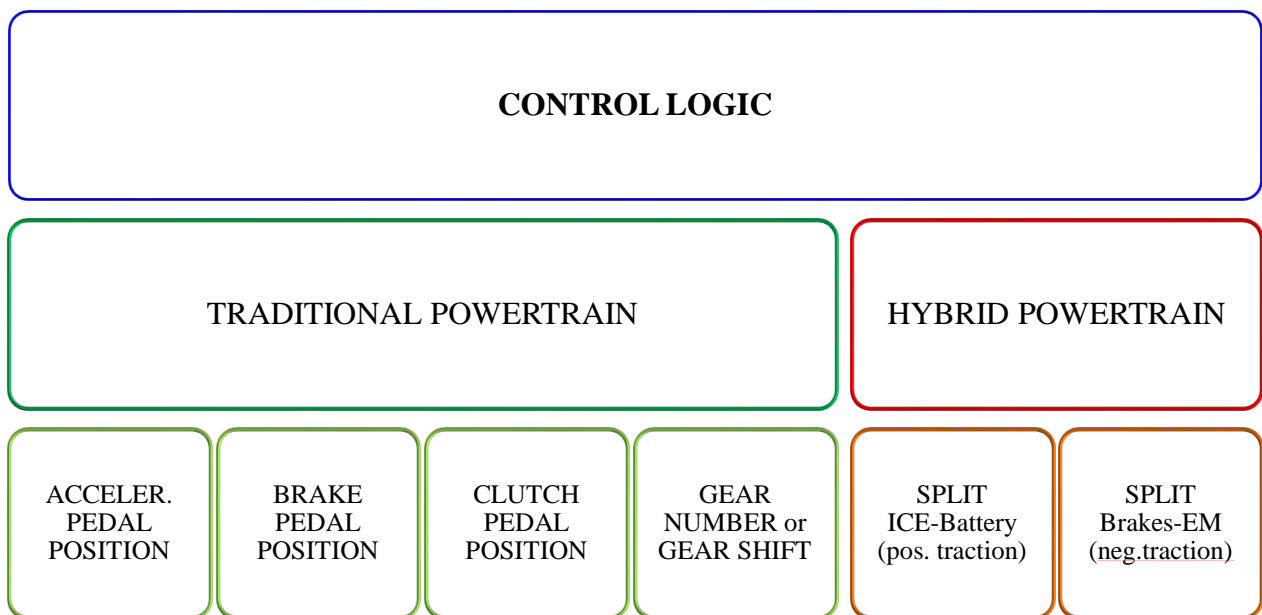
Figure 3.9 – Implemented Control logic

The virtual driver creates a dynamic feedback to any required driving pattern. In particular, the accelerator (APP) and the brake pedal (BPP) positions are defined through a PI (Proportional and Integral) controller as a function of the difference between the target and actual vehicle speeds (Fig. 3.10):

$$[APP, BPP] = c_1 \Delta v_{car} + c_2 \int_0^{t^*} \Delta v_{car} dt \qquad (3.11)$$

where c_1 and c_2 are calibration constants that characterize the readiness of the driver to follow the driving cycles and t^* is the actual simulation time.

Figure 3.10 – Target and actual vehicle speed profiles

Two different modes, depending on the sign of the traction power, are considered:

➤ **negative traction power**: the hybrid powertrain employs regenerative braking by means of a special system that can apply up to 90% of the total power ([11]). The remaining share is guaranteed by the traditional brakes in order to allow a smooth transition in case of safety braking or in case of power limitation of the electric machine

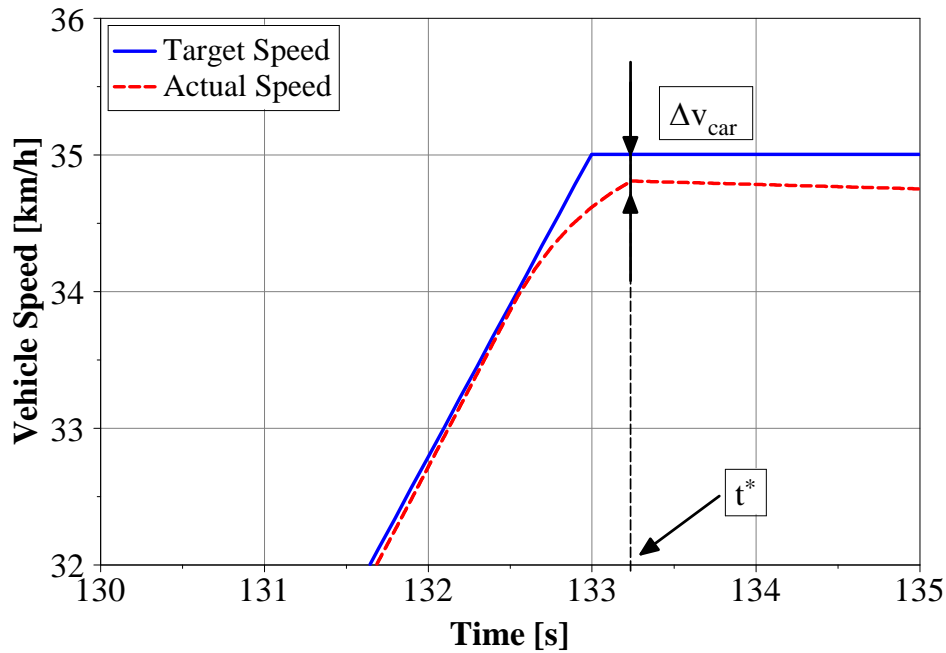➤ **positive traction power:** the hybrid powertrains split the traction power between the available power sources. The purpose of the Hybrid Operating Strategy is to guarantee the best power split

As already mentioned, this study deals with the minimization of the fuel consumption and NO_x emissions (for the only CI engine), by selecting the optimal operating strategy. In particular:

➤ **Parallel Hybrid Electric Vehicle:** the electric machine and the engine have to guarantee the required mechanical traction power, their speed is determined by the speed profile and the gear shift strategy. The EM power profile is set as variable, while the ICE operation derives from the following power balance equation:

$$P_{ICE}=P_{req,cs}-P_{EM}+(I_{ICE} + I_{EM})\omega_{ICE}\dot\omega_{ICE} \tag{3.12}$$

where $P_{req,shaft}$ is the required traction power at the crankshaft.

➤ **Series Hybrid Electric Vehicle:** the battery and generator (EM2 in Fig. 3.1) have to guarantee the required electric power, the speed of the engine is independent on the driving pattern (electric transmission). It results a double degree of freedom (power and the speed)

in the engine operation. As assumption, it is considered the system ICE+EM2 to work along its Optimal Operating Points (OOPs), according to the following equation:

$$P_{EM2,el} = \varepsilon_{EM2}(P_{ICE} - (I_{ICE} + I_{EM2})\omega_{ICE}\dot{\omega}_{ICE}) \tag{3.13}$$

where ε_{EM2} is the total efficiency of the generator.

The OOPs are function of the operating strategy target, i.e. the minimization of the fuel consumption (Eq. 3.14a) or the minimization of the NO_x emissions (Eq. 3.14b):

$$MIN\ (M_{fuel})\ \implies\ P_{ICE}(\omega_{ICE}, \dot{\omega}_{ICE}, \theta_{ICE}) = P_{ICE}(\omega_{ICE}{}^*, \dot{\omega}_{ICE}{}^*, \theta_{ICE}{}^*) : \left.\frac{P_{EM2,el}}{\dot{m}_{fuel}}\right|_{max} \tag{3.14a}$$

$$MIN\ (M_{NOx})\ \implies\ P_{ICE}(\omega_{ICE}, \dot{\omega}_{ICE}, \theta_{ICE}) = P_{ICE}(\omega_{ICE}{}^*, \dot{\omega}_{ICE}{}^*, \theta_{ICE}{}^*) : \left.\frac{P_{EM3,el}}{\dot{m}_{NOx}}\right|_{max} \tag{3.14b}$$

The resulting OOPs (Fig. 3.11) are function of the engine speeds, engine acceleration and engine equivalent temperature (that influences the BSFC and $BSNO_x$).
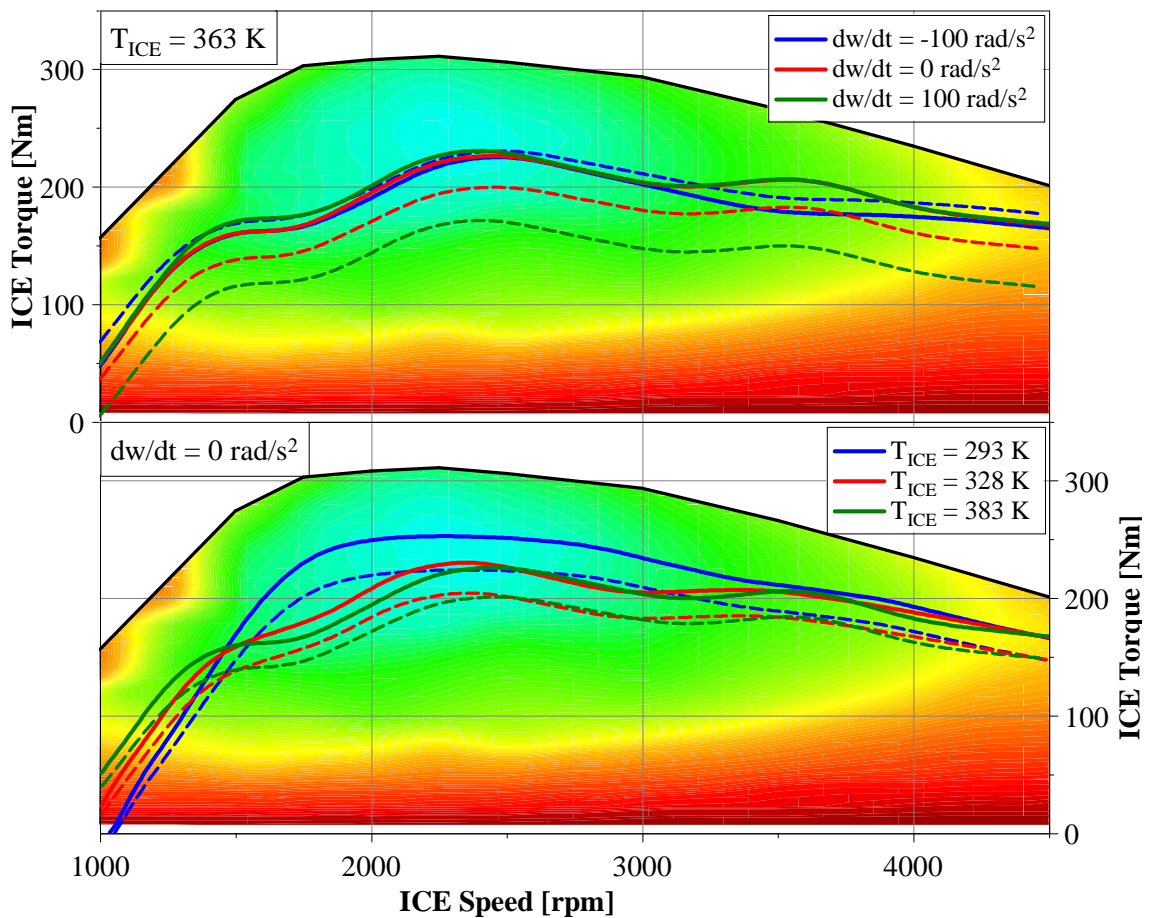

Figure 3.11 – SHEV Optimum Operating Line at constant engine temperature and acceleration. P_{ICE}: solid line; $P_{EM2,el}$: dashed line

The ICE speed is set as variable in the optimization procedure, whereas the generator electric power ($P_{EM2,el}$) and the engine brake power result respectively from the above mentioned OOP maps and Eq. 3.13. The battery electric power is calculated from the following power balance equation:

$$P_{Batt}=P_{req,el}-P_{EM2,el} \tag{3.15}$$

where $P_{req,el}$ is the electric power required by the traction electric machine (EM1).

It is interesting to notice that, the operation of SHEVs is very similar to that of PHEVs from a hybrid operating strategy point of view. In parallel hybrid architectures, the electric machine works together with the engine in order to supply the required mechanical traction power (Eq. 3.12). In series hybrid architectures, the generator (motored by the ICE) works together with the battery in order to supply the required electric traction power (Eq. 3.15).

From the operating strategy point of view, PHEV and SHEV could be renamed, respectively, as Mechanical Parallel Hybrid Electric Vehicle and Electrical Parallel Hybrid Electric Vehicle.

SERIES HYBRID ELECTRIC VEHICLES   PARALLEL HYBRID ELECTRIC VEHICLES
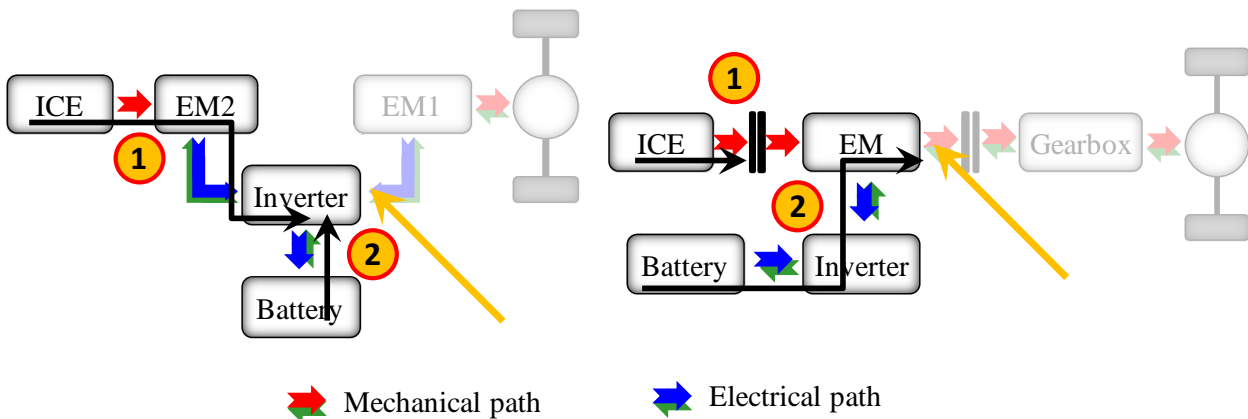
Figure 3.12 - SHEV vs PHEV: components involved in the hybrid optimization and focus on the two energy paths

Figure 3.12 compares the two energy paths of the SHEV and the PHEV. In the case of the series architecture the electric power required by the e-motor (EM2) is supplied by the engine-generator system and/or by the battery. The e-motor represents a fixed ring in the energy chain between the power sources and wheels and, after it, no degree of freedom is available in the optimization of the operating strategy. Therefore, the HOS will take in consideration only the drivetrain component above EM1 (see left diagram in Fig. 3.12).

In the case of the parallel architecture the mechanical power required by the gearbox is supplied by the engine and/or by the battery-inverter-electric machine system. After this component, the energy flow is fixed. Therefore, the optimization of the hybrid strategy consider the only drivetrain component above the gearbox (see right diagram in Fig. 3.12).

As far as the optimization of the Hybrid Operating Strategy is concerned, three different realized were developed in Matlab environment, un novel benchmark and two real-time optimizers ([25]). In particular:

1. novel Benchmark Optimizer (BO): based on Genetic Algorithm methods, it determines the best possible operating strategy for the selected target, driving cycle and powertrain design. The single solution is characterized by a vector of *independent variables*, in which every scalar defines the P_{EM} *for the PHEV or the* w_{ICE} *for the SHEV*, *at each time step* of the selected driving cycle

2. Real-time optimizer 1 – Total Losses Minimization (TLM): based on Genetic Algorithm methods, it *minimizes the total loses of the hybrid drivetrain*. It involves a *vector-approach* (for further details, please refers to Chapter 3.2.2) and requires a reduced number of calibration parameters. It is computationally fast and adequate to work in real-world applications

3. real-time optimizer 1 – Total Load-Switch Thresholds (TLST): based on Genetic Algorithm methods, it *switches the operating mode depending on the load and speed signals*. It involves a *scalar-approach* and requires a reduced number of calibration parameters. It is by far the computationally fastest method here analyzed

3.2.1   Genetic Algorithm based methods

The optimum searching procedure is carried out by applying Genetic Algorithm (GA) based methods. As underlined by Montazeri et al. [(26)], due to HEV properties, gradient-based optimization methods may converge toward one of the several local optima:

"Due to the complex nature of HEV, a control strategy based on the engineering intuition frequently fail to achieve satisfactory overall system efficiency, and therefore an optimization algorithm must be used. […] powertrain system characteristics are highly nonlinear and non-continuous that may have a large number of local optimums."

Genetic algorithm are statistical-based methods able to solve optimization problems whose objective function is non-continuous, non-differentiable, stochastic and highly non-linear ([27]). As shown in Fig. 3.13, this optimization methodology allows the optimal solution to evolve along the entire problem region in order to find the global optimum.

GAs are inspired by the mechanism of natural selection, in which better individuals are likely be the winners in a competing environment. A population of candidate solutions (the so called individuals) encoded by a series of genes are selected to evolve toward the best possible solution. The evolution usually starts from a population of randomly generated individuals. At each generation, the performance of every individual is evaluated by means of a fitness function. Some individuals are then stochastically selected based on their fitness and modified through recombination and random mutation to form the population for the next generation. The optimization algorithm will terminate when either a maximum number of generations has been produced or the best individual (the final solution) has achieved a satisfactory fitness level.
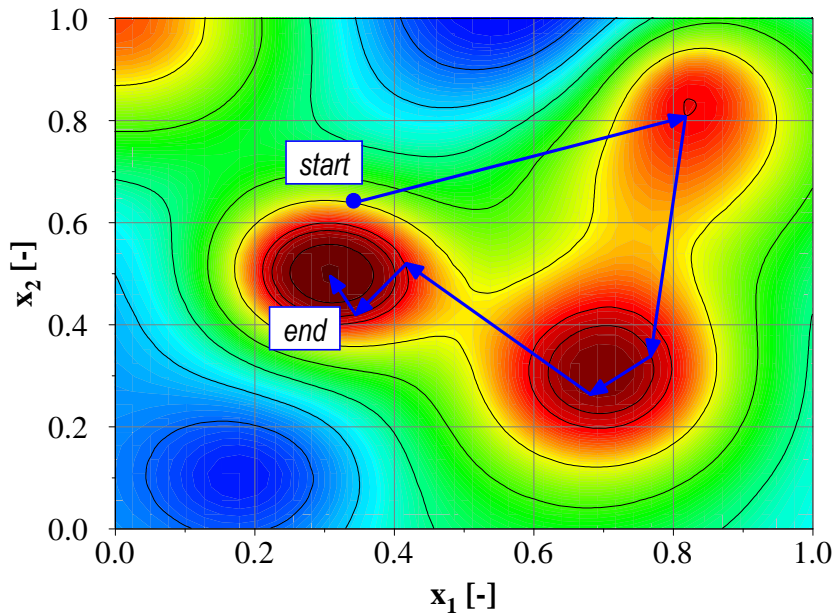
Figure 3.13 – GA method: sample of the global optimum search

The GA procedure can be summarized by the following five main steps ([28, 29]):

1. Initialization: an N-individuals initial population is randomly generated. The population size depends on the nature of the problem, but it typically needs to be at least of the same order of magnitude of the number of variables. Moreover the randomly population should be generated in order to cover the entire range of possible solutions (the so called search space of the optimization procedure)

2. Evaluation: each individual is estimated by means of a fitness function. The evaluation is always problem dependent and is used to measure the quality of each individual

3. Selection: individuals, called parents, are selected deterministically or stochastically. The selection is realized through a fitness-based procedure, during which fitter solutions are more likely to be selected

4. Reproduction: genetic operators (elite individuals, crossover and mutation) are applied to recombine the parents and produce new individuals (the children). These processes ultimately result in the next generation offspring that is different from the previous one and, hopefully, better. The next generation is a combination (Fig. 3.14) of:

> ➢ **elite children**: best individuals that automatically survive without variation

> ➢ **crossover children**: combinations of two (or more) parents

> ➢ **mutation children**: random changes of single parents. The mutation factor initially is high enough to lead the method toward all possible search regions, then it decreases to allow a faster convergence of the population
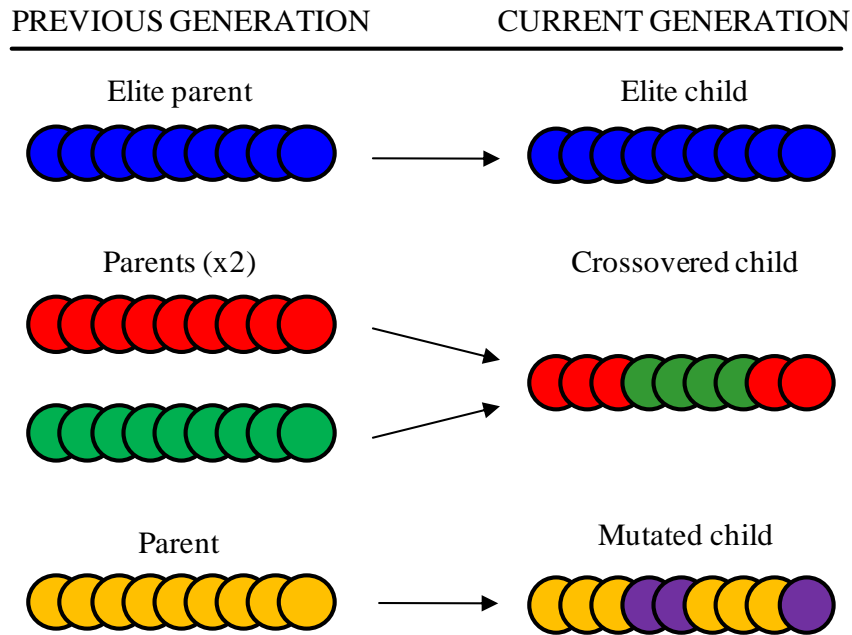
Figure 3.14 – GA method: reproduction methods

5. **Return or Stop:** return to the step 2, unless termination criteria are fulfilled. Termination criteria are based on the improvement of the optimization target (i.e. the reduction of the M_{fuel} or M_{NOx}) from one generation to the following one

GA methods are directly applicable to unconstrained optimization processes; in case of constrained problems the restrictions are introduced through penalty functions that penalize the infeasible solutions by reducing their effective fitness [(30)]. The fitness function J, adopted to address the desired optimization target (FC: $w_1=1$, $w_2=0$ or NO_x $w_1=0$, $w_2=1$), is defined as follows:

$$J(P_{mgu}) = w_1 M_{fuel} + w_2 M_{NOx} + w_3 \Delta SOC + w_4 \Delta E_{req} \tag{3.16}$$

where the global variation of the battery State Of Charge and the difference between the total energy required to drive the vehicle compared to what the powertrain actually supplies are taken into consideration.

3.2.2 Benchmark Optimizer

It defines the best possible operating strategy for the selected target, driving cycle and powertrain design. In order not to take into consideration any restriction to the operating strategy but only the technological ones, the single individual genes encode the considered independent variable at each time step of the driving pattern ([31]).

In the case of the **Parallel Hybrid Electric Vehicle**:

> *the individual determines the EM brake power time history*
> *the single gene is the EM brake power for a given time step*

In the case of the **Series Hybrid Electric Vehicle**:

the individual represents the ICE speed time history
the single gene is the ICE speed for a given time step
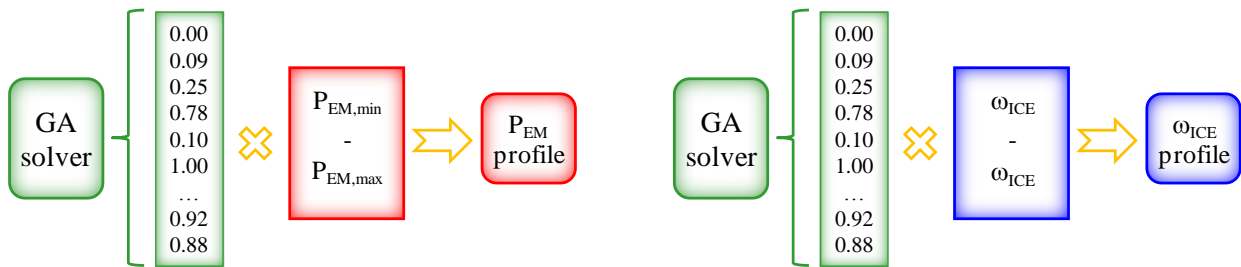
Figure 3.15 – Benchmark Optimizer: basic structure

The size of the calculation matrix (Fig. 3.16) is a critical factor in the modeling procedure: it highly influences both the calculation time and the RAM memory required by the Matlab code. On the other hand, a minimum number of time steps (M-variables) and individuals (N-individuals) is required in order to guarantee respectively the time-independence of the solution and the genetic diversity of the population.
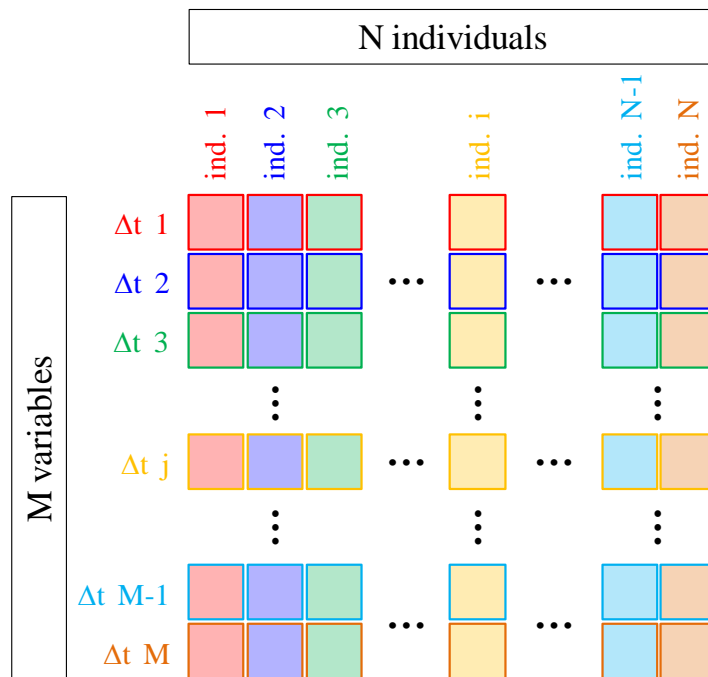
Figure 3.16 – GA method: structure of the benchmark optimization procedure matrix

A time-independence analysis of the objective function was carried out. The appropriate number of variables was chosen for all the driving cycles in order to guarantee an unvaried amount of total fuel consumption, NO_x emissions and final SOC (Fig. 3.17). The population size was then

selected in a way to guarantee the individual diversity (the most important factor that affects GA performance) ([31]).
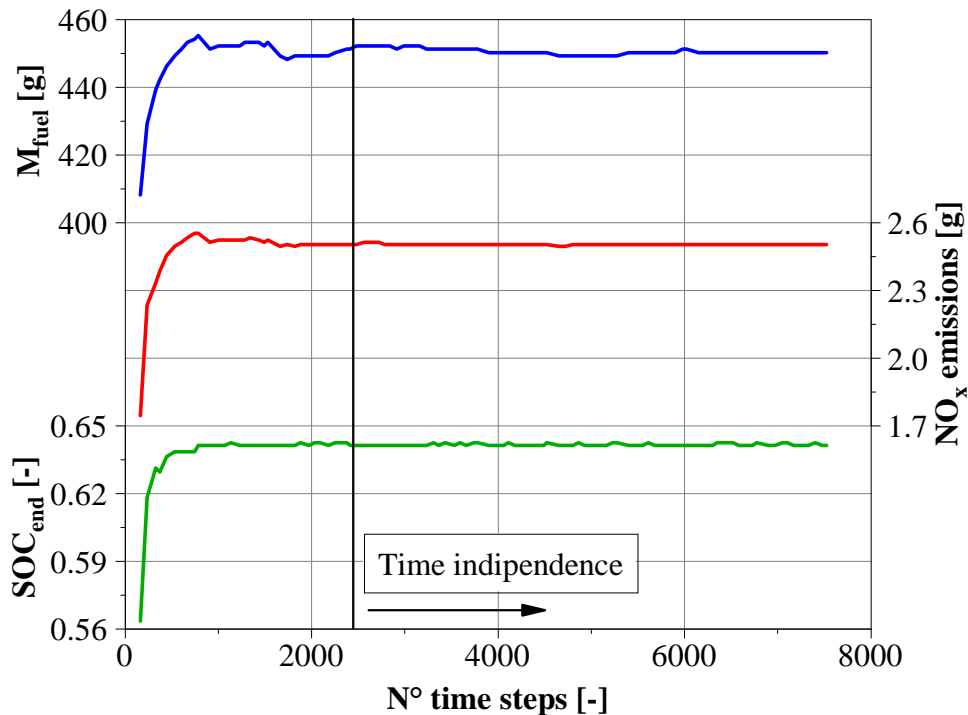
Figure 3.17 – GA method: time-independence analysis for NEDC

The main shortcoming of this approach is the huge size (NxM) of the population genomes, which leads to a highly time-consuming calculations (up to 5-7 days for a single NEDC optimization). However, the approach allows the solver to stochastically find the global optimum without any fictitious penalties or restrictions, apart from the technological limits. This novel approach can be applied to establish whenever a target has to be achieved globally along the driving cycle, i.e. for the total fuel consumption and NO$_x$ emissions. However, when a quantity has to be "locally" optimized (i.e., optimized with respect to a specific time or operating mode), this approach is not suitable. This is the case of the combustion noise optimization analyzed in the proposed case study, for which a different optimization criteria has been applied (for further details, please refer to Chapter 4.3).

3.2.3 Real-time optimizer 1 – Total Losses Minimization (TLM)

The first proposed real-time optimizer is based on the minimization of the total drivetrain losses (P$_{tot,l}$). *At each time step, it chooses the power level of the electric machine* (in the PHEV, Eq. 3.11) *or the engine speed* (in the SHEV, Eq. 3.12) *that minimize the total system losses*. As example, the engine and the electric line losses of the PHEV are minimized in Fig. 3.18 (first two terms in Eq. 3.17a) ([23, 31, 32]). In particular, the left diagram show the trend of the ICE and (EM & Battery) losses with respect to the electric motor power and engine brake power (in stationary conditions).

These losses are summed together to obtain the total system losses. The algorithm will search the minimum of this profile and will let the system to work on this (optimal) operating point. Moreover, in order to achieved the desired final battery SOC, a calibration of the multiplication coefficient has to be addressed (right diagrams in Fig. 3.18).
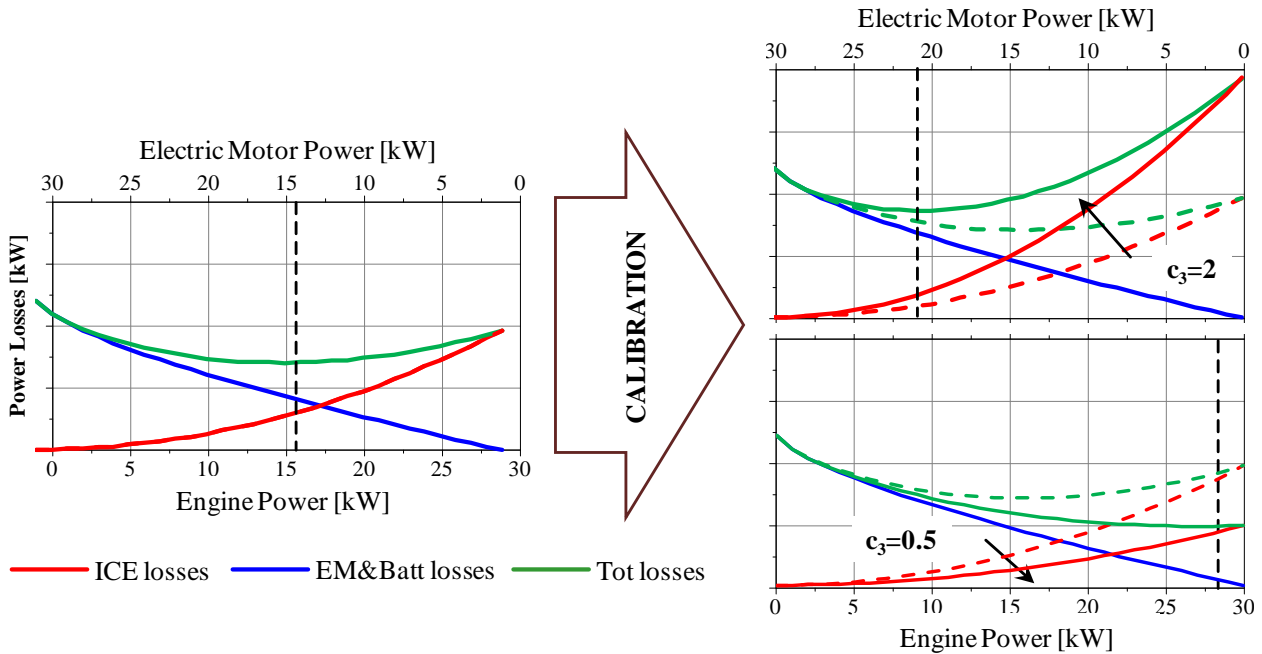
Figure 3.18 – Total Losses Minimization: example of the overall structure

In order to find the minimum of the system losses, the following equations are considered:

PHEV: $P_{tot,l}=c_1 \cdot P_{ICE,l}+c_2 \cdot P_{T(ICE),l}+c_3 \cdot P_{EM\&Batt,l}+c_4 \cdot P_{SOC,l}+c_5 \cdot P_{NOx,l}$ (3.17a)

SHEV: $P_{tot,l}=c_1 \cdot P_{ICE\&EM2,l}+c_2 \cdot P_{T(ICE),l}+c_3 \cdot P_{Batt,l}+c_4 \cdot P_{SOC,l}+c_5 \cdot P_{NOx\&EM2,l}$ (3.17b)

Genetic Algorithm based methods are applied as search algorithm to find the best set of the c_1 - c_6 tuning parameters. Their values are constant for any defined mission profile (NEDC, Artemis Urban Cycles,…).

Parallel Hybrid Electric Vehicle

$P_{ICE,l}$ in Eq. 3.17a characterizes the internal combustion engine energy losses. Two different approaches are proposed:

➤ **Total ICE losses $P_{ICE,tot,l}$:** the difference between the fuel chemical energy per unit time and the brake output power

$P_{ICE,tot,l}=Q_{HV} \cdot \dot{m}_{fuel}-P_{ICE}=(1-\varepsilon_{ICE}) \cdot \dot{m}_{fuel} \cdot Q_{HV}$ (3.18a)

> ➢ **Recoverable ICE losses $P_{ICE,rec,l}$:** the power losses with respect to the optimal condition for the considered engine speed. They do not consider the unavoidable ICE losses, i.e. the rate of fuel heat energy loss that occurs assuming the engine operation at the peak efficiency for the given speed:

$$P_{ICE,rec,l}=[\varepsilon_{ICE,max}(\omega_{ICE})\text{-}\varepsilon_{ICE}]\cdot\dot{m}_{fuel}\cdot Q_{HV}=\frac{\dot{m}_{fuel}}{BSFC_{min}(\omega_{ICE})}-P_{ICE} \tag{3.18b}$$

Fig. 3.19 shows the $P_{ICE,rec,l}$ and $P_{ICE,tot,l}$ profiles as a function of the brake power at 1500 rpm for the CI engine and at 2000 rpm for the SI engine.
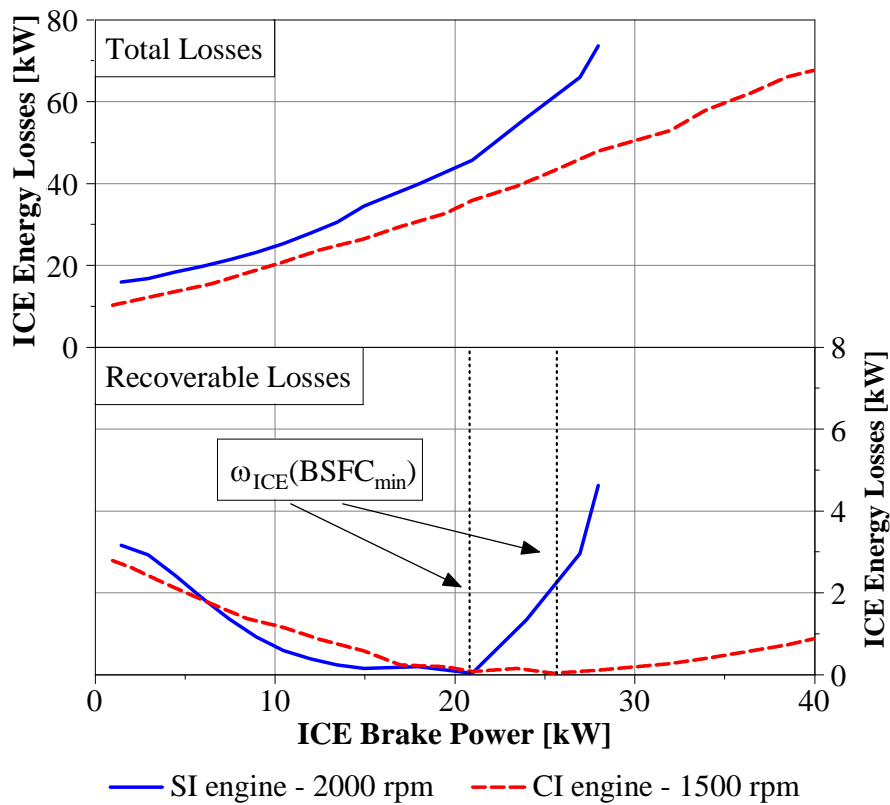
Figure 3.19 - recoverable and total engine energy losses

Total ICE energy losses decrease as P_{ICE} decreases, whereas the recoverable share is zero for the optimal ICE operation and increases as the engine brake power moves away from the optimal power level. $P_{ICE,rec,l}$ makes the engine to work (more intensively) on its maximum efficiency point trough a load point shift strategy operated by the electric machine.

$P_{EM\&Batt,l}$ characterizes the electric machine, inverter and battery energy losses. In motor mode it is the difference between the electro-chemical power of the battery and the mechanical power of the electric machine; vice versa, in generator mode:

Motor: $\quad P_{EM\&Batt,l}=P_{Batt,chem}\text{-}P_{EM}=i\cdot V_{OC}\text{-}P_{EM}$ \hfill (3.19a)

Generator: $P_{EM\&Batt,l}=P_{EM}-P_{Batt,chem}=P_{EM}-i\cdot V_{OC}$ (3.19b)

$P_{l,T,ICE}$ represents the ICE thermal losses. This term takes into consideration that the ICE warm-up is slowed down if part of the traction power is supplied by the electric machine, and friction losses are increased until the engine reaches fully warmed operation conditions. It is calculated based on the semi-empirical formulation used for the calculation of the ICE equivalent temperature ([18]):

$$P_{T(ICE),l}=\left(\frac{\theta_{ICE,warm}-\theta_{ICE}}{\theta_{ICE,warm}-\theta_{ICE,cold}}\right)^{2}\cdot P_{Batt}$$ (3.20)

$P_{SOC,l}$ controls the State of Charge of the battery. As in the case of the engine equivalent temperature, the SOC is responsible for cross-effects on the total fuel consumption of the NO_x emissions: changing the battery energy content at a certain time will influence the voltage of the electric system during the remaining time history. $P_{SOC,l}$ introduces fictitious losses that are proportional to the deviation of the battery SOC with respect to the target (SOC_{start} in case of not plug-in HEVs, SOC_{min} in case of plug-in HEVs):

$$P_{SOC,l}=C_{SOC,l}\cdot\left(P_{Batt}-P_{Batt,shift}\right)$$ (3.21)
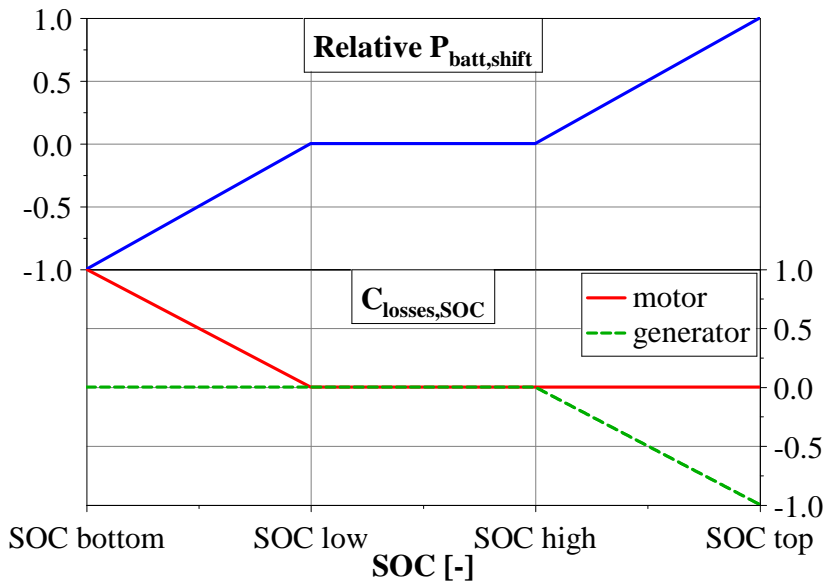
Figure 3.20 – State Of Charge Losses

The $C_{SOC,l}$ and $P_{batt,shift}$ depend on the SOC (Fig. 3.20). Both the values of the SOC at the bottom, low, high and top levels and the corresponding $P_{batt,shift}$ and $C_{SOC,l}$ are tuned according to the vehicle mission.

The last term, **$P_{NOx,l}$**, is responsible for the minimization of the NO_x emissions (in the case of the only CI engine). In order to be properly assessed, a calibration constant that within this study

will be called, *equivalent NO$_x$ heating value Q$_{NOx}$*, has been introduced. It correlates the mass flow rate of the NO$_x$ emissions to the engine brake power (equivalent to the Q$_{HV}$ for the fuel mass flow rate). It is not a intrinsic property of the fuel, but it depends on the BSNO$_x$ map and engine operating points during the considered driving cycle. It is *set as calibration constant* in the optimization procedure together with the parameters c_1 to c_6. P$_{NOx,l}$, similarly to P$_{ICE,l}$, are defined in two different ways:

> **Total NO$_x$ losses P$_{NOx,tot,l}$:** the difference between the NO$_x$ equivalent input power ($P_{NOx} = \dot{m}_{NOx} \cdot Q_{NOx}$) and the engine brake power:

$$P_{NOx,tot,l} = Q_{NOx} \cdot \dot{m}_{NOx} - P_{ICE} = (1-\varepsilon_{NOx}) \cdot \dot{m}_{NOx} \cdot Q_{NOx} \tag{3.22a}$$

where $\varepsilon_{NOx} = \dfrac{P_{ICE}}{P_{NOx}} = \dfrac{P_{ICE}}{\dot{m}_{NOx} \cdot Q_{NOx}}$, represents the equivalent efficiency of the engine considering as input the NO$_x$ equivalent power ($P_{NOx} = \dot{m}_{NOx} \cdot Q_{NOx}$)

> **Recoverable NO$_x$ losses P$_{NOx,rec,l}$:** the NO$_x$ equivalent losses with respect to the optimal condition for the considered engine speed. They neglect the unavoidable NO$_x$ losses, i.e. the rate of equivalent NO$_x$ losses that occurs assuming the engine operation at the minimum BSNO$_x$ for the given speed:

$$P_{NOx,rec,l} = [\varepsilon_{NOx,max}(\omega_{ICE}) - \varepsilon_{NOx}] \cdot \dot{m}_{NOx} \cdot Q_{NOx} = \frac{\dot{m}_{NOx}}{BSNOx_{min}(\omega_{ICE})} - P_{ICE} \tag{3.22b}$$

where ε_{NOx} represents the equivalent engine efficiency, considering as input the NO$_x$ equivalent power ($P_{NOx} = \dot{m}_{NOx} \cdot Q_{NOx}$) and $\varepsilon_{NOx,max}(\omega_{ICE})$ is the maximum ε_{NOx} for the given ICE speed.
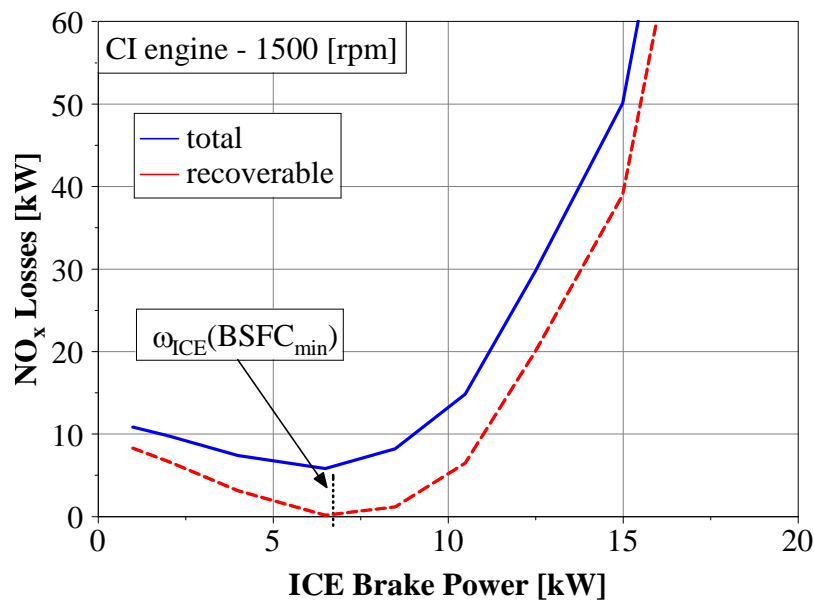

Figure 3.21 - recoverable and total NO$_x$ equivalent losses (ω_{ICE}=1500 rpm)

Figure 3.21 shows the $P_{NOx,rec,l}$ and $P_{NOx,tot,l}$ patterns as a function of the ICE brake power at 1500 rpm of the CI engine.

Series Hybrid Electric Vehicle

$P_{ICE\&EM2,l}$ in Eq. 3.17b expresses the energy losses of the system: ICE, EM2 and Inverter. Two different approaches are proposed:

> **Total ICE&EM2 losses $P_{ICE\&EM,tot,l}$:** the difference between the fuel chemical energy per unit time and the electric output power at the net of any variation of the (ICE+EM2) inertia:

$$P_{ICE\&EM2,tot,l} = Q_{HV} \cdot \dot{m}_{fuel} - P_{EM2,el} - (I_{ICE} + I_{EM2}) \cdot \omega_{ICE} \cdot \dot{\omega}_{ICE} =$$

$$\left(1 - \varepsilon_{ICE\&EM2}\right) \cdot \dot{m}_{fuel} \cdot Q_{HV} - (I_{ICE} + I_{EM2}) \cdot \omega_{ICE} \cdot \dot{\omega}_{ICE} \qquad (3.23a)$$

where $\varepsilon_{ICE\&EM2}$ stands for the total efficiency of the (ICE, EM2 and Inverter) system and I_{ICE}, I_{EM2} represent the inertia of respectively engine and generator. The last term of Eq. 3.23a is a main difference with respect to the PHEV operating strategy. It characterizes the possibility of the series mode of varying the ICE speed independently on the driving conditions, considering as positive effect the increase of the traction system speed. The resulting energy accumulated as inertia will be available in future instants during decelerating phases.

> **Recoverable ICE losses $P_{ICE\&EM2,rec,l}$:** the power losses with respect to the optimal condition. They do not consider the unavoidable ICE&EM2 losses, i.e. the rate of energy loss that occurs assuming the (ICE, EM2 and Inverter) system at the peak efficiency of the whole operating map:

$$P_{ICE,rec,l} = \left[\varepsilon_{ICE\&EM2,max} - \varepsilon_{ICE\&EM2}\right] \cdot \dot{m}_{fuel} \cdot Q_{HV} - (I_{ICE} + I_{EM2}) \cdot \omega_{ICE} \cdot \dot{\omega}_{ICE}$$

$$= \varepsilon_{ICE\&EM2,max} \cdot \dot{m}_{fuel} \cdot Q_{HV} - P_{EM2,el} - (I_{ICE} + I_{EM2}) \cdot \omega_{ICE} \cdot \dot{\omega}_{ICE} \qquad (3.23b)$$

$P_{Batt,l}$ characterizes the battery energy losses. In motor mode it is the difference between the electro-chemical power and the electric machine of the battery. Vice versa, in generator mode.

Motor: $P_{Batt,l} = P_{batt,chem} - P_{Batt} = i \cdot (V_{OC} - V_{EM})$ $\qquad\qquad\qquad$ (3.24a)

Generator: $P_{Batt,l} = P_{Batt} - P_{batt,chem} = i \cdot (V_{EM} - V_{OC})$ $\qquad\qquad\qquad$ (3.24b)

$P_{I,T,ICE}$ and $P_{SOC,l}$ have the same formulation as in the case of the Parallel Hybrid Electric Mode (please refer respectively to Eq. 3.20 and to Eq. 3.21).

The last term, $P_{NOx\&EM2,l}$, is responsible for the minimization of the NO_x emissions (in the case of the only CI engine). Similarly to $P_{ICE\&EM2,l}$, it is defined in two different ways:

> **Total NO$_x$&EM2 losses P$_{NOx\&EM2,tot,l}$:** the difference between the NO$_x$ equivalent power and the electric output power of the generator inverter at the net of any variation of the ICE+EM2 inertia:

$$P_{NOx\&EM2,tot,l} = Q_{NOx} \cdot \dot{m}_{NOx} - P_{EM2,el} - P_{Inertia} =$$

$$= \left(1 - \varepsilon_{NOx\&EM2}\right) \cdot \dot{m}_{NOx} \cdot Q_{NOx} - \left(I_{ICE} + I_{EM2}\right) \cdot \omega_{ICE} \cdot \dot{\omega}_{ICE} \qquad (3.25a)$$

where $\varepsilon_{NOx\&EM2}$ represents the equivalent efficiency of the (ICE, EM2 and Inverter) system considering as input the NO$_x$ equivalent power: $P_{NOx} = \dot{m}_{NOx} \cdot Q_{NOx}$.

> **Recoverable NO$_x$&EM2 losses P$_{NOx,rec,l}$:** the NO$_x$ equivalent losses with respect to the optimal condition. They do not consider the unavoidable NO$_x$&EM2 losses, i.e. the rate of equivalent NO$_x$ losses that occurs assuming the (ICE, EM2 and Inverter) system at the minimum BSNO$_x$ of the whole operating map:

$$P_{NOx\&EM2,rec,l} = \left[\varepsilon_{NOx\&EM2,max} - \varepsilon_{NOx\&EM2}\right] \cdot \dot{m}_{NOx} \cdot Q_{NOx} - P_{Inertia}$$

$$= \varepsilon_{NOx\&EM2,max} \cdot \dot{m}_{NOx} \cdot Q_{NOx} - P_{EM2,el} - \left(I_{ICE} + I_{EM2}\right) \cdot \omega_{ICE} \cdot \dot{\omega}_{ICE} \qquad (3.25b)$$

where $\varepsilon_{NOx\&EM2,max}$ is the maximum ε_{NOx} of the whole operating map.

3.2.4   Real-time optimizer 2 – Total Load-Switch Thresholds (TLST)

The second real-time optimizer is based on the total load-switch thresholds. At each time step, it defines the brake power of the Internal Combustion Engine based on thresholds equations with tuning parameters to be optimized depending on the mission target. It employs a scalar-approach that allows an extremely reduced computational time and is based on the considerations of Balazs et al. in ([11]).

Parallel Hybrid Electric Vehicle

For the optimization of the PHEV control strategy, two equations with two tuning parameters (c_1 and c_2) are adopted.

Only electric mode is active for low required traction powers. Parameter **c_1** defines the maximum power up to which electric driving is active (Fig. 3.22): if the required traction power ($P_{req,cs}$) is lower than c_1, the vehicle will be driven electrically, otherwise the combustion engine is switched-on. If c_1 is set to 0 kW, electric driving is not allowed at all.

If $P_{req,cs} < c_1$:

$$P_{EM} = P_{req,cs}; \qquad P_{ICE} = 0 \qquad (3.26)$$

Figure 3.22 - Total load-switch thresholds HOS: pure electric mode

Hybrid parallel mode is active for intermediate and high required traction powers. Calibration parameter c_2 defines the engine Load Point Shift (LPS) on the basis of the difference between the target SOC and the actual SOC (Fig. 3.23).
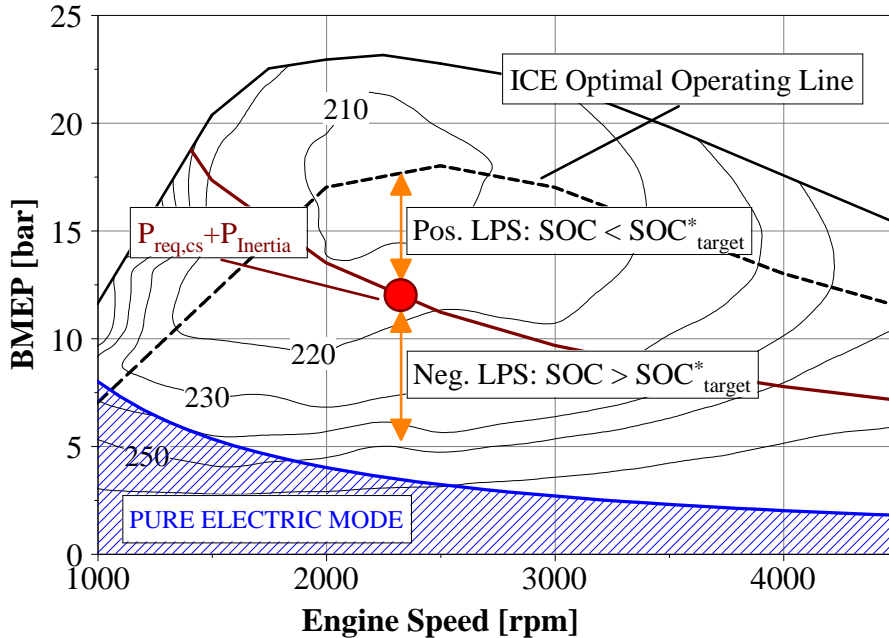
Figure 3.23 - Total load-switch thresholds HOS: parallel mode

Parameter c_2 is then introduced in the model taking into consideration the kinetic energy recoverable through regenerative braking (the total regenerative braking efficiency is assumed $\varepsilon_{reg,br}=60\%$):

$$P_{ICE} = P_{req,cs} + (I_{ICE} + I_{EM})\omega_{ICE}\dot{\omega}_{ICE} - c_2 \cdot (SOC - SOC^*_{target}) \tag{3.27}$$

$$\text{with: } SOC^*_{target} = \frac{E_{Batt}SOC_{Target} - \varepsilon_{reg,br}{}^1\!/_2 M_{car}v_{car}^2}{E_{Batt}} \tag{3.28}$$

If c_2 is set to 0, the SOC does not influence the hybrid operating strategy, whereas large values of c_2 result in a high ICE load point shift. In case of ICE positive load point shift (SOC<SOC^*_{Target}), the increase in the ICE brake power is limited to its optimal operating line.

Series Hybrid Electric Vehicle

For the optimization of the SHEV control strategy two equations with two tuning parameters (c_1 and c_3) are adopted.

Only electric mode: as in the case of the PHEV, **c_1** defines the maximum power up to which electric driving is active (see Fig. 3.22):

If $P_{req,el} < c_1$:

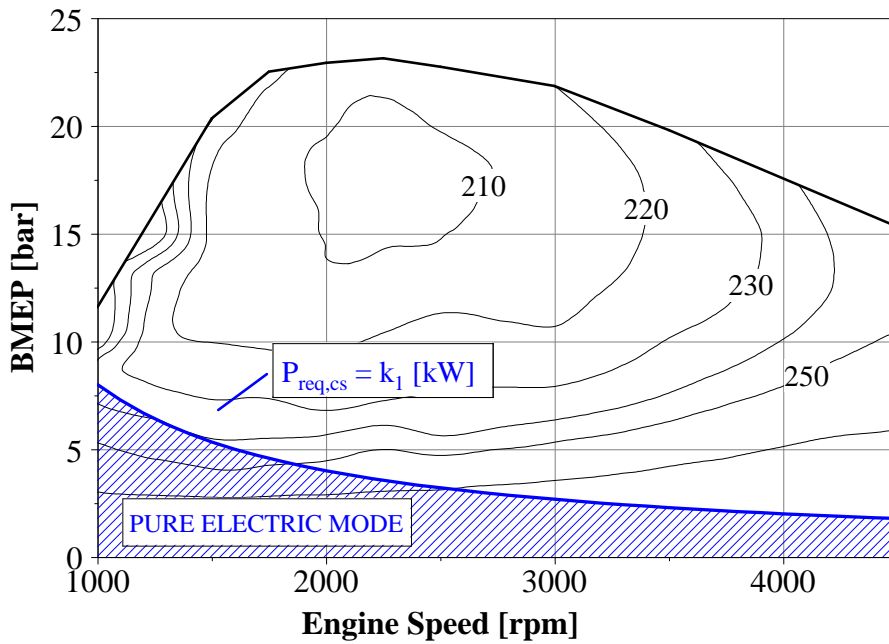$$P_{Batt} = P_{req,el}; \qquad P_{gen,el} = 0 \tag{3.29}$$
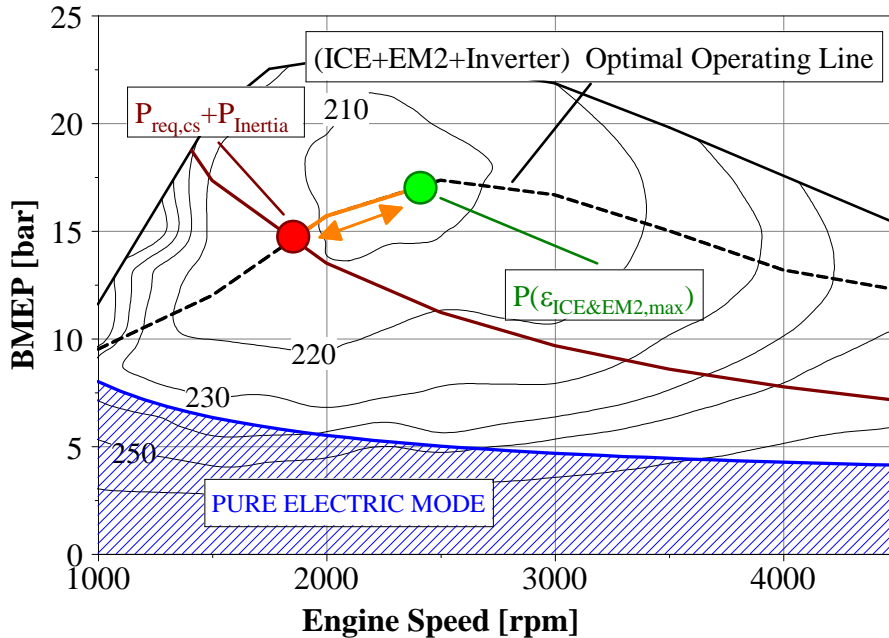
Figure 3.24 - Total load-switch thresholds HOS: series mode

Hybrid series mode is active for intermediate and high required traction powers. As in the case of the benchmark optimizer and the other real-time optimizer, the ICE is forced to work only on the (ICE+EM) optimal operating points. Calibration parameter c_3 defines the engine Load Point

Shift towards the optimal operating point of the whole operating map, on the basis of following equation:

Target M_{fuel}: $P_{gen,el} = P_{req,el} + c_3 \cdot \left(P\left(\max(\varepsilon_{ICE\&EM2,max}) \right) - P_{req,el} \right)$ (3.30a)

Target M_{NOx}: $P_{gen,el} = P_{req,el} + c_3 \cdot \left(P_{req,el} - P\left(\max(\varepsilon_{NOx\&EM2,max}) \right) - P_{req,el} \right)$ (3.30b)

With $c_3 = 0$ there is no load point shift and the (ICE, EM2 and Inverter) system provides exactly the required electric power, whereas constant $c_2 = 1$ requires the (ICE, EM2 and Inverter) system to operate at its maximum efficiency point. Figure 3.24 shows the corresponding operating points of the engine with respect to Eq. 3.30a, reported on the BSFC map.

4. RESULTS AND DISCUSSION

Before proceeding with the analysis of the results, it should be underlined that the model was assessed in previous project phases ([23, 31, 32]). In particular, both the fuel consumption, NO_x emissions and combustion noise (please refer to Chapter 4.3) were tested along the NEDC for a parallel hybrid application: a Belt Alternator Starter coupled to a middle size Diesel engine. Due to intellectual property reasons, all the results regarding this specific application are expressed in non-dimensional terms, normalized with respect to a reference condition.

Table 4.1- NEDC: total NO_x emissions

Case	Relative Fuel Consumptions	Relative NO_x Emissions
Experimental (hot-start)	100	100
Simulation (cold-start)	101.3 (**+1.3%**)	105.7 (**-5.7%**)
Experimental (cold-start)	110	104.2
Simulation (cold-start)	109.8 (**-0.2%**)	107.7 (**+3.4%**)

The test rig was equipped with:

➢ 'ELIN AVL APA 100' cradle-mounted AC dynamometer, featuring a power of 220 kW, a nominal torque of 525 Nm and a maximum speed of 12000 rpm

➢ 'AVL KMA 4000' system to continuously meter the engine fuel consumption

➢ 'AVL AMAi60' raw exhaust-gas analyzer

➢ AVL PUMA OPEN 1.3.2 automation system in order to control the abovementioned measuring instruments, interfaced to the AVL Indicom software for indicated data acquisition

> ➢ AVL ISAC 400 software for the simulation of the vehicle dynamics and the driver's behavior ([31]).

The adopted methodology takes into account system dynamics by means of a *"quasi-static" modeling approach*: even though the fuel consumptions and pollutant emissions are calculated as a function of the dynamic engine speed and load, each instantaneous condition is based on experimentally-derived hot stationary maps. This approach has been proved to be appropriate in the case of the fuel consumption. As far as the NO_x emissions are concerned, only the cycles characterized by modest speed and load transients, such as the NEDC, are properly analyzed ([33]).
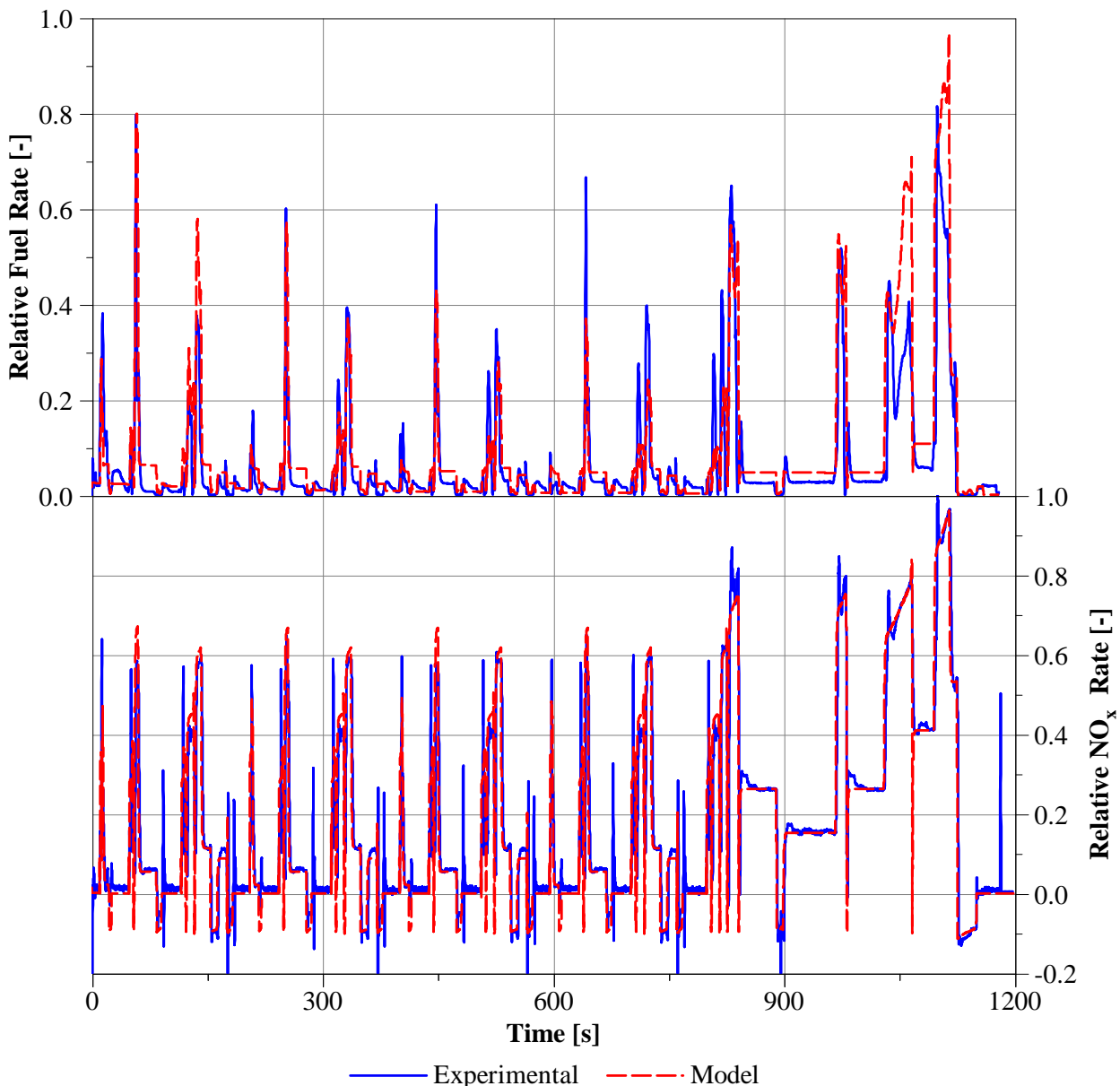
Figure 4.1- Assessment: Relative fuel and NO_x emission rate with cold start ICE (NEDC)

Two test cases, in which the traction power is provided by the engine alone, as in conventional vehicles, have been considered: a cold-start NEDC and a warm-start NEDC.

4. Results and Discussion

The assessment (Tab. 4.1 and Fig. 4.1, for the cold start cycle) shows a good agreement between the experimental and simulated values, with an overall difference of less than 1% in the case of the fuel consumption and 6% in the case of the NO_x emissions (Tab. 4.1).

4.1   Parallel Hybrid Electric Vehicle

In PHEVs, the ICE and EM directly supply the mechanical torque to the wheels, according to the power split determined by the control logic; their speed is function of the vehicle velocity and gear shift strategy. The electric machine power profile is set as variable in the HOS, while the engine operation derives from Eq. 3.12.

Concerning the figures of the "Results and Discussion" chapter, the following abbreviations have been employed:

Baseline: conventional vehicle configuration. The same powertrain of the parallel architecture is considered, excluding the electric components (EM, inverter and battery)

TLM TOT: Total Losses Minimization with Total engine or NO_x losses

TLM REC: Total Losses Minimization with Recoverable engine or NO_x losses

TLST: Total Load Switch Thresholds

BO: Benchmark Optimizer

NPI, PI: Not Plug-In hybrid electric vehicle or Plug-In hybrid electric vehicle

FC, NO$_x$: the minimization of the fuel consumption or the minimization of the NO_x emissions

is the target of the operating strategy

Stop&Start: engine Stop & Start feature

4.1.1   Benchmark Optimizer

As far as the benchmark optimizer is concerned, Fig. 4.2 reports the targets (M_{fuel} or M_{NOx}) as a function of the generation number, for the best (solid blue line) and worst (dashed red line) individuals. As examples, four different cases are shown. The difference in the performance between the best and the worst individuals, shown in Fig. 4.2, is fundamental in GA based methods in order to guarantee the genetic diversity of the population. Moreover, both the convergence rate and the improvement in the total fuel consumption or total NO_x emissions have an arbitrary behavior: they depend on the random generation of the initial individuals and the stochastic evolution of the population.

Regarding the New European Driving Cycle, a total number of 1051 independent variables and a population of 17053 individuals were defined. As an example, in the case of the CI Engine, w/o plug-in feature and optimizing the NO_x emissions along the NEDC (top left diagram in Fig. 4.2), the total number of calculated cycle is:

$$N(Total\ Calculations) = N(individuals) \cdot N(generations) = 17'053 \cdot 4'493 = 76'619'129 \ !!$$

Around 10-100 million complete cycles were required for each benchmark optimization. A remarkable effort was required in order to improve the Matlab script to reach acceptable calculation times. The final release of the model is able of achieving this huge calculation effort (i.e.

N(Total Calculations)≈10E7) in about 4-7 days, with a 64-bit computer, featuring 16 GB of RAM memory and eight 3.2 GHz processors.
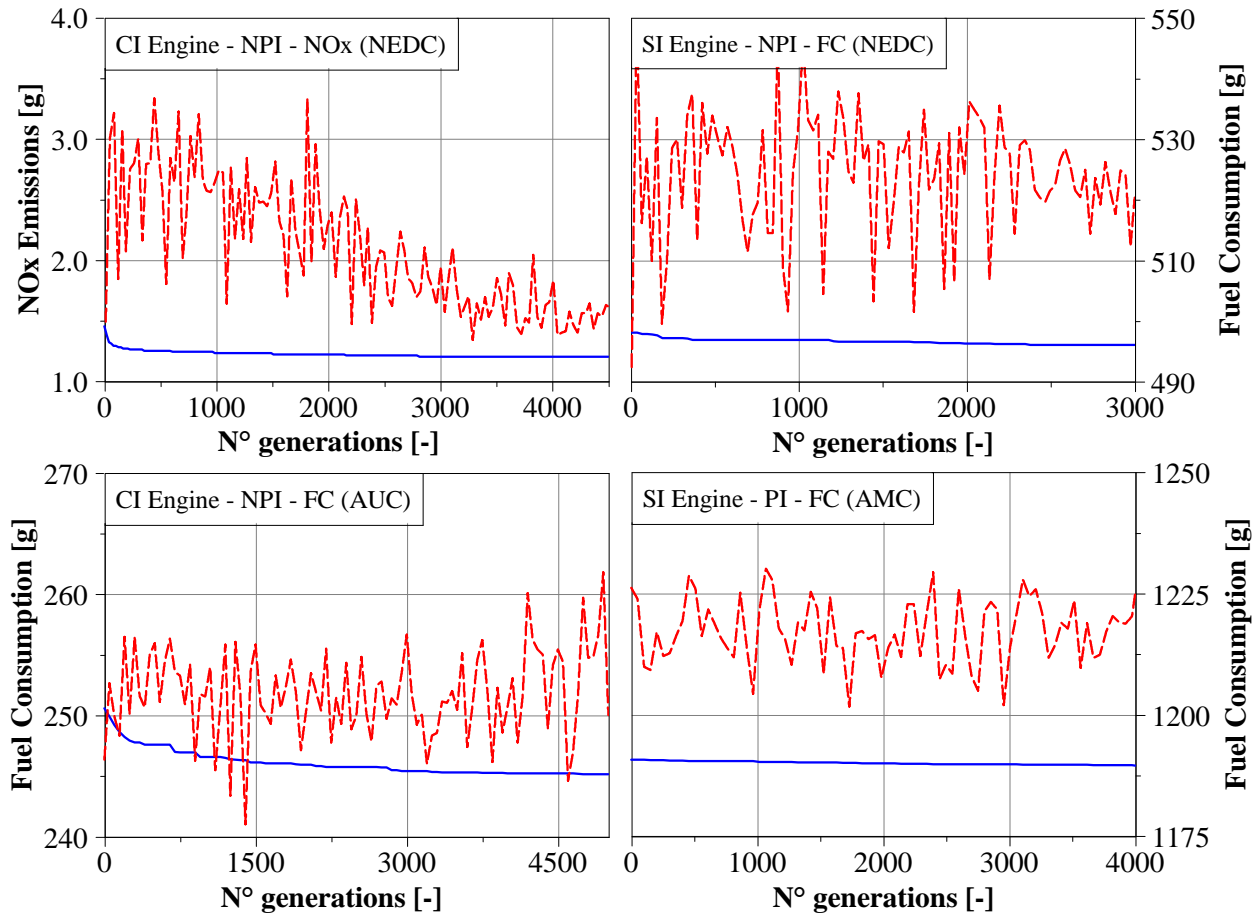
Figure 4.2- PHEV Benchmark Optimizer: fuel consumption or NOₓ emission convergence

Figure 4.3 shows the time histories of the electric machine and engine brake power (respectively blue solid line and dashed red line) and the battery SOC (green dash-dot line) along the NEDC cycle for all the analyzed parallel hybrid vehicles and obtained with the benchmark optimizer.

For both the CI engine and the SI engine NPI, in case of the M_{fuel} target (respectively top left and intermediate left graphs in Fig. 4.3), the EM works as a generator only during deceleration phases (regenerative braking). The only exception is a weak engine positive load point shift for the SI engine during the EUDC. The energy stored in the battery pack is used to run the electric machine in motor mode mainly at low speed and at low/medium load (pure electric mode, with the clutch, between ICE and EM, open), whereas the share of electric assist is negligible during high traction torque phases. In case of the not plug-in CI engine with M_{NOx} as target (bottom left graph in Fig. 4.3), the electric machine works as generator during the speed plateaus, in order to shift the ICE load, towards the minimum brake specific NO_x line (positive load point shift). Regenerative braking and positive LPS are applied to increase the SOC; the energy available in the battery is then used, during the EUDC, to shift the ICE load downwards towards the $BSNO_{x,min}$ line. As in the previous cases, a zero net usage of the battery is guaranteed (i.e. $SOC_{end}=SOC_{start}$).
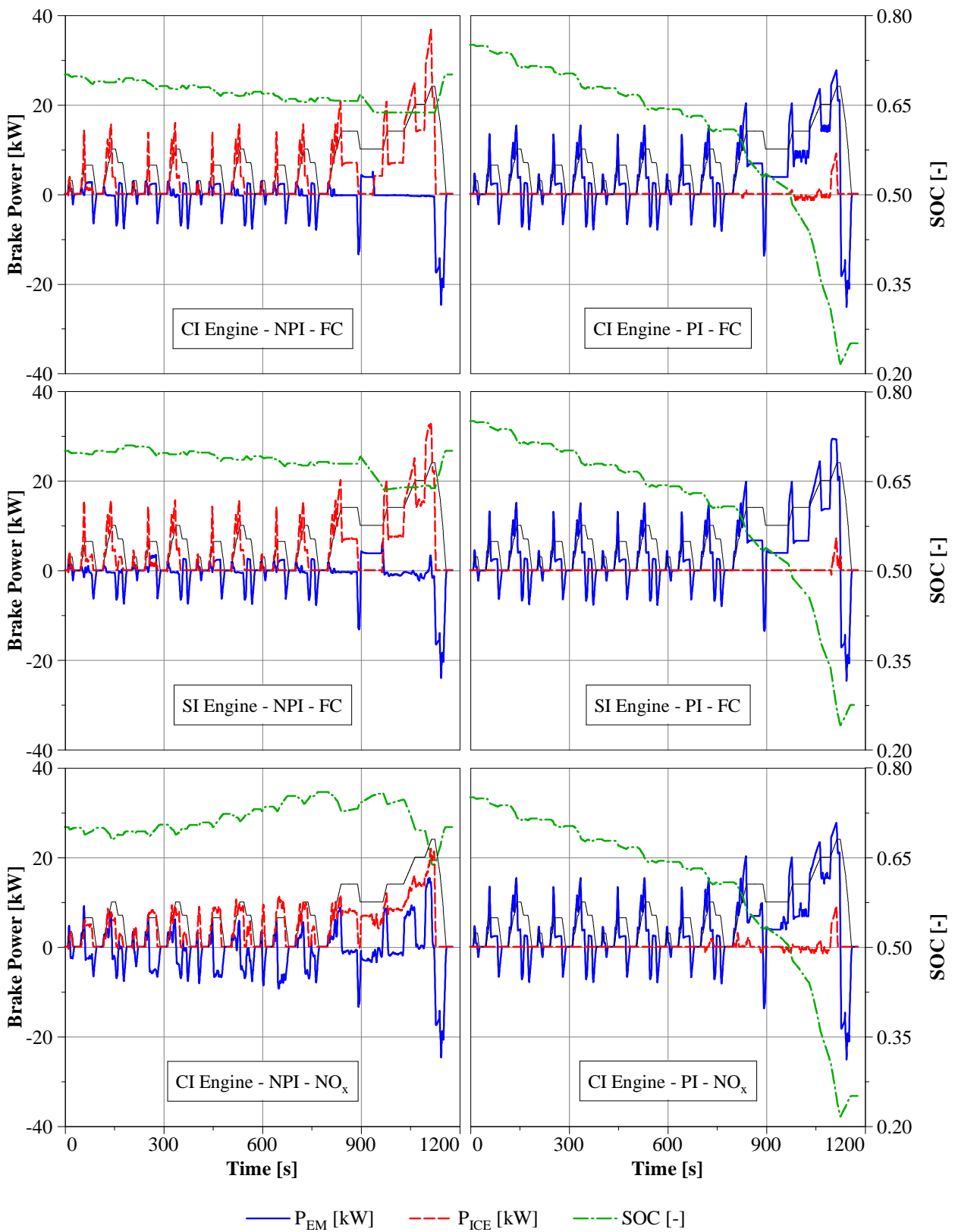
Figure 4.3- PHEV Benchmark Optimizer: ICE and EM brake power profiles and battery State Of Charge (NEDC)

As far as the plug-in PHEVs are concerned, (right column graphs of Fig. 4.3), the electric machine supplies all the required traction power during the four successive urban cycles. The engine is not switched-on until the extra-urban phase, when the battery SOC reaches the lower limit. As a consequence, the minimum fuel consumption and NO_x emissions are guarantee; in counterbalance a net usage of the energy battery content is required (i.e. $SOC_{end} \approx 0.25$, and $SOC_{start} \approx 0.75$).

Figure 4.4 shows the time distribution of the engine operating points (in terms of BMEP and ICE speed) during the NEDC for the not plug-in PHEVs (right column). They are compared to the conventional vehicle configurations (left column). The color scale indicates the total time during which the engine operates at a specific point of the diagram. The solid black line represents the full-load conditions. Regarding the CI engine, the minimum BSFC operating line (top plots in Fig. 4.4) is significantly above the minimum $BSNO_x$ one (bottom plots in Fig. 4.4). Accordingly, the minimization of the M_{NOx} and the minimization of the M_{fuel} lead to completely different operating strategies (see Fig. 4.3).

The NEDC is characterized by low load conditions with a maximum required traction power of about 35 kW during the 100-120 km/h speed transient. As a consequence, in case of the traditional vehicle, the CI engine always operates below the minimum BSFC line (top left in Fig. 4.4). Concerning the SI engine, only a reduced fraction of the operating points is above the $BSFC_{min}$ condition (at around 3000 rpm and 7 bar of BMEP, intermediate left graph in Fig. 4.4). When negative LPS mode is actuated, the ICE load is reduced even further. This leads to a decrease in the FC, even though the engine efficiency deteriorates. Instead, as mentioned, the minimum $BSNO_x$ operating line is significantly below the minimum BSFC line. The operation of the traditional vehicle results to be also above the $BSNO_{x,min}$ operating conditions (bottom graph in Fig. 4.4).

Top graphs in Fig. 4.4, show the variation in the time distribution of the ICE operation for the not plug-in PHEV by means of the benchmark optimizer with respect to the conventional vehicle. The two operating areas at 2-3 bar of BMEP and respectively 1250 and 1750 rpm of engine speed are almost completely avoided by means of the only electric mode (see speed plateaus in Fig. 4.3). No relevant ICE load shift strategy is implemented and the other operating areas result to be unvaried. Concerning the SI engine (intermediate graphs in Fig. 4.4), the conditions at low load (below 2 bar of BMEP) are almost completely substituted by the electric mode: this allows the system to avoid the lowest efficiency points of the SI engine. Moreover, a weak negative load point shift strategy of the ICE is applied for the operating points above the $BSFC_{min}$ line (at about 3250-3750 rpm and 7-9 bar) and a positive engine load point shift for the operating points at about 1250-1750 rpm toward the optimal $BSFC_{min}$ line.

Finally, the optimization of the NO_x emissions for the CI engine (bottom graphs in Fig. 4.4) implies a completely different operating strategy with respect to the previous ones and a marked (positive and negative) engine load point shift is implemented. This is a consequence of the lower $BSNO_{x,min}$ line respect to the $BSFC_{min}$ one and the higher derivatives of the $BSNO_x$ with respect to the load than in the case of the BSFC (see Fig. 4.5):

$$abs\left(\frac{dBSNO_x}{dBMEP}\bigg|_{\omega_{ICE}=\omega_{ICE}^*}\right) \gg abs\left(\frac{dBSFC}{dBMEP}\bigg|_{\omega_{ICE}=\omega_{ICE}^*}\right) \qquad (4.1)$$
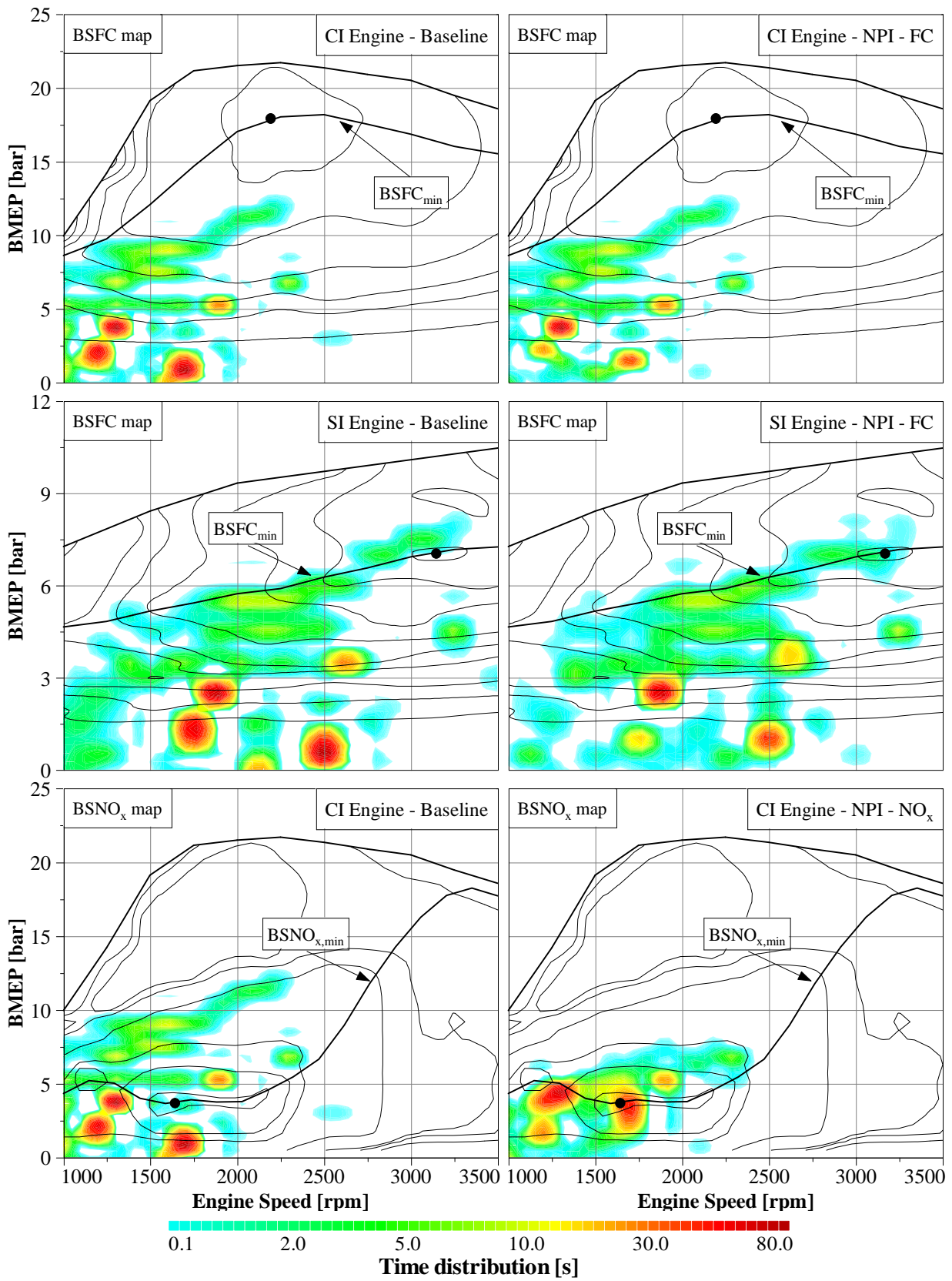
Figure 4.4 – PHEV Benchmark Optimizer: time distribution of the ICE operating points for the not plug-in HEVs compared to the baseline (NEDC)

Equation 4.1 and Fig. 4.5 underline how, at fixed engine speed, a load difference implies low variations in the BSFC (i.e. in the engine efficiency), but high deviations in the $BSNO_x$. Therefore, in the case of the fuel consumption minimization, the benchmark optimizer mainly uses the energy accumulated during the regenerative braking for the electric mode. Whereas, in case of the NO_x minimization, the engine is operated along the minimum $BSNO_x$ emission line by means of a significant load point strategy that guarantees dramatic reductions in terms of total NO_x emissions.
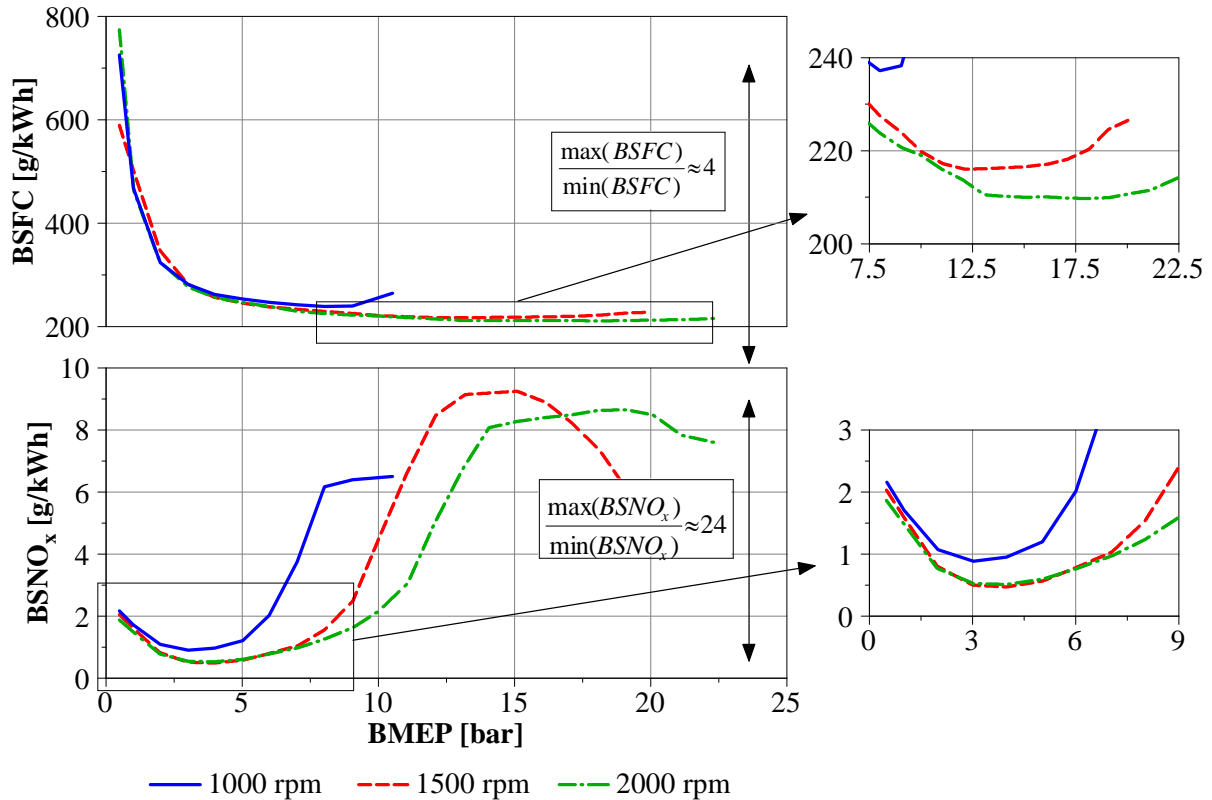
Figure 4.5- PHEV: BSFC and BSNO$_x$ with respect to BMEP at fixed engine speeds (CI Engine)

All the results analyzed so far underline that the efficiency of the electric line (electric machine-inverter-battery, ε_{EL}) is a key factor in the selection of the hybrid operating mode. One method that can be used to investigate the hybrid powertrain losses, during LPS phases, is the overview of the Sankey diagrams (Fig. 4.6 and Fig. 4.7). They consider the powertrain up to the mechanical input power of the gearbox (for further details on the optimized hybrid components, please refer to Fig. 3.12).

Figure 4.6 shows the system losses (up to the EM-Gearbox clutch) in case of the pure thermal mode, with the only engine supplying the required traction power (left column), compared to the case of the hybrid system with load point shift strategy (right column). Regarding the pure thermal mode, two operating points at 1500 rpm are considered: at 8 bar and 16 bar of BMEP. They are respectively below and above the minimum BSFC point, that is located at BMEP = 12 bar (see Fig.s 4.4 and 4.5) and they are characterized by an efficiency of 35.7% and 37.6%. It is considered the engine working on each operating point for a time interval of 1 sec, with the following fuel energy consumption:

$$E_{ICE,source}(baseline) = P_{ICE,source,1} - \Delta t + P_{ICE,source,2} \cdot \Delta t = 47.6 \cdot 1 + 83.5 \cdot 1 = 131.1 \text{ kJ}$$

Conventional Vehicle

Load Point Shift Strategy

$P_{ICE,source}$ = 47.6 kW

$P_{ICE,source}$ = 67.8 kW

ε_{ICE}=35.7 %

ε_{ICE}=37.8 %

$P_{req,cs}$ = 17.0 kW

$P_{batt,source}$ = -7.1 kW

$P_{req,cs}$ = 17.0 kW

ε_{EL}=81.9 %

$P_{ICE,source}$ = 83.5 kW

$P_{ICE,source}$ = 67.8 kW

ε_{ICE}=37.6 %

ε_{ICE}=37.8 %

$P_{req,cs}$ = 31.4 kW

$P_{batt,source}$ = 7.1 kW

$P_{req,cs}$ = 31.4 kW

ε_{EL}=82.3 %

$E_{ICE,source}$ (1 sec + 1 sec) = 131.1 kJ

$E_{ICE,source}$ (1 sec + 1 sec) = 135.6 kJ

ICE Source	ICE Loss	Battery Source	Electric Loss	Required Power

Figure 4.6- PHEV Load point shift strategy for the minimization of the total fuel consumption (CI engine – ω_{ICE}=1500 rpm)

Concerning the load point shift strategy, right column in Fig. 4.6 reports a positive LPS (top diagram) and a negative LPS (bottom diagram) that allow the engine to work always on its optimal operating point (with the highest efficiency of 37.8%). In the both cases, the electric line is characterized by an efficiency of about 82%, underling how the ICE loss share is predominant. As for the conventional vehicle, it is considered an operation of 1 sec for the both conditions, with a resulting zero net balance of the battery energy content:

$$E_{ICE,source}(LPS\ strategy) = P_{ICE,source,1} \cdot \Delta t + P_{ICE,source,2} \cdot \Delta t = 67.8 \cdot 1 + 67.8 \cdot 1 = 135.6\ kJ$$

An overall expense of 135.6 kJ of fuel energy source is obtained, higher than the conventional vehicle (+3.4 %): *the improvement in the Compression Ignition Engine efficiency during its load point shift is too low and it is more than counterbalanced by the energy losses of the electric line.*

Figure 4.7 compares the pure thermal mode (left column) with respect to the load point shift strategy (right column), in the case of the NO_x minimization. Regarding the pure thermal mode, two operating points at 1500 rpm are considered: at 1 bar and 7 bar of BMEP. They are respectively below and above the minimum $BSNO_x$ point, at about 4 bar of BMEP (see Fig.s 4.4 and 4.5).

In order to allow the system overview through the Sankey diagrams, an equivalent Q_{NOx} heating value of 220 MJ/kg is considered (for further details, see Eq. 3.22a): the two operating points result to be characterized by an equivalent efficiency of respectively: 14.7 % and 18.5 %. It is once more considered the engine working on each operating point for 1 sec, with the following NO_x equivalent energy consumption:

$$E_{NOx,source}(baseline) = P_{NOx,source,1} \cdot \Delta t + P_{NOx,source,2} \cdot \Delta t = 15.0 \cdot 1 + 81.1 \cdot 1 = 96.1 \text{ kJ}$$
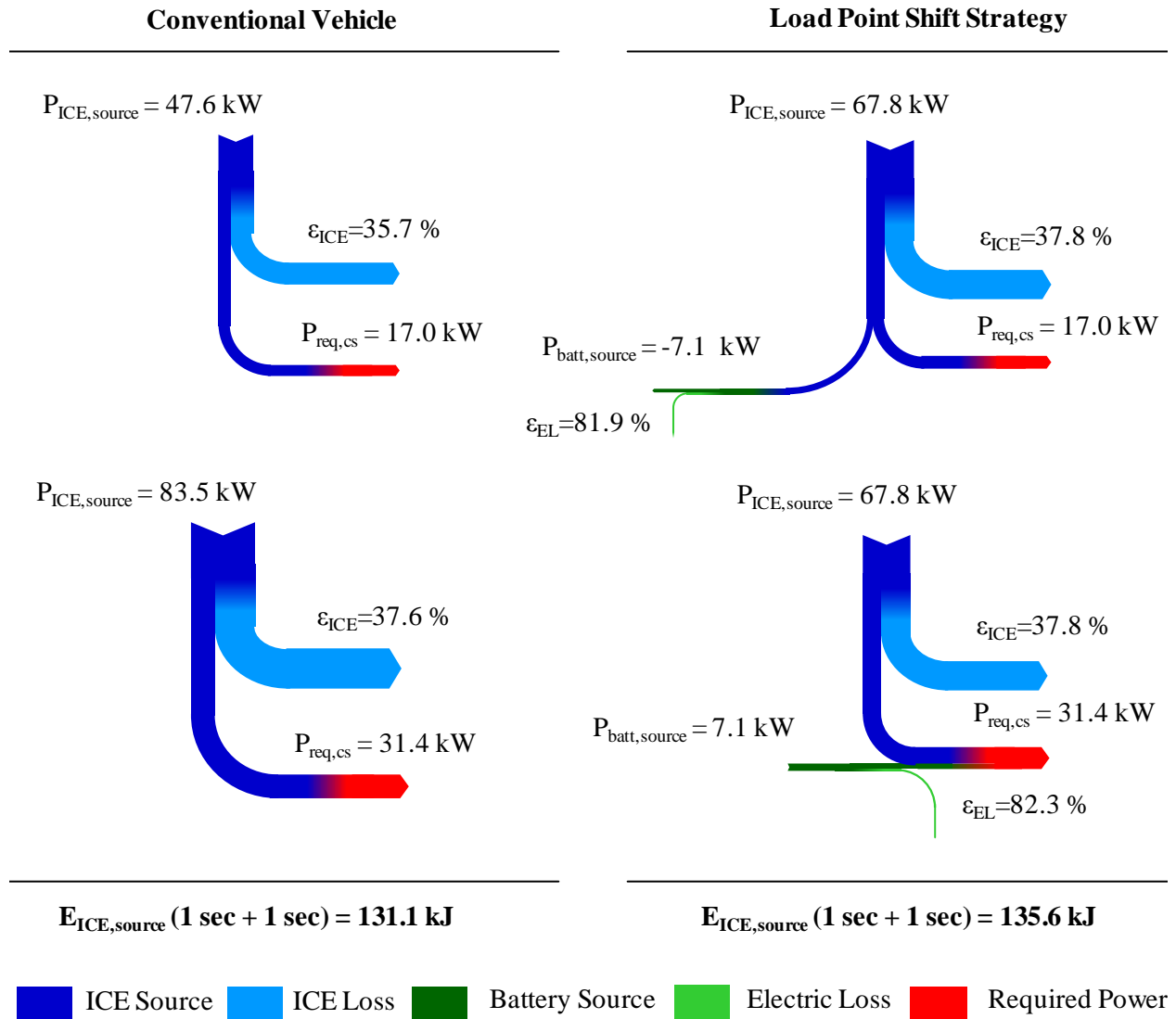

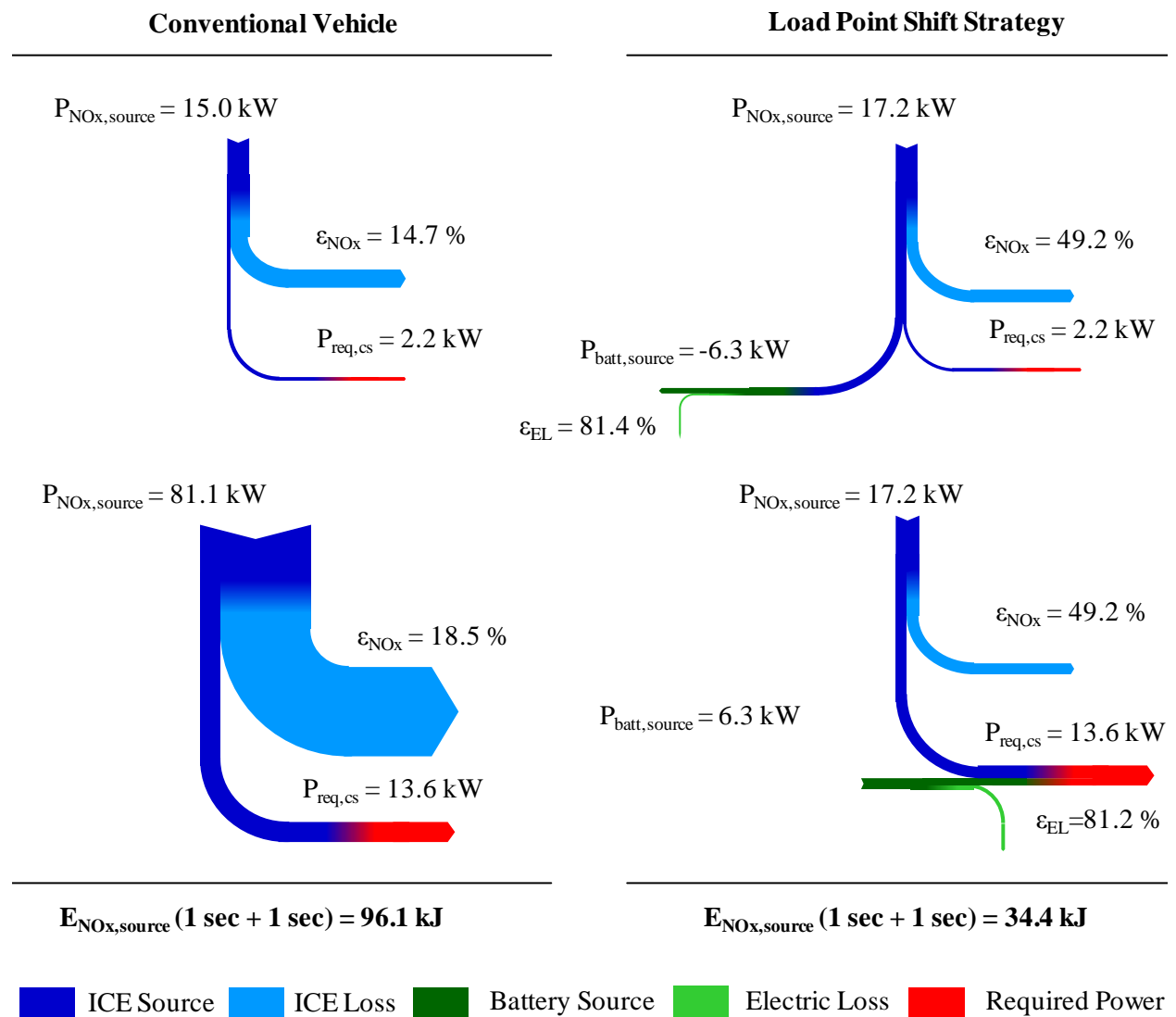**Figure 4.7- PHEV Load point shift strategy for the minimization of the total NO_x emissions (CI engine – ω_{ICE}=1500 rpm)**

Concerning the load point shift strategy, the right column in Fig. 4.7 shows a positive LPS (top diagram) and a negative LPS (bottom diagram) that allow the engine to work on its minimum $BSNO_x$ (featured by the highest equivalent efficiency of 49.2 %). In the both cases, the electric line is characterized by an efficiency of about 81%. As in the case of the conventional vehicle, it is considered an operation of 1 sec for the two conditions (with a resulting zero net balance of the battery energy content: $P_{batt,source}$=-7 kW for the positive LPS and $P_{batt,source}$=+7 kW for the negative LPS):

$$E_{NOx,source}(LPS\ strategy) = P_{NOx,source,1} \cdot \Delta t + P_{NOx,source,2} \cdot \Delta t = 17.2 \cdot 1 + 17.2 \cdot 1 = 34.4\ kJ$$

It results an NO_x equivalent energy consumption of 34.4 kJ (*-76.4 % with respect to the traditional mode*), that confirms *the importance of the engine load point shift strategy to minimize the NO_x emissions*.

Figure 4.8 reports an overview of the well-to-wheel CO_2 emissions (left diagram) and NO_x emissions (right diagram) along the NEDC for all the considered PHEVs. It is important to underline that all the CO_2 and NO_x emissions of this study, do not represent the benchmark of the considered technology, because the optimization procedure considers the only operating strategy. At the beginning of the project, a drivetrain layout based on the experience of the author was assumed (see Tab. 3.1) and no further redesign of the hardware was considered. *The real intention of this study is to show how different operating strategies exploit as best as possible the selected hybrid powertrains with reference to a selected target*. For further details on possible techniques to optimize the hybrid powertrain design, please refer to ([10, 11, 34]).

The wheel-to-well CO_2 emissions are calculated as the sum of two different terms: the CO_2 from the combustion of the fuel ($CO_{2,ICE}$) and, in the case of the only plug-in hybrids, the indirect CO_2 emissions from the electric energy required by the net to recharge the battery ($CO_{2,Batt}$):

$$CO_2 = CO_{2,ICE} + CO_{2,Batt} \tag{4.2}$$

$$CO_{2,ICE} = \frac{M_{fuel} \cdot x_{CO2,Fuel}}{\rho_{Fuel} \cdot Range} \tag{4.3}$$

$$CO_{2,Batt} = \frac{V_{OC} \cdot \Delta SOC \cdot Q_{Batt} \cdot x_{CO2,el\ net}}{\varepsilon_{Ch,el,net} \cdot Range} \tag{4.4}$$

where:

> $x_{CO2,Fuel}$ **[g_{CO2}/l]**: represents the grams of CO_2 released per liter of burned fuel. It is a property of the considered fuel. The following values, defined from the stochiometric combustion, are considered:

Gasoline: $x_{CO2,Fuel} = 2340\ [g_{CO2}/l]$

Diesel: $x_{CO2,Fuel} = 2640\ [g_{CO2}/l]$

> $x_{CO2,el\ net}$ **[g_{CO2}/kWh$_{el}$]**: represents the grams of CO_2 released per kWh of electric energy absorbed from the electric net. It is a property of the electric network (function of the type of

installed power plants, grid efficiency, etc.). For the European Union, the following value is considered ([10]):

$$x_{CO2,el,net} = 400 \ [g_{CO2}/kWh]$$

➢ $\varepsilon_{Ch,el,net}$ **[%]**: characterizes the efficiency of the vehicle battery recharging through the electric net. It is assumed to be 93% ([10])

➢ **Range [km]**: is the total distance driven by the vehicle; for further details on the considered driving cycle, please refer to Tab. 3.3
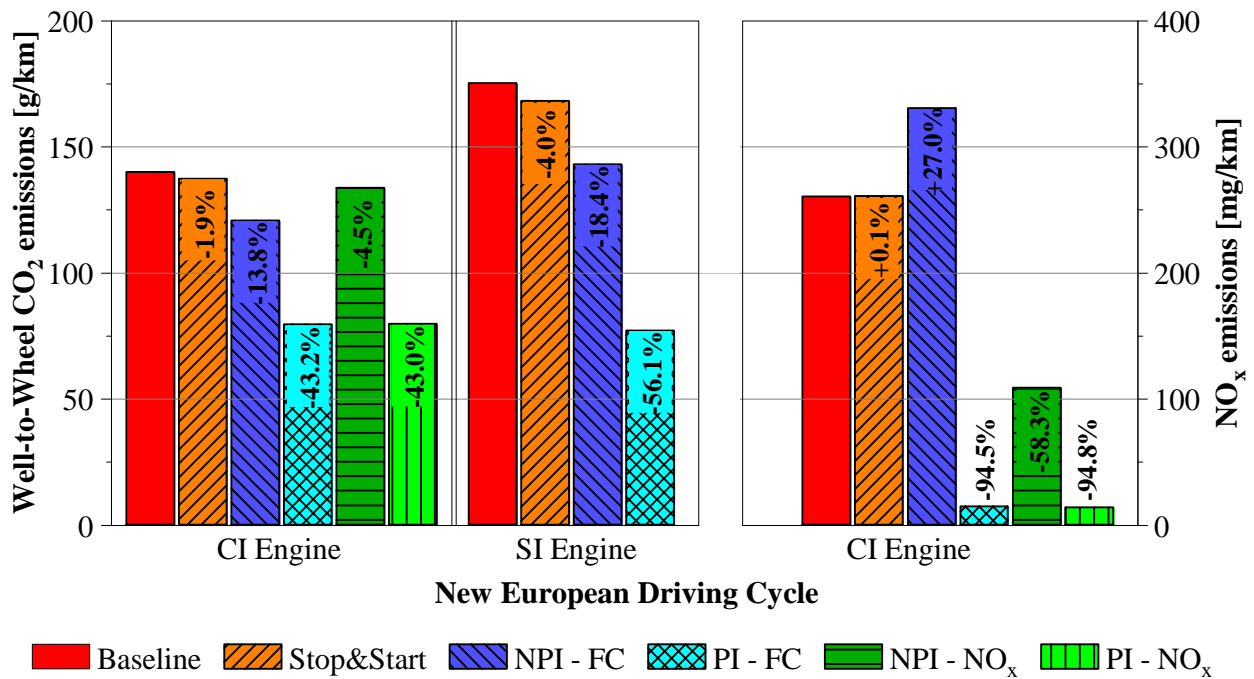
Figure 4.8 - PHEV Benchmark Optimizer: Well-to-Wheel CO₂ emissions and NOₓ emissions (NEDC)

As far as the CO_2 emissions are concerned, the CI engine guarantees about 140 g_{CO2}/km in case of the conventional vehicle (left red bar in Fig. 4.8), whereas the SI engine about 175 g_{CO2}/km (+25 %, intermediate red bar). Both the Stop&Start feature and the hybridization result to have a stronger impact in case of the SI engine, with an overall reduction for the not plug-in, in terms of the CO_2 emissions, close to 20 %. This is due to the higher variation of the BSFC of the SI engine, with respect to the CI engine (Fig.s 2.3 and 2.4). However, the CI engine, due to its better average efficiency, reaches the lowest CO_2 emissions between the not plug-in vehicles (about 120 g_{CO2}/km). Finally, targeting the NO_x emissions, the fuel consumption is strongly compromised and less than 5 % reduction in terms of CO_2 emissions is achieved.

In the plug-in PHEVs, the battery energy content and the electric motor maximum power allow the vehicle to be driven almost completely in electric mode and the engine is switched-on only during the EUDC. The both engines and optimization targets (M_{fuel} and M_{NOx}) perform almost the same CO_2 emissions, the majority of which (about 85 %) is due to the battery recharge ($CO_{2,batt}$, see Eq. 4.4).
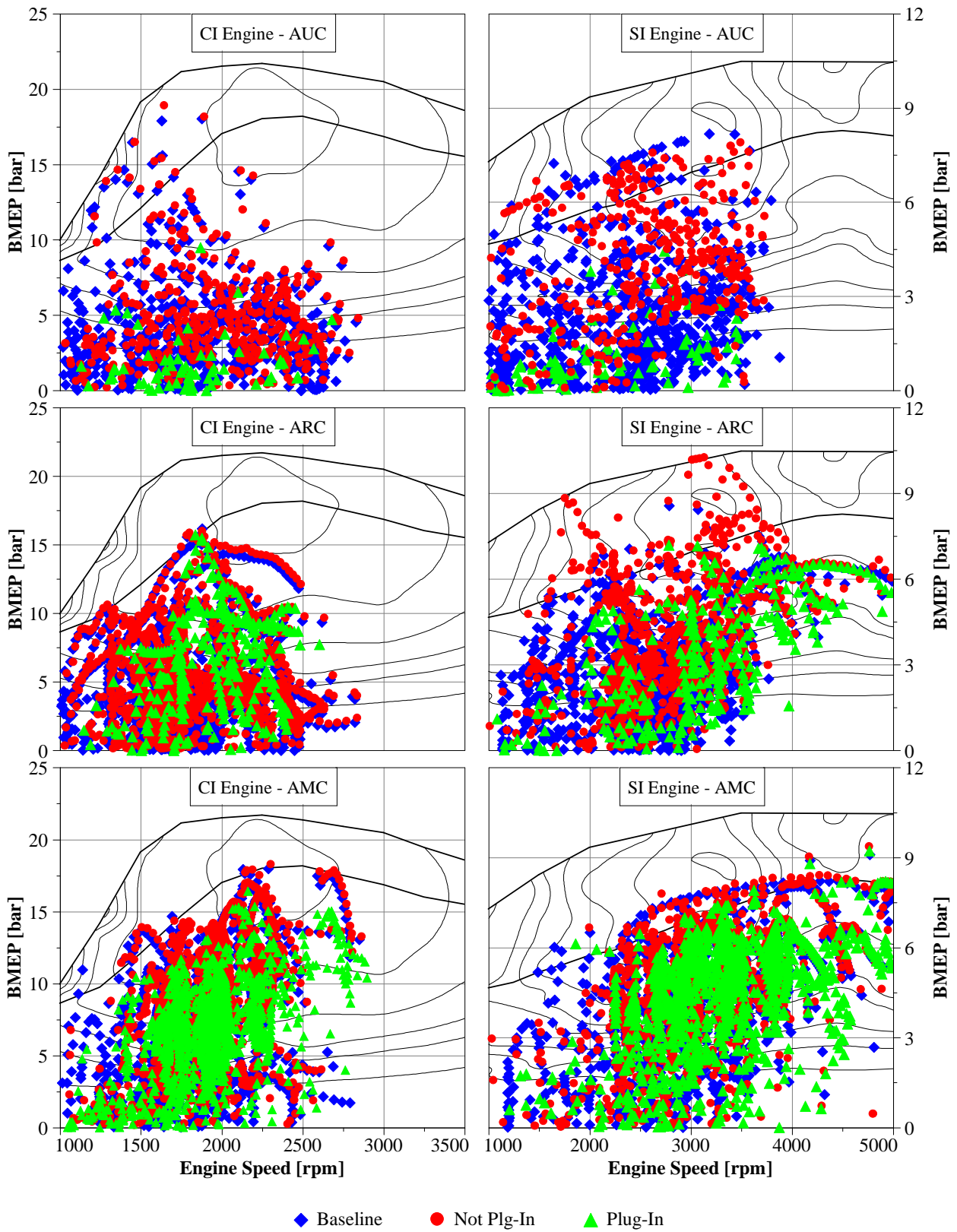
Figure 4.9 - PHEV Benchmark Optimizer: ICE operating points for the not plug-in and plug-in PHEVs compared to the baseline (Artemis Driving Cycles)

Regarding the NO_x, only local emissions are taken into consideration and the plug-in feature prevents any NO_x emissions at all. The hybridization has a major impact and the not plug-in PHEV achieve a decrease close to 60 %. This result is compromised in case of the FC target, that implies an increase of the NO_x emissions. Finally, the plug-in almost avoid any emissions (due to the only short switching-on of the engine) and their performance is independent on the optimization target.

The vehicle was also simulated, for the only fuel consumption minimization, along real world representative driving profiles: the Artemis (Urban, Road and Motorway) driving Cycles. Figure 4.9 compares the operating points of the baseline (conventional vehicle configuration without Stop&Start feature) with respect to the plug-in and not plug-in PHEVs. The hybridization allows the engine to partially avoid low speed and load operating points during which the engine is characterized by the lowest efficiencies (especially the SI engine). Only in the case of the SI ICE a relevant load point shift strategy is implemented, especially in the case of the AUC. Moreover, the plug-in feature is more effective in the case of urban driving cycles, for which the total required energy is limited and comparable to the initial battery energy content.

Finally, Fig. 4.10 shows the wheel-to-well CO_2 emissions in case of the three Artemis Cycles for all the parallel hybrid electric vehicles and compared to the baseline (with and without Stop&Start strategy). The conventional vehicle without Stop&Start feature (baseline) is considered as reference for the percentage reductions in the diagram: red bar for the CI engine and dark-blue bar with horizontal-line hatch for the SI engine. With reference to Fig. 3.8 and Tab. 3.3, the AUC is characterized by the longest standstill time and the high peak and mean vehicle accelerations. As a consequence, the Stop&Start function is very significant (5.8% and 2.6% of CO_2 reduction respectively in the case of the SI engine and CI engine) and the optimizer effectively exploits the powertrain electrification.
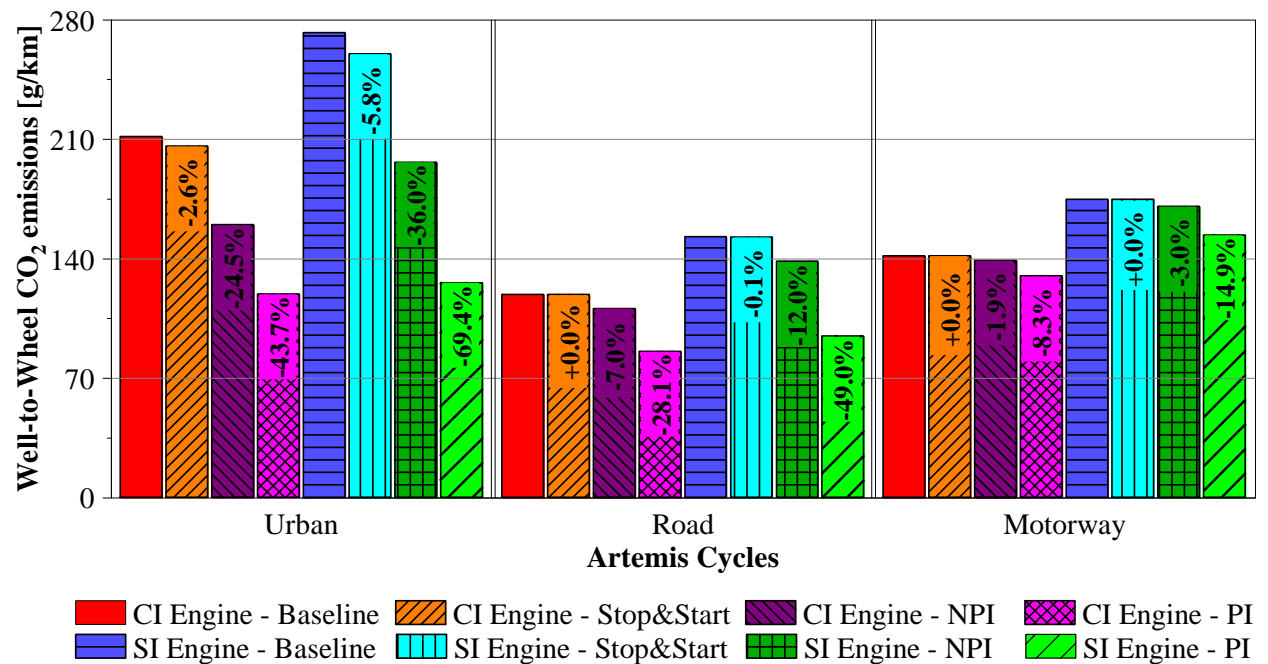

Figure 4.10 - PHEV Benchmark Optimizer: Well-to-Wheel CO_2 emissions (Artemis Driving Cycles)

The higher is the average speed and the longer are the constant load time intervals (i.e. in the case of the Road and even more of the Motorway AC), *the less impacting is the hybridization of the vehicle*. The ARC and especially the AMC are characterized by higher engine speeds and load operating points (Fig. 4.9), that imply the baseline engine to operate at high efficiencies. Only a weak load point shift strategy is required and the electric mode is not convenient or not possible. As a consequence, the PHEV guarantees lower and lower improvements in terms of CO_2 emissions in the case of the Artemis Road and Motorway Cycles: from 36 % of the AUC, to 12 % of the ARC, to 3 % of the AMC in case of the SI engine without plug-in. Similarly, the plug-in feature is more effective in the case of the AUC and its benefits are compromised for highway conditions. As in the case of the NEDC, the CI engine performs the lowest CO_2 emissions even if its hybridization and the plug-in feature guarantee less improvements in terms of fuel consumption with respect to the conventional vehicle.

4.1.1   Real-time optimizers

Figures 4.11-4.13 show the time histories of the electric machine brake power resulting from the real-time operating strategies and the benchmark (respectively blue solid line and dashed red line) and the battery SOC of the real-time operating strategies (green dash-dot line) along the NEDC for the not plug-in parallel hybrid vehicles. All the three RTOs are taken into consideration.

In the case of the CI engine with M_{fuel} as target (Fig. 4.11), the three operating strategies have a comparable behavior:

➢ low load driving conditions are driven in pure electric mode (the only exception is the first part of the first UDC with the TLM REC). This feature prevents the ICE to work on its lowest efficiency operating points during the speed plateaus of the UDCs (excluding the 50 km/h) and the 70 km/h in the EUDC (not for the TLST)

➢ in general, no load point shift strategy is implemented

The TLM TOT is the operating strategy that is more close to the BO and only negligible differences can be noticed. Accordingly, result the Well-to-Wheel CO_2 emissions reported in Fig. 4.14: the TLM TOT shows almost the same reduction with respect to the baseline (-13.7%) as the benchmark (-13.8%), whereas the TLM REC (-13.1%) and even more the TLST (-12.4%) guarantee lower benefits. However, in all the cases, performance remain close. This can be attributed to the flat CI engine efficiency map and the very simple strategy to be implemented: or electric mode in case of low load conditions or pure thermal mode.

Regarding the SI engine with M_{fuel} as target and not plug-in feature (Fig. 4.12), a similar behavior to the CI engine is obtained. The main difference are the more intense load-point shift strategy during the EUDC for the TLM TOT and the BO and the electric share during the first UDC in the case of the TLM REC and the TLST. As in the case of the Compression Ignition engine, the TLM TOT (-18.2 %) is the real-time operating strategy that performs more closely to the benchmark (-18.4 %), whereas the other two optimizers have a worse behavior: 16.4% for the TLM REC and -15.4% for the TLST.

Figure 4.11 – PHEV Real-Time Optimizers: EM brake power profiles and battery State Of Charge for the CI engine with M_fuel as target (NEDC)
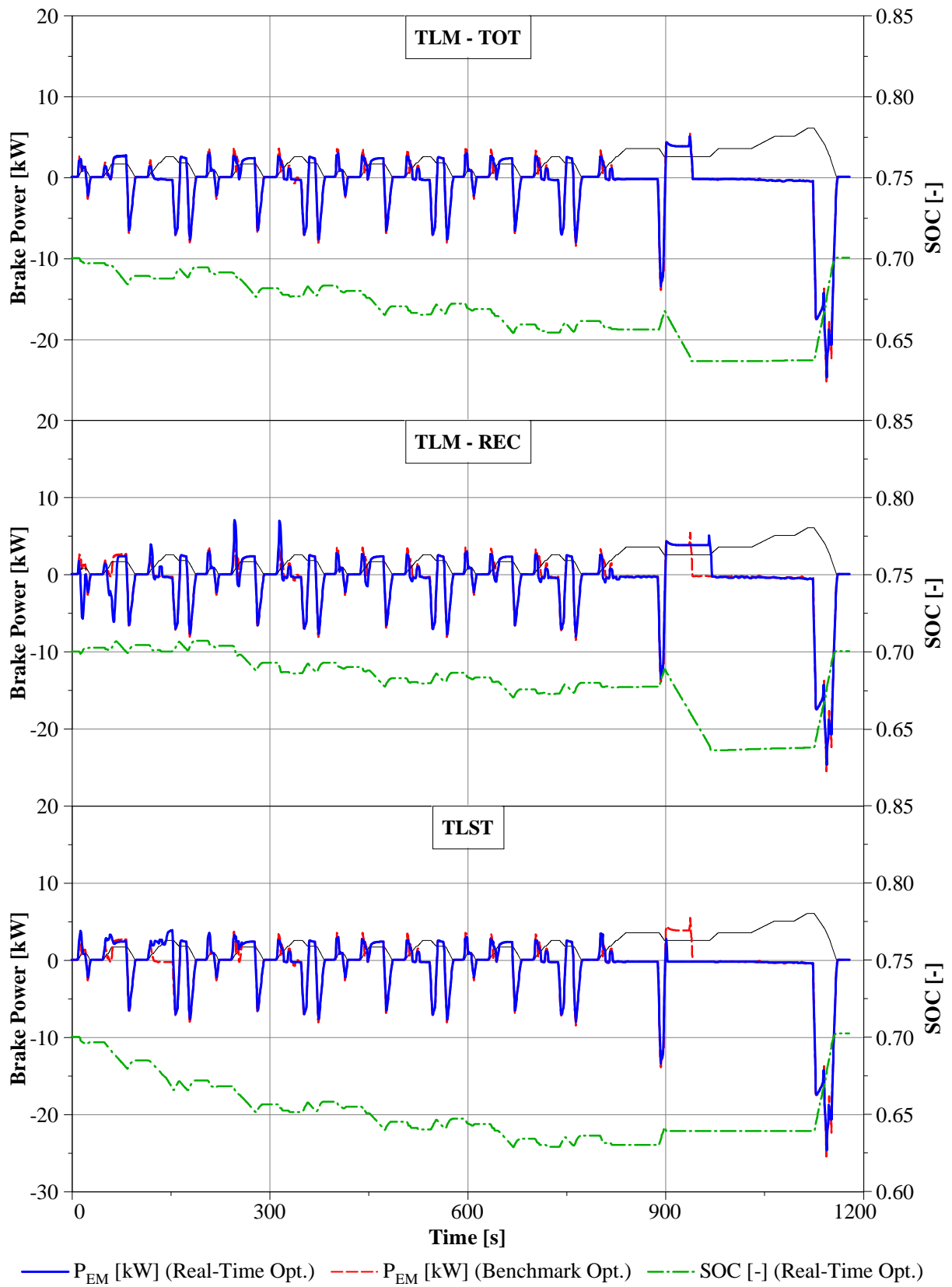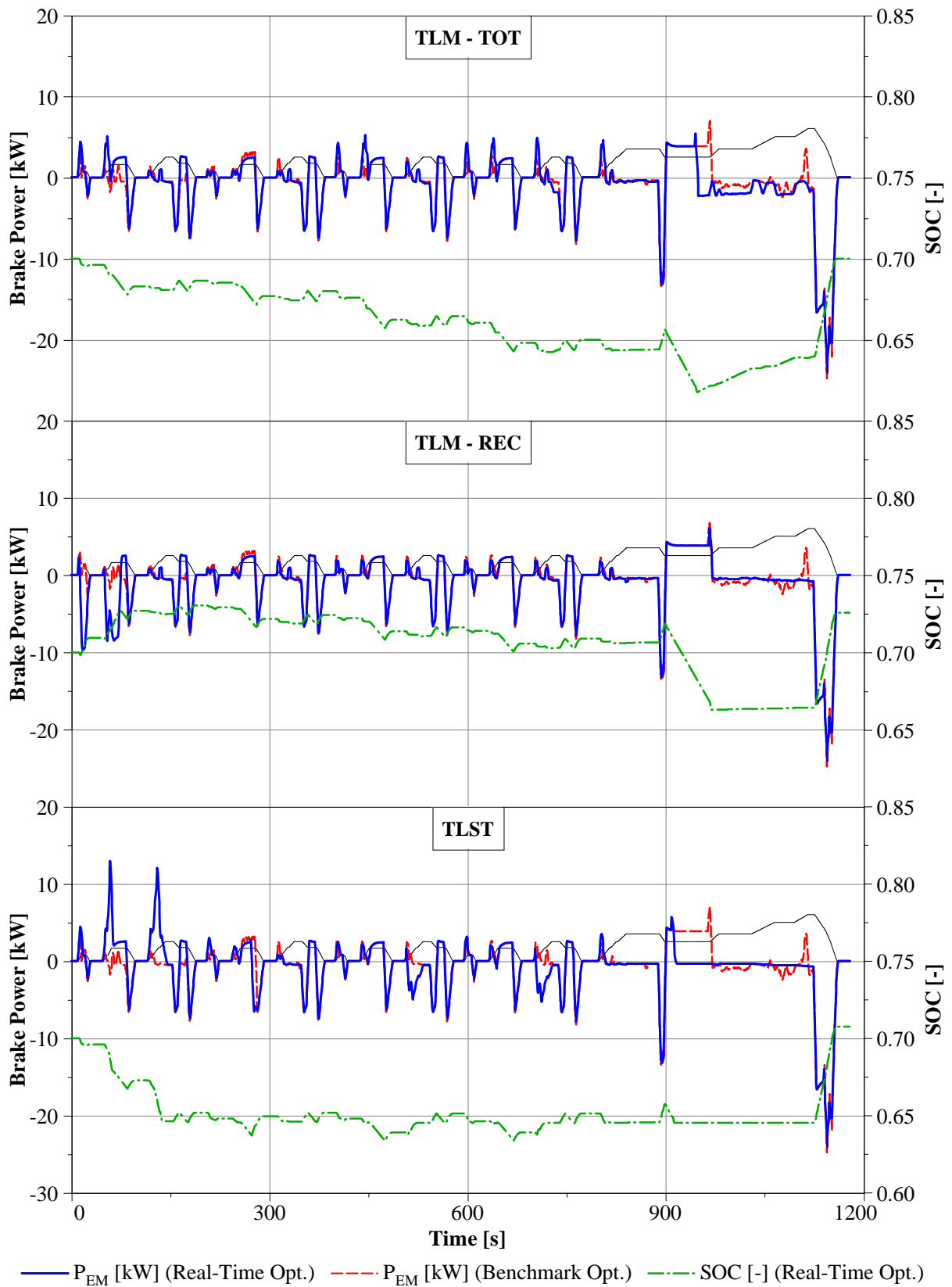
Figure 4.12 – PHEV Real-Time Optimizers: EM brake power profiles and battery State Of Charge for the SI engine with M_fuel as target (NEDC)
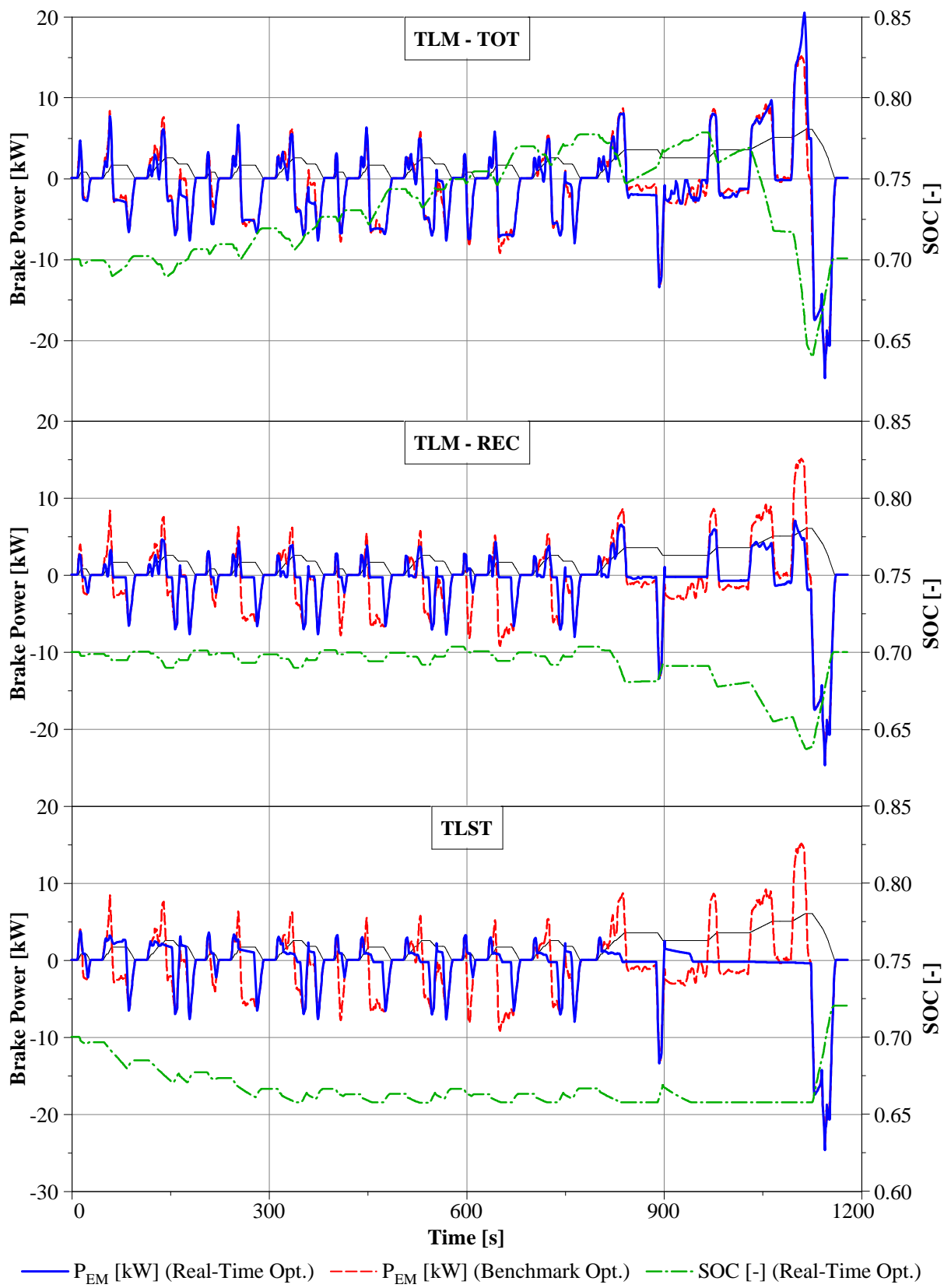
Figure 4.13 – PHEV Real-Time Optimizers: EM brake power profiles and battery State Of Charge for the CI engine with M$_{NOx}$ as target (NEDC)

Finally, in case of the CI engine with M_{NOx} as target and not plug-in feature (Fig. 4.13), the electric machine works as a generator along the speed plateaus, in order to shift the engine load towards the minimum brake specific NO_x line (positive load point shift) and to save energy in the battery that will be used during the extra-urban phase. Being the ICE load point shift the key strategy to reduce NO_x emissions, the recoverable formulation of the NO_x losses (Eq. 3.22b) was expected to be more effective than the total expression (Eq. 3.22a) for the TLM strategy.
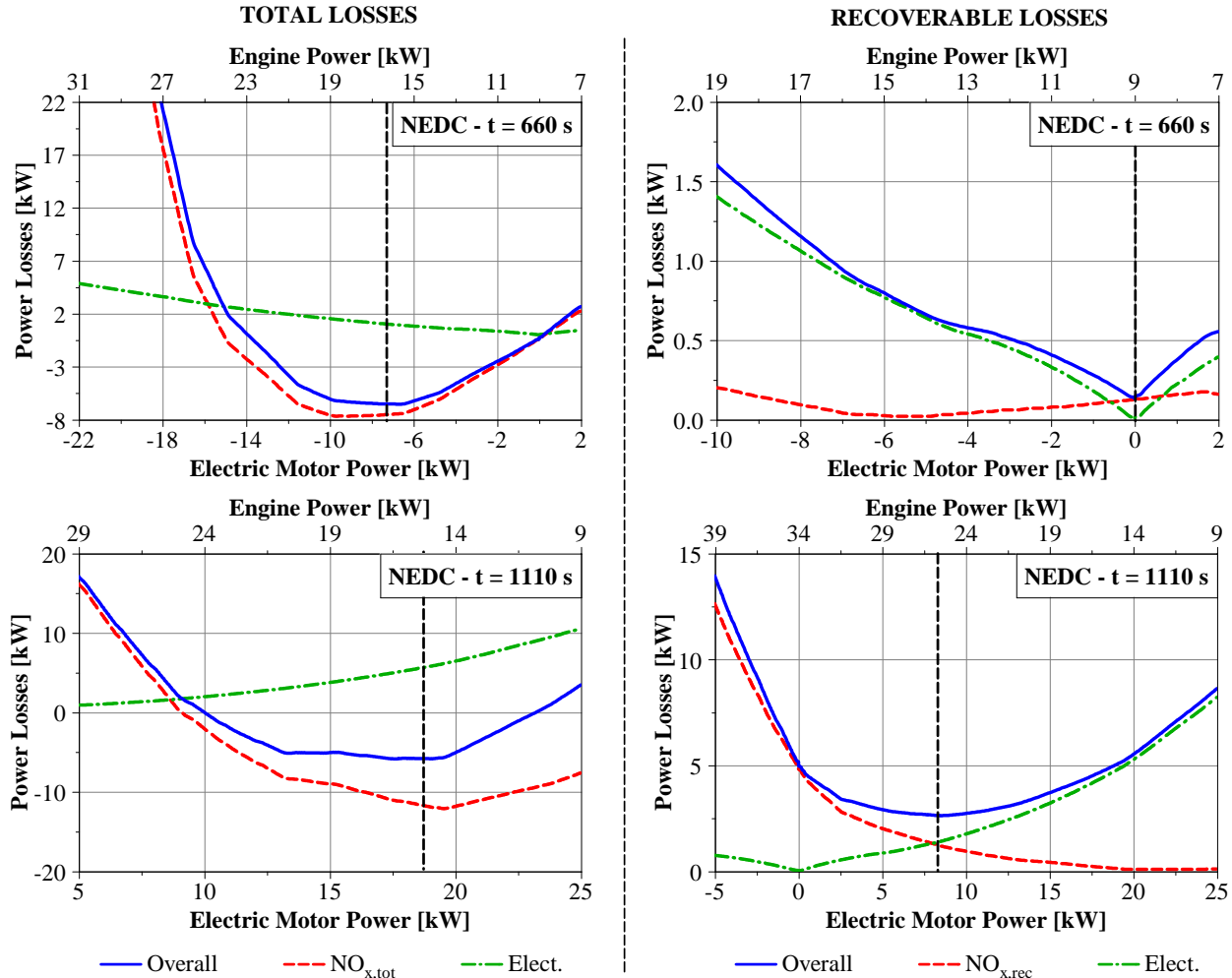
Figure 4.14 – PHEV TLM: NO_x, electric and overall losses for the CI engine with M_{NOx} as target (left column: total losses, right column: recoverable losses).

Nevertheless, the recoverable NO_x losses (second plot of Fig. 4.13) implement a less effective load point shift strategy than the total NO_x losses (first plot of Fig. 4.13) with a resulting lower reduction in terms of NO_x emissions (refer to Fig. 4.14). This behavior can be explained through Fig. 4.14, where the NO_x, electric and overall losses of the total (left column) and recoverable (right column) formulation are compared. Two distinguishing instants have been considered along the NEDC: 35 km/h speed plateau of the last ECE (at 660 s) and the 100-to-120 km/h speed transient during the EUDC (at 1110 s). The two top plots show how the total losses formulation finds the best condition at about [P_{EM} = -7 kW – P_{ICE} = 16 kW] with a significant positive load shift of the ICE, while the recoverable losses formulation at [P_{EM} = 0 kW – P_{ICE} = 9 kW] employs pure thermal mode. Concerning the extra-urban operating condition, both the strategies require a negative load point

shift of the engine, however the total NO_x losses are more effective and allow a stronger reduction of the engine power toward the minimum $BSNO_x$ line.

Total NO_x or ICE losses
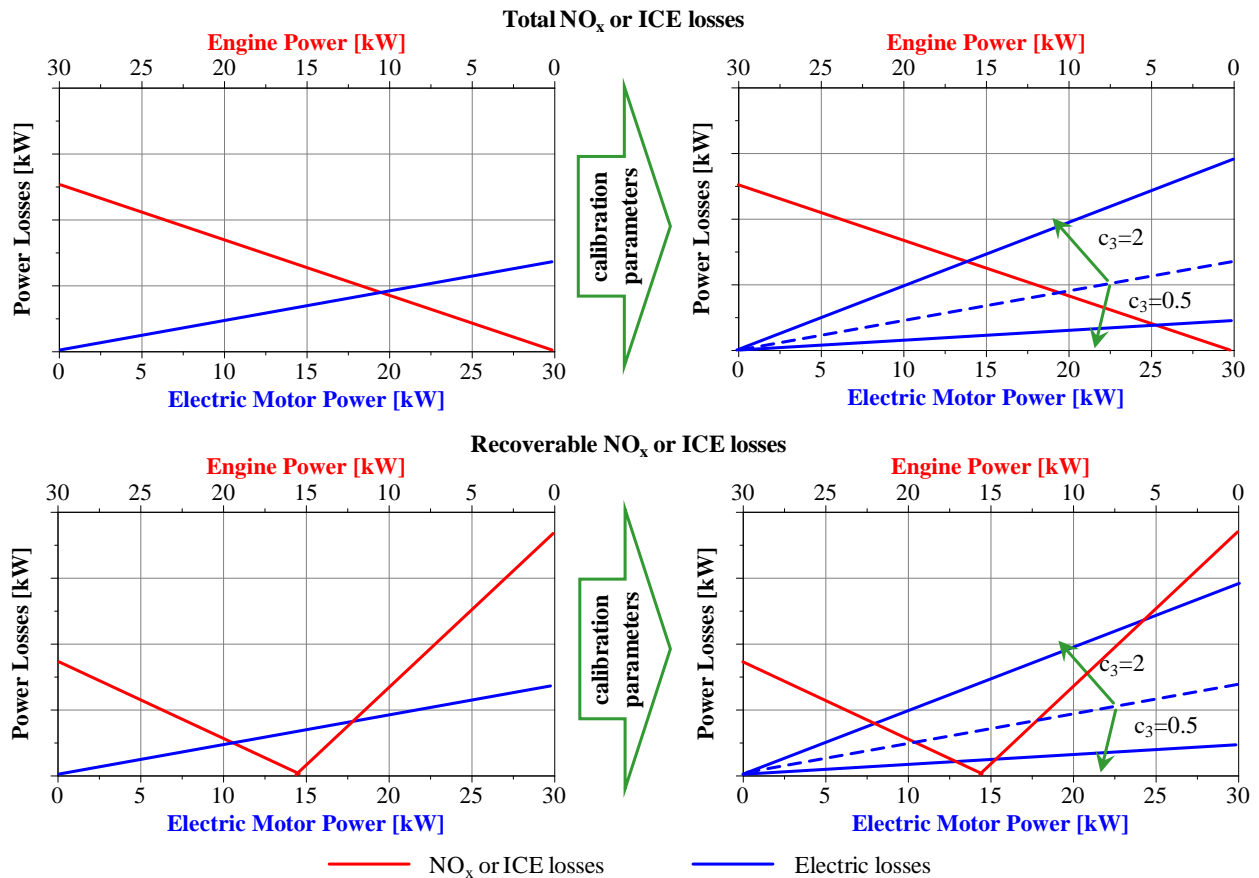
Figure 4.15 – PHEV TLM: NO_x (or ICE) and electric losses for the CI engine (top row: total losses, bottom row: recoverable losses).

This unexpected behavior is due the worse control of the final SOC by adopting the recoverable formulation of the NO_x losses. Figure 4.15 shows a schematic overview of this concern. In the top left plot the total NO_x (or ICE) losses are compared to the electric ones: the firsts increase from right (zero value) to left, together with the raise of the engine power, whereas the second increase from left (zero value) to right with the raise of the electric machine power. For reasons of simplicity, only positive P_{EM} are considered. As explained in the Chapter 3.2, the losses are calibrated in the optimization procedure, through the multiplication factor of Eq. 3.17a, until the required final SOC is achieved (see top right plot). Concerning the recoverable losses, these are characterized by a not-monotonic trend (bottom left plot) with a zero value at the minimum $BSNO_x$ (or BSFC) operating point. The calibration through the electric losses, that tend to balance the usage of the energy accumulated in the battery, have to be enhanced (compare top plots in Fig. 4.14). As a consequence, the NO_x losses achieve a lower impact on the overall strategy and a worse reduction, in terms of NO_x emissions, is achieved.

In general, recoverable losses can have better performance than the total ones, but their calibration is more challenging and is highly dependent on the boundary conditions.
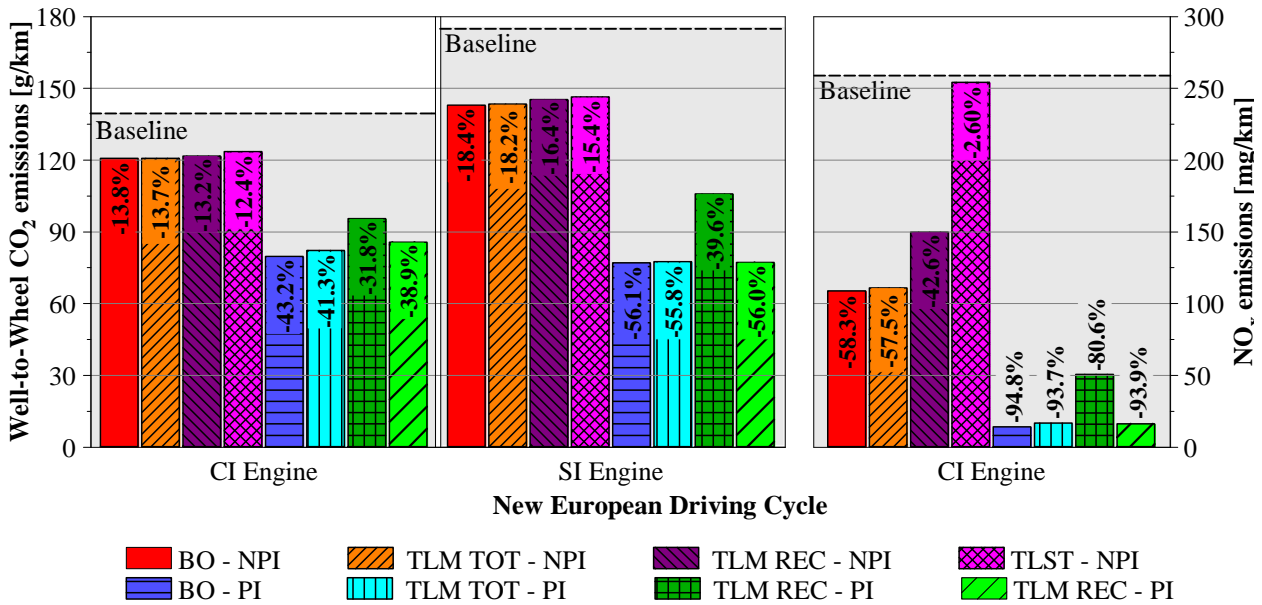
Figure 4.16 – PHEV Real-Time Optimizers: Well-to-Wheel CO₂ emissions and NOₓ emissions (NEDC)

Figure 4.16 shows an overview of the well-to-wheel CO_2 emissions and NO_x emissions obtained along the NEDC. The gray background represents the baseline condition of the conventional vehicle and the bars in red and blue (with horizontal lines hatch) report the benchmark optimization (see Fig. 4.8). The real-time optimization shows an overall good match with respect to the benchmark.. The TLM-TOT results to be the best real-time optimization strategy with close performance to the BO: the difference, in terms of CO_2 and NO_x reduction is less than respectively 1.5 %, in the case of the not plug-in, and 5 %, in the case of the plug-in. The TLST achieves reductions in terms of fuel consumption close to the TLM-TOT (about 2% more in the case of the not-plug PHEVs), instead is not suitable for the minimization of the NO_x emissions. Possible improvements could be achieved introducing another term in its control equation (Eq. 3.27) that would enhance the ICE load point shift:

$$P_{ICE} = P_{req,cs} + P_{Inertia} - c_2 \cdot \left(SOC - SOC^*_{target}\right) + \mathbf{c_3} \cdot \left[\mathbf{P_{ICE,BSNO_{x,min}}} - \mathbf{P_{req,el}}\right] \tag{4.5}$$

The drawback of this solution would be the necessity of a third calibration parameter and therefore a higher computational effort.

The real time optimizers worsen in the case of the plug-in PHEVs. This is due to the adoption of a too simplified operating strategy, that does not considered the range extender feature of the plug-in HEVs. Figure 4.17 shows the typical trend of the battery SOC of a plug-in hybrid in a real-world application. Two are the main phases:

➢ **Charge Depleting mode**: the hybrid powertrain exploit the electric energy accumulated in the battery until a lower threshold ($SOC_{CS,start}$, in the figure) is reached

➢ **Charge Sustaining mode**: no net battery energy consumption is allowed ($SOC_{end} = SOC_{CS,start}$). The system works as a not plug-in HEV.
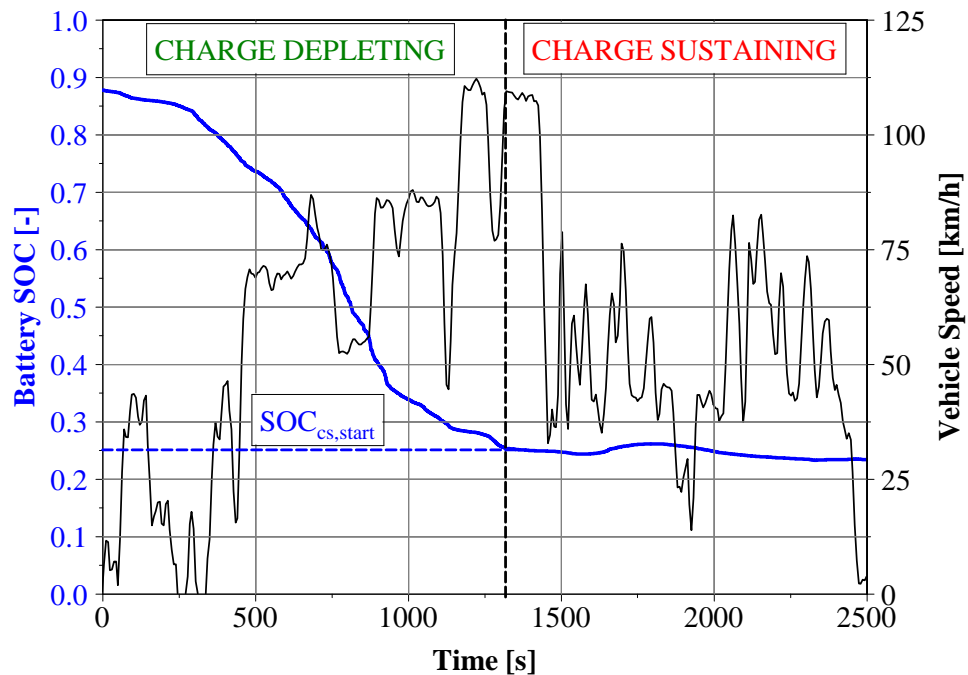
Figure 4.17 – Plug-In HEV: charge depleting and charge sustaining modes

The $SOC_{SC,start}$ is a key parameter, since it indentifies the instant at which the charge sustaining mode is activated. Regarding the charge depleting mode, two main operating strategies can be implemented:

➢ **Only electric mode**: the powertrain is allowed to work only in electric mode (if no technological constraint requires the switching-on of the engine). This mode has a straightforward implementation and it assures, in real world conditions, to exploit with the maximum priority the battery energy content

➢ **Hybrid mode**: the powertrain works in hybrid mode. It is required a double optimization of the Operating Strategy: one for the charge depleting hybrid mode and one for the charge sustaining hybrid mode. The number of calibration parameters and, therefore, also the computational effort is highly increased. This method allows the maximum potentiality of fuel consumption and NO_x emissions minimization

The first approach, that employs the only electric mode during charge depleting, has been implemented. As mentioned, it was necessary to consider a supplementary calibration parameter that defines the SOC at which the system switches from only electric to charge sustaining mode. This methodology guarantees good performance and, on average, *reduced of one third the difference between the real-time optimizers and the benchmark*. This improvements is even more remarkable in the case of the Artemis Urban Cycle. For further improvements, the hybrid mode during charge depleting should be taken into consideration.

Figure 4.18 shows an overview of the well-to-wheel CO_2 emissions for the Artemis cycles. The gray background represents the baseline condition of the conventional vehicle and the bars in red and blue (with horizontal lines hatch) report the benchmark optimization (see Fig. 4.10)
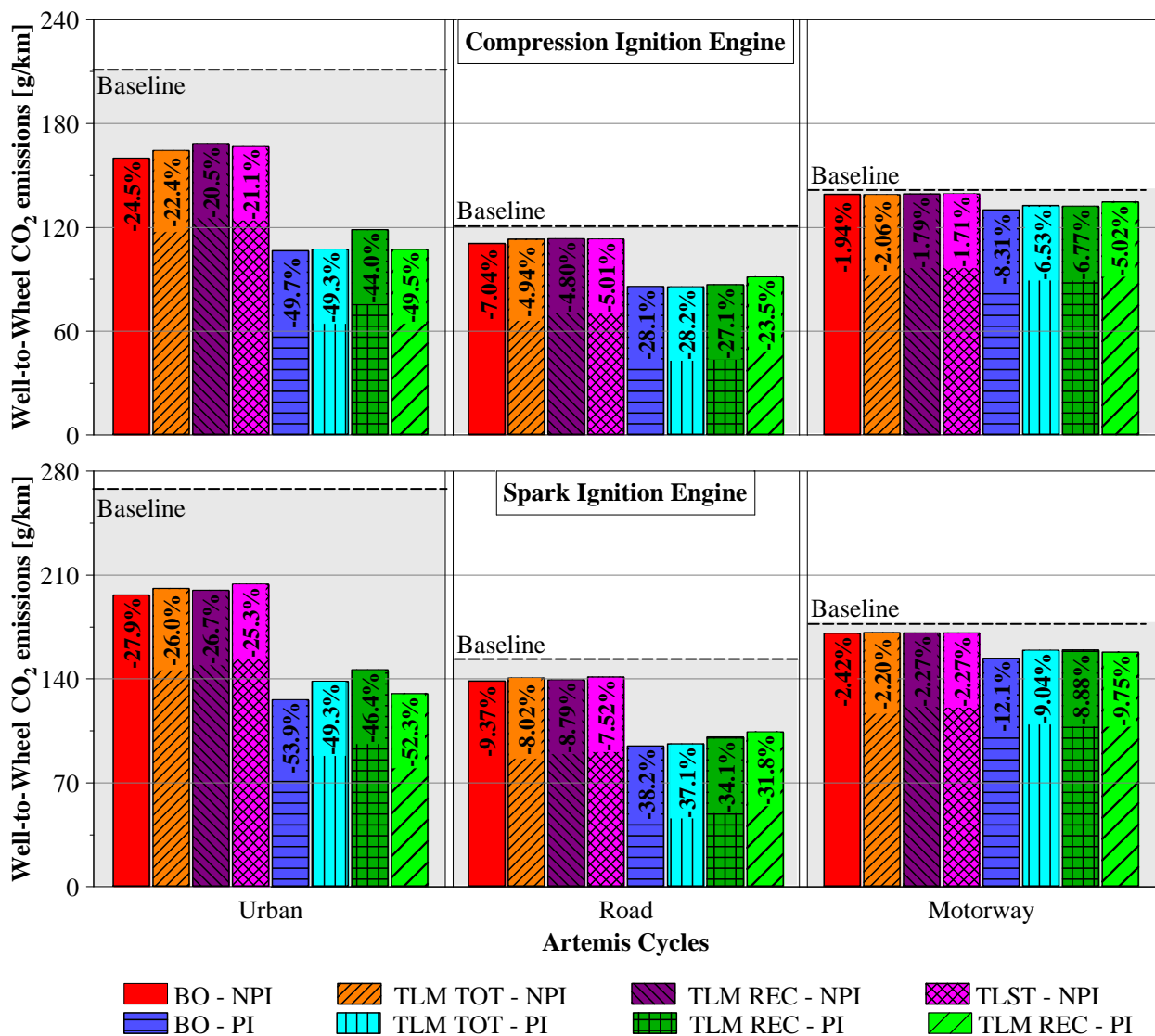
Figure 4.18 – PHEV Real-Time Optimizers: Well-to-Wheel CO$_2$ emissions (Artemis Driving Cycles)

The evaluation of the real-time optimizer and the benchmark is comparable to what examined along the NEDC. In general the TLM-TOT is the best real time optimizer, even if the TLM-REC performs slightly better in the case of the not plug-in SI engine PHEVs. Finally, as mentioned, the plug-in PHEVs show a higher difference between the benchmark and the real-time optimizers, underling the necessity of a more complete operating strategy (see Fig. 4.17)

Before examining the SHEV, it should be underlined that the both real-time optimizers can be implemented in real-world applications, provided calibration parameters (c_1-c_5 for the TLM and c_1, c_2 for the TLST) are adapted to the mission profile. The coefficients should be initially calibrated on the basis of a reference driving cycle (dashed red line in Fig.s 4.19, 4.20), which is estimated from the available route information (destination, traffic conditions, …) and from the driving style of the end-user. A second route, referred to as "Achieved Cycle" (solid blue line), shows the actual progress of the driving pattern.
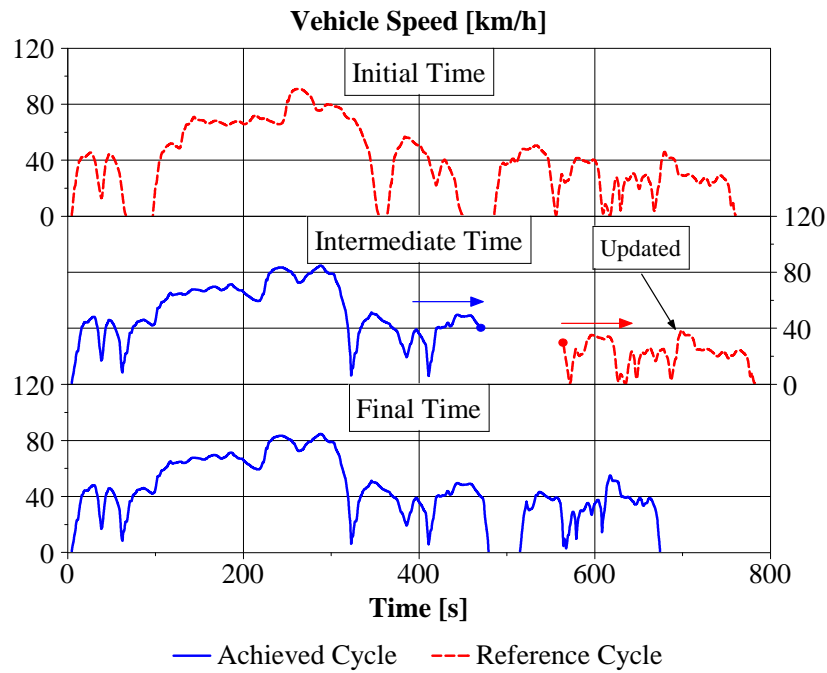
Figure 4.19 – PHEV Real-Time Optimizers (TLM TOT): reference and achieved driving cycles in a real-world application

The real-time optimizer recalculates the c-vector for the remaining part of the (reference) cycle at regular time intervals. This speed profile can also be updated on the basis of on-time traffic information (see intermediate plot in Fig. 4.19).
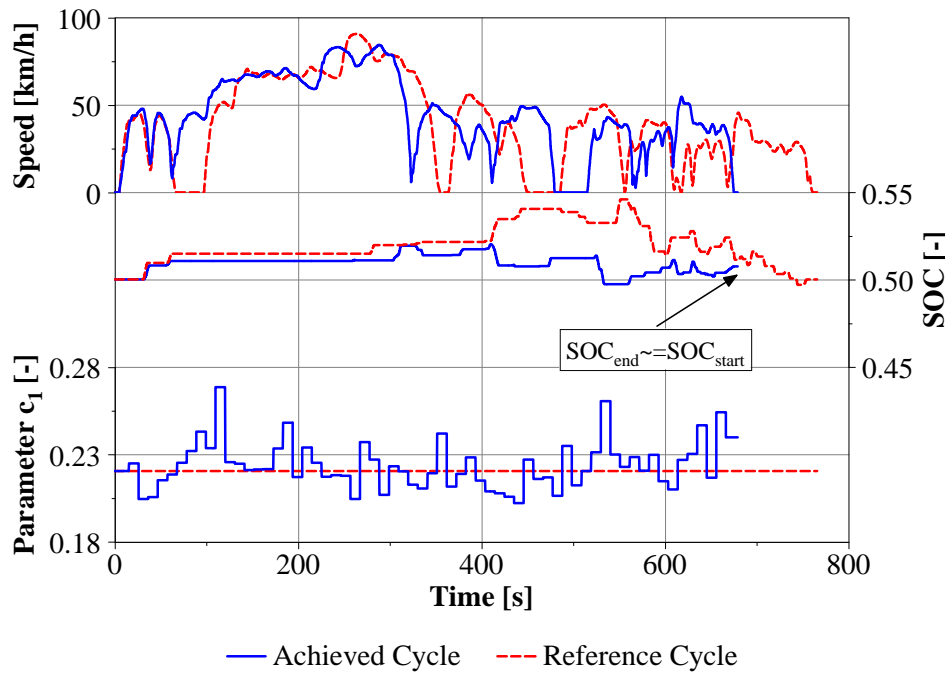
Figure 4.20 – PHEV Real-Time Optimizers (TLM TOT): tuning of coefficient c_1 during a real-world application

As example, the lower graph in Fig. 4.20 shows the time history of c_1, obtained by recalibrating the c-vector every 10 seconds. The on-time correction of the c-coefficients results to be essential in order to achieve the largest possible reduction in terms of fuel consumption and pollutant emissions and a final SOC close to the target. However, the GA solver, here adopted, is not suitable for direct implementation on vehicle control units: low-throughput methods have to be employed, such as the so-called "golden-section" search approach.

4.2 Series Hybrid Electric Vehicle

In Series Hybrid Electric Vehicles, there are two Electrical Machines (EMs) connected through a power converter. One electric machine (EM2) mainly features as generator, in order to convert the mechanical power supplied by the engine into electrical power. It is also employed in motor mode in order to start the engine. The other electric machine (EM1) works as traction motor, converting the electric power from the battery and/or generator into mechanical power. The result is a double degree of freedom for the operation of the engine: both the load and the speed are independent on the driving condition. As assumption, the system ICE+EM2 works along its Optimal Operating Points (OOPs), according to Eq. 3.14a, for the fuel consumption minimization, and Eq. 3.14b, for the NO_x emissions minimization.

The speed of the engine is set as optimization parameter, whereas the engine power level is defined through the Optimal Operating Point maps (for further details, please refer to Fig. 3.11) and the battery operation derives from Eq. 3.13.

4.1.1 Benchmark Optimizer

As far as the benchmark optimizer is concerned, the same number of independent variables, and total population were defined as in the case of the PHEV, resulting with a comparable computational effort.

Figure 4.21 shows the time histories of the battery and e-motor EM1 electric power (respectively blue solid line and dashed red line) and the battery SOC (green dash-dot line) along the NEDC cycle for all the analyzed series hybrid vehicles and obtained with the benchmark optimizer.

In the case of the compression ignition engine, without plug-in feature and with M_{fuel} as target (top left graphs in Fig. 4.21), virtually no load point shift strategy is adopted and the battery absorbs electric power only during deceleration phases (regenerative braking). The only exception are the weak engine positive load point shifts in the 70 km/h and 90 km/h speed plateaus of the EUDC. The energy stored in the battery during the regenerative braking and positive LPS of the extra-urban phase, is used to run the electric machine in motor mode mainly at low speed and at low/medium load, whereas the share of electric assist is negligible during high-required torque phases. Therefore, as in the case of the not plug-in CI engine PHEV, the electric machine predominantly drives the vehicle in pure electric mode. Being a not plug-in hybrid, a zero net usage of the battery is achieved: $SOC_{end}=SOC_{start}$.

In the case of the spark ignition engine, without plug-in feature and with M_{fuel} as target (intermediate left graphs in Fig. 4.21), the operating strategy, in overall, is comparable to the one adopted in the case of the CI engine, even if a more intensive load point shift strategy is employed. The energy is stored in the battery during the regenerative braking and positive LPS phases and is used to run the electric machine in motor mode mainly at low speed and at low/medium load, whereas the share of electric assist is negligible during high traction torque phases.
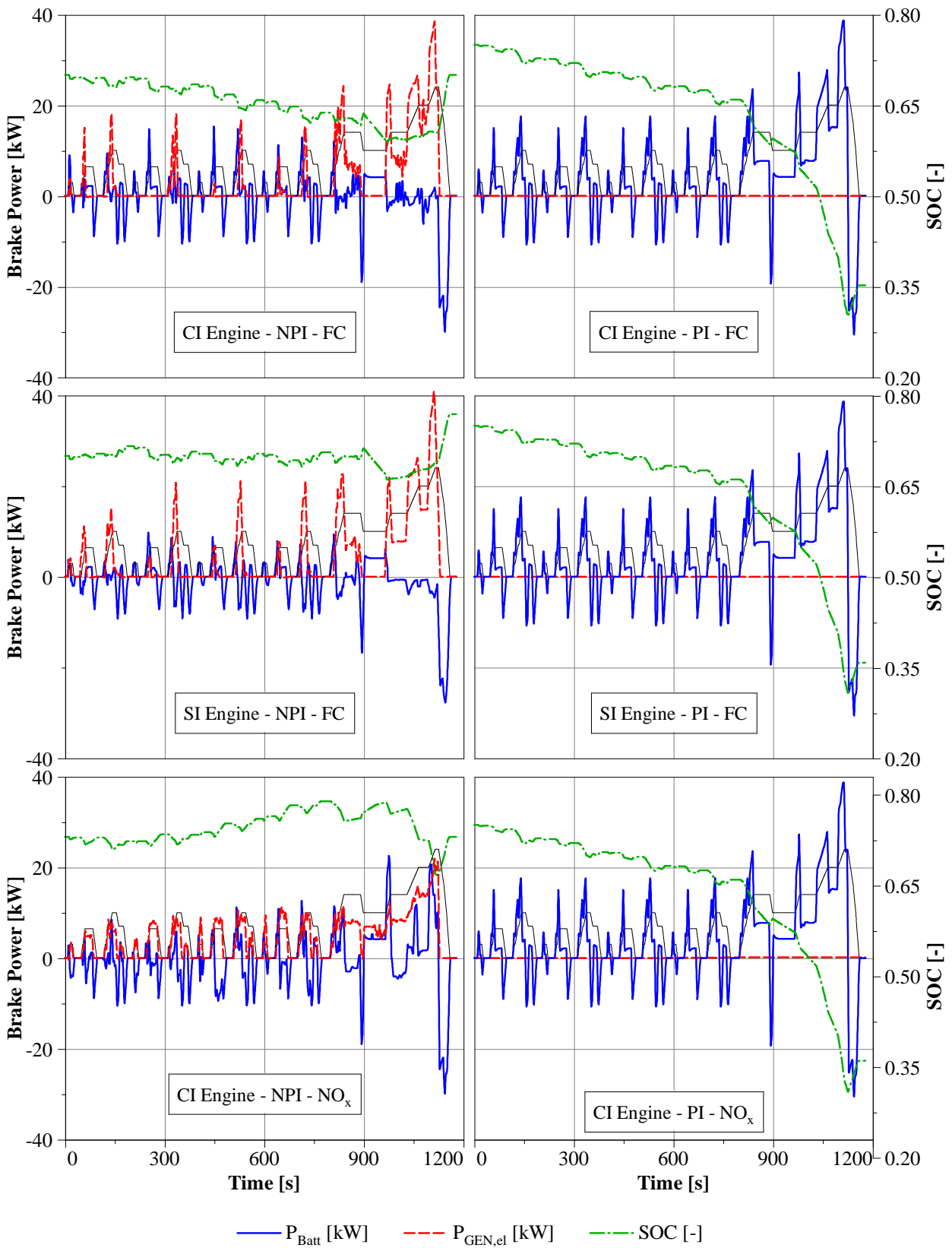
Figure 4.21 - SHEV Benchmark Optimizer: battery and EM electric power profiles and battery State Of Charge (NEDC)

4. Results and Discussion

Concerning the CI engine, not plug-in and with M_{NOx} as target (bottom left graph in Fig. 4.21), the electric machine works as generator during the speed plateaus, in order to shift the ICE load towards the minimum brake specific NO_x line (positive load point shift). As in the case of the PHEV, regenerative braking and positive LPS increase the battery energy content that is afterwards employed in the EUDC, to reduce the ICE load towards the minimum $BSNO_x$ condition..

As far as the plug-in SHEVs are concerned, (three graphs in the right column of Fig. 4.21), no maximum power limit is reached of the electric component (as in the case of the PHEV) and the battery can supply all the required electric power. Moreover, the battery energy content is sufficient for the whole driving cycle and the minimum SOC is never reached. The ICE-GEN system is not activated and the minimum fuel consumption and NO_x emissions are guaranteed at the cost of a net usage of the battery (i.e. $SOC_{start} \approx 0.75$ and $SOC_{end} \approx 0.3$).

SERIES HYBRID ELECTRIC VEHICLES   PARALLEL HYBRID ELECTRIC VEHICLES
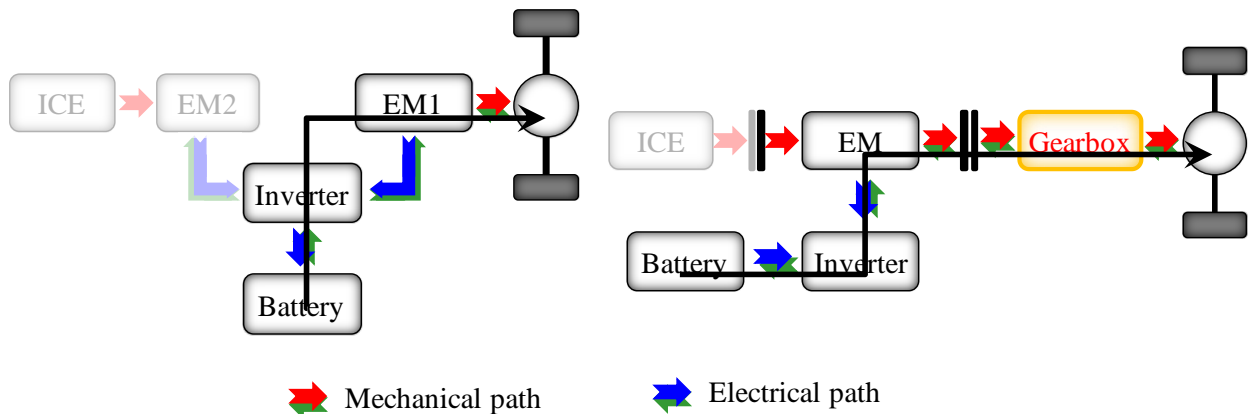
Figure 4.22 - SHEV vs PHEV: only electric mode

Moreover, *the electric mode of the SHEV guarantees a better system efficiency than in the PHEV architecture, because no gear box is installed*. This component is essential in the case of a traditional powertrain in order to couple the ICE performance to the vehicle requirements. In the case of high toque electric machines, it is not necessary and its inefficiency can be avoided (Fig. 4.22).

The considered gearbox is characterized by an average transmission efficiency of about 80-95% along the considered driving cycles (for further details, please refer to Section 3.1.4). Accordingly, in the plug-in PHEVs, even if the engine is switched-on, the final SOC is close to 0.25. Whereas the plug-in SHEVs, featured by the same battery and a slightly higher vehicle weight, work only in pure electric mode and the final SOC is higher than 0.30.

Figure 4.23 shows the time distribution of the engine operating points (as a function of BMEP and speed). The figures refer to the not plug-in SHEVs (right column) along the NEDC. They are compared to the conventional vehicles (left column), already evaluated with the PHEVs in Fig. 4.4. The color scale indicates the total time during which the engine operates on a specific point of the diagram.

85
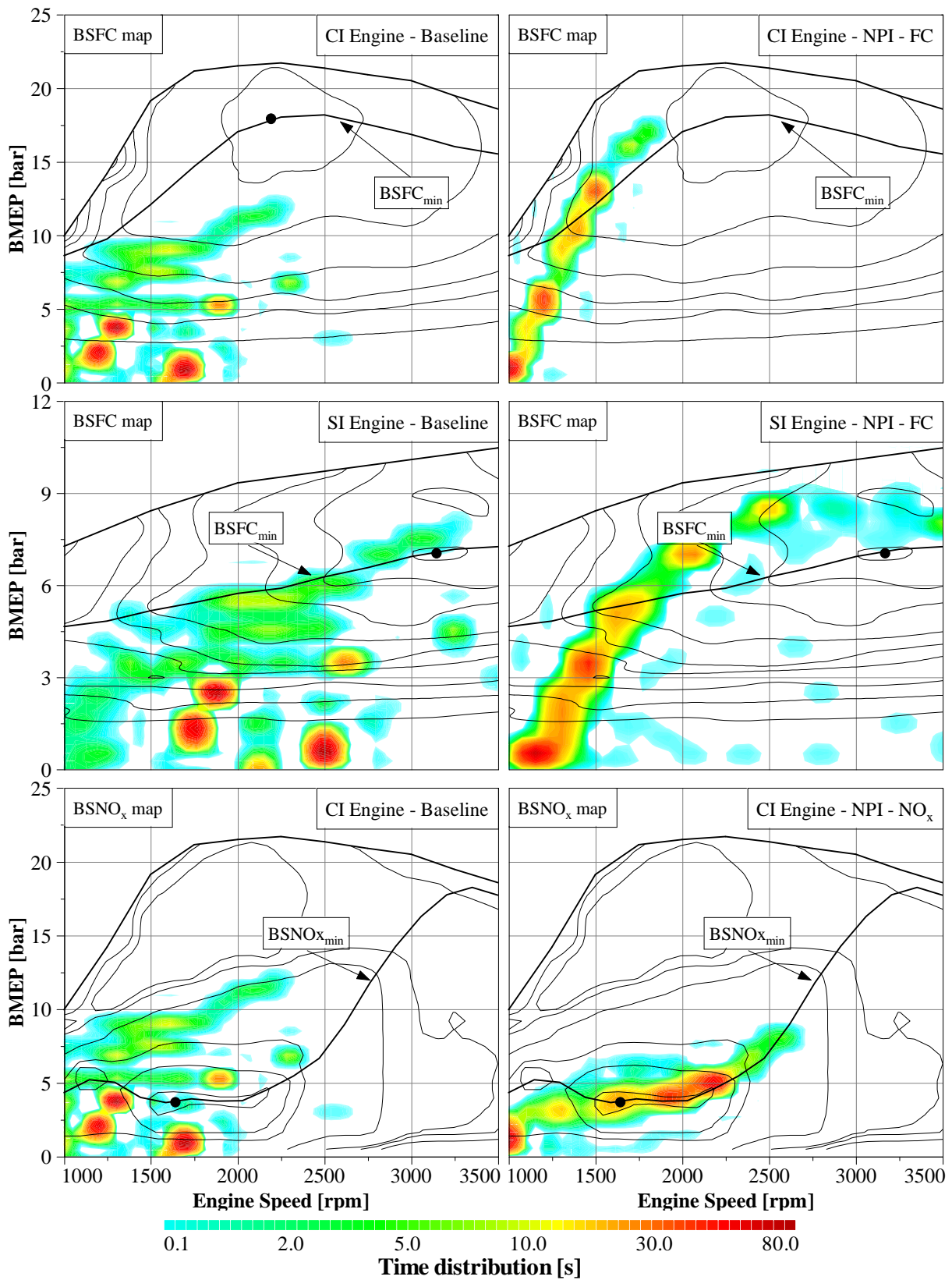
Figure 4.23 – SHEV Benchmark Optimizer: time distribution of the ICE operating points for the not plug-in HEVs compared to the baseline (NEDC)

The operating points of the three considered cases are located close to the minimum brake specific operating line. However, for two main reasons, they do not coincide with the engine optimum operating line:

1. *in order to avoid the so-called "big bang" behavior, a linear transition between the motoring condition and the optimum operation is introduced as limitation to the engine output power. Such a linear restriction works between the idle speed (zero output power of the engine) and 1500 rpm for the CI engine with FC target, 1100 rpm for the CI engine with NO_x target, and 1700 rpm for the SI engine. This is a model assumption and further improvements should be achieved in a real vehicle applications, to obtain the best compromise between comfort and system efficiency*

2. the target of the operating strategy is to minimize the system fuel consumption or NO_x emissions, and it is not proper to consider the optimization of a single component (i.e. the engine). In particular, during the generation of the Optimum Operating Points the total engine-to-generator system was taken into consideration implying the definition of cubic OOP maps, function of engine-generator speed, engine equivalent temperature and engine-generator angular acceleration (for further details please refer to Eq.s 3.14a and 3.14b)

Table 4.2- SHEV, CI engine and not plug-in: variation of the total fuel consumption depending on the considered OOP maps (NEDC)

Case	CO_2 emissions [g/km]	Delta CO_2 emissions [%]
1. ICE - only hot - stationary	128.9	-7.7
2. ICE - stationary	125.0	-10.5
3. System - only hot - stationary	126.5	-9.4
4. System - stationary	120.4	-13.8
5. System - transient	119.6	-14.4
Baseline	139.7	-

In order to further underline the importance of defining a system optimization approach with three independent variables (ω_{ICE}, $\Delta\omega_{ICE}$ and θ_{ICE}), Tab. 4.2 reports the comparison of the fuel consumption of the not plug-in SHEVs with CI Engine along the NEDC. The following cases are considered:

1. optimization of the only engine efficiency in hot (no variation of the operating points of the ICE map is considered during the warm-up phase) and stationary condition (OPPs function of ω_{ICE})

2. optimization of the only engine efficiency in stationary condition (OPPs function of ω_{ICE} and θ_{ICE})

3. optimization of the total system (engine+generator) in hot and stationary condition (OPPs function of ω_{ICE})

4. optimization of the total system (engine+generator) in stationary condition (OPPs function of ω_{ICE} and θ_{ICE})

5. optimization of the total system (engine+generator) in transient condition (OPPs function of ω_{ICE} and θ_{ICE}). This is the actually adopted methodology.

Table 4.2 shows how, the approach simplification comes together with a decline in the FC performance. The transient behavior of the ICE-GEN system has a limited influence: this is partially due to the modest speed and load transients that characterize the NEDC. In case of real-world driving cycles, a higher impact is expected. The system overview results to be more important and it is responsible of about 2% in the fuel economy improvement: this factor is strongly dependent on the engine and generator efficiency maps. Finally, also the ICE warm-up (i.e. θ_{ICE}) represents a main aspect and it has to be considered, in order not to compromise the FC reduction.

Referring to Fig. 4.23, it is straightforward the effect of the series hybrid architecture on the operation of the ICE. The engine can work completely independently on the profile requirement due to the electrical transmission and the operating areas result to be completely different with respect to the conventional vehicle. Concerning the fuel consumption target (top and intermediate graphs in Fig. 4.23) the operation of the both engine at low load and high speed is avoided. The engine tends to follows the required electric power of the NEDC, in order to avoid the battery losses, with a resulting slightly uniform distribution of the operating points along the optimum operating line. In the case of the SI engine the load point shift strategy, underlined in Fig. 4.21, results in the operating area above 2250 rpm. As far as the optimization of the NO_x emissions of the CI engine is concerned (bottom graphs in Fig. 4.23), a completely different operating strategy with respect to the previous ones is implied. As already shown in Fig. 4.21, a remarkable engine load point shift strategy is implemented in order to allow the engine to work on its lowest $BSNO_x$ conditions. As in the case of the PHEV, this is a consequence of the low engine power related to the $BSNO_{x,min}$ point, much below the maximum power required during the NEDC. Moreover, the $BSNO_x$ is characterized by higher derivatives with respect to the load along the defined Optimum Operating Lines than the BSFC one (see Fig. 4.5):

$$abs\left(\frac{dBSNO_x}{dBMEP}\bigg|_{\omega_{ICE}=\omega_{ICE,OOLs}^*}\right) \gg abs\left(\frac{dBSFC}{dBMEP}\bigg|_{\omega_{ICE}=\omega_{ICE,OOLs}^*}\right) \tag{4.6}$$

Figure 4.24 graphically emphasizes this concept. In particular:

➢ the top plot shows the variation of the generator (ε_{GEN}, green dash-dot line), engine (ε_{ICE}, red dashed line) and total system (ε_{TOT}, engine + generator, blue solid line) efficiencies as a function of the engine-generator speed along the predefined optimum operating lines in hot and stationary conditions ($\theta_{ICE}=90°C$ and $\Delta\omega_{ICE}=0$ rpm/s)

➢ the bottom plot shows the variation of the generator efficiency (ε_{GEN}, green dash-dot line), the engine equivalent efficiency considering as input the NO_x emissions (ε_{NOx}, red dashed line, with an equivalent Q_{NOx} heating value of 220 MJ/kg)

$$\varepsilon_{NOx} = \frac{P_{ICE}}{P_{NOx}} = \frac{P_{ICE}}{\dot{m}_{NOx} \cdot Q_{NOx}} \qquad\qquad (4.7)$$

and the total system engine (NO_x) + generator efficiency (blue solid line) as a function of the engine-generator speed along the predefined optimum operating line in hot and stationary conditions (θ_{ICE}=90°C and $\Delta\omega_{ICE}$=0 rpm/s)

Figure 4.24- SHEV Benchmark Optimizer: ICE (FC and NO_x), GEN and total efficiency with respect to the engine speed along the OOLs (CI Engine – θ_{ICE}=90°C, $\Delta\omega_{ICE}$=0 rpm/s)

In the both cases the generator guarantees high efficiencies, ranging from 80% to 92%. In particular, for speeds above 1200 rpm (power limitation not active), it shows a very flat profile. Therefore, it has a minor influence on the total system efficiency. Regarding the engine, the energy efficiency is characterized by a flat trend, with no significant improvement after the threshold of the linear limitation. The engine reaches 38.5 % of best efficiency at about 2500 rpm.

As far as the NO_x emissions are concerned, the best operating points are located at 1100-1300 rpm and a significant reduction in the NO_x equivalent efficiency is implied for speeds above 1500 rpm. The total efficiency is a straight consequence of the previous two, being, in stationary conditions, the simple multiplication of the engine and generator efficiency. Figure 4.24 once more underlines how the engine is the predominant component in the overall powertrain efficiency.
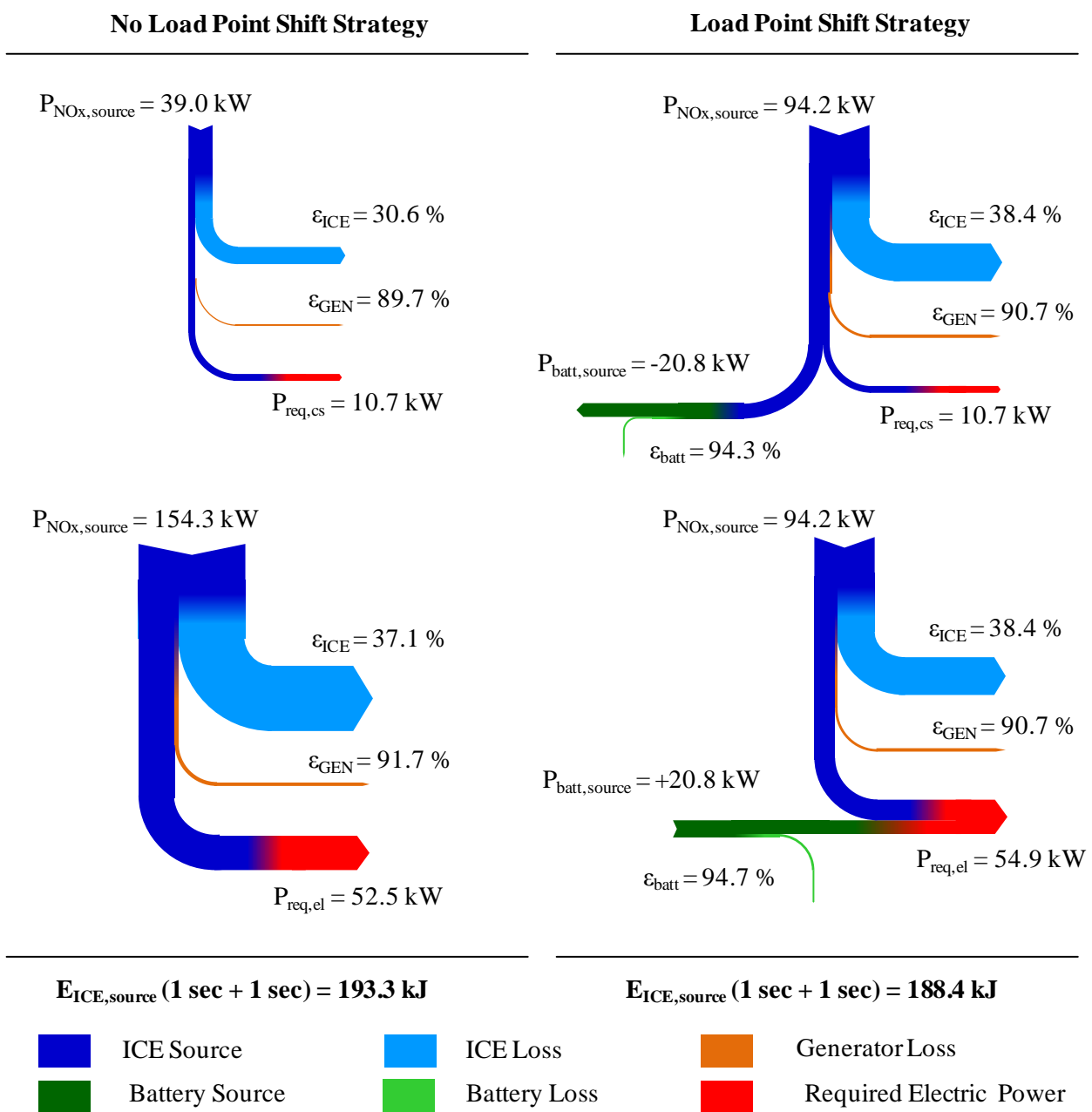
Figure 4.25 - SHEV Load point shift strategy for the minimization of the total fuel consumption (CI Engine – θ_{ICE}=90°C, $\Delta\omega_{ICE}$=0 rpm/s)

In order to give a detailed analysis of the powertrain performance during LPS phases, Fig. 4.25 and Fig. 4.26 show the Sankey diagrams of the considered SHEV. The load point shift strategy, to optimize the fuel consumption (right column of Fig. 4.25) and the NO_x emissions (right column of Fig. 4.25) is compared to the no LPS operation (left columns of Fig.s 4.25, 4.26). The Sankey diagrams entail all the hybrid powertrain components up to the inverter of the electric traction motor (for further details about the optimized hybrid system, please refer to Fig. 3.12)

Regarding the "No load point shift strategy" two operating points at respectively (ω_{ICE}=1250 rpm, P_{ICE}=10.7 kW) and (ω_{ICE}=3250 rpm, P_{ICE}=52.5 kW) are investigated. They are respectively

below and above the minimum BSFC point, that is located at about (ω_{ICE}=2050 rpm, P_{ICE}=36.1 kW) and they are characterized by an efficiency of the engine-generator system of respectively 27.5 % and 34.0 %. As in the case of the PHEV, it is considered that the engine works on each operating point for a time interval of 1 sec, with a resulting fuel energy consumption of:

$$E_{ICE,source}(baseline) = P_{ICE,source,1} \cdot \Delta t + P_{ICE,source,2} \cdot \Delta t = 39.0 \cdot 1 + 154.3 \cdot 1 = 193.3 \text{ kJ}$$

Concerning the load point shift strategy, right column in Fig. 4.25 reports a positive LPS (top diagram) and a negative LPS (bottom diagram) that allow the engine-generator system to operate on its optimal operating point (with the highest efficiency of 34.8 %). In the both cases the battery is characterized by an efficiency of about 94-95 %. As for the "No load point shift strategy", it is considered an operation of 1 sec for the two conditions, with a resulting zero net balance of the battery energy content:

$$E_{ICE,source}(LPS\ strategy) = P_{ICE,source,1} \cdot \Delta t + P_{ICE,source,2} \cdot \Delta t = 94.2 \cdot 1 + 94.2 \cdot 1 = 188.4 \text{ kJ}$$

An overall expense of 188.4 kJ of fuel energy source is obtained, slightly lower than in the case of the no LPS operation (-2.5%): *even if the load point shift strategy implies low improvements in the efficiency of the (CI engine & generator) system, it can guarantee an overall reduction in the fuel consumption due to the low losses of the battery component.* Moreover, the operating scheme proposed in Fig. 4.25, has to be only considered as a example: the operating strategy will more probably implement a positive load point shift strategy (top-right diagram) with an increase of the battery SOC coupled to a more widespread only electric mode.

Figure 4.26 shows the hybrid powertrain losses, up to the electric side of the traction e-motor, in the case of the NO_x minimization. Regarding the no LPS strategy, two operating points at respectively (ω_{ICE}=1000 rpm, P_{ICE}=1.3 kW) and (ω_{ICE}=1250 rpm, P_{ICE}=11.5 kW) are considered. In order to allow an efficiency overview through the Sankey diagrams, an equivalent Q_{NOx} heating value of 220 MJ/kg is employed (for further details, see Eq. 3.22a): the two operating points result to be characterized by a system equivalent efficiency of respectively: 16.9 % and 17.2 %. Considering that the engine works on each operating point for 1 sec:

$$E_{NOx,source}(baseline) = P_{NOx,source,1} \cdot \Delta t + P_{NOx,source,2} \cdot \Delta t = 6.2 \cdot 1 + 66.7 \cdot 1 = 72.9 \text{ kJ}$$

Concerning the load point shift strategy, the right column in Fig. 4.26 shows a positive LPS (top diagram) and a negative LPS (bottom diagram) that allows the engine to work close to its optimal operating point: (ω_{ICE}=1100 rpm, P_{ICE}=6.76 kW) with the equivalent efficiency of 43.1 %. In the both cases, the battery is characterized by an efficiency of about 95%. As for the conventional vehicle, it is considered an operation of 1 sec on the two operating conditions (with a resulting zero net balance of the battery energy content: $P_{batt,source}$=±4.6 kW):

$$E_{NOx,source}(LPS\ strategy) = P_{NOx,source,1} \cdot \Delta t + P_{NOx,source,2} \cdot \Delta t = 17.5 \cdot 1 + 17.5 \cdot 1 = 35.0 \text{ kJ}$$

It results an NO_x equivalent energy consumption of 35.0 kJ (*-81.9 % with respect to the no load point shift mode*), that proves, as in the case of the PHEV, *the importance of the (engine-generator) load point shift in order to allow a dramatic reduction in the total NO_x emissions.*

No Load Point Shift Strategy

$P_{NOx,source} = 6.2\,kW$

$\varepsilon_{NOx} = 20.5\,\%$

$\varepsilon_{GEN} = 82.2\,\%$

$P_{req,cs} = 1.3\,kW$

$P_{NOx,source} = 66.7\,kW$

$\varepsilon_{NOx} = 17.2\,\%$

$\varepsilon_{GEN} = 89.7\%$

$P_{req,el} = 11.5\,kW$

Load Point Shift Strategy

$P_{NOx,source} = 17.5\,kW$

$\varepsilon_{NOx} = 43.1\,\%$

$\varepsilon_{GEN} = 87.3\,\%$

$P_{batt,source} = -4.6\,kW$

$P_{req,cs} = 1.3\,kW$

$E_{batt} = 95.2\,\%$

$P_{NOx,source} = 17.5\,kW$

$\varepsilon_{NOx} = 43.1\,\%$

$\varepsilon_{GEN} = 87.3\,\%$

$P_{batt,source} = +4.6\,kW$

$\varepsilon_{batt} = 95.3\,\%$

$P_{req,el} = 11.5\,kW$

$E_{ICE,source}$ (1 sec + 1 sec) = 72.9 kJ

$E_{ICE,source}$ (1 sec + 1 sec) = 35 kJ

	NO$_x$ Source		ICE Loss		Generator Loss
	Battery Source		Battery Loss		Required Electric Power

Figure 4.26 - SHEV Load point shift strategy for the minimization of the total NO$_x$ emissions (CI Engine – θ_{ICE}=90°C, $\Delta\omega_{ICE}$=0 rpm/s)

As general comparison between the load point shift strategy of the SHEV and PHEV, the following guidelines can be drawn:

➢ *in the PHEV higher improvements in the engine efficiency can be obtained with respect to the ones achievable by the (engine-generator) system of the SHEV*. This is because, in the SHEV,

the (engine-generator) system is decoupled from the driving condition and it already works along the optimum operating line

➤ *in the Series Hybrid Electric Vehicle, the load point shift strategy implies the storage/absorption of the energy in/from the battery, involving to only battery losses ($\varepsilon_{Batt} \approx 94\text{-}95\%$). In the case of the PHEV also the electric machine is included in the electric line, with a resulting total electric efficiency of about $\varepsilon_{EM} \cdot \varepsilon_{Batt} \approx 80\text{-}82\%$.* This implies that the load point shift strategy is more effective in the case of the series architecture and a this technique is more extensively employed

➤ due to the higher derivative of the $BSNO_x$ with respect to the load (see Eq. 4.1 for the PHEV and Eq. 4.6 for the SHEV) than in the case of the BSFC map, *the NO_x optimization features a much more significant load point shift strategy than the optimization of the fuel consumption*
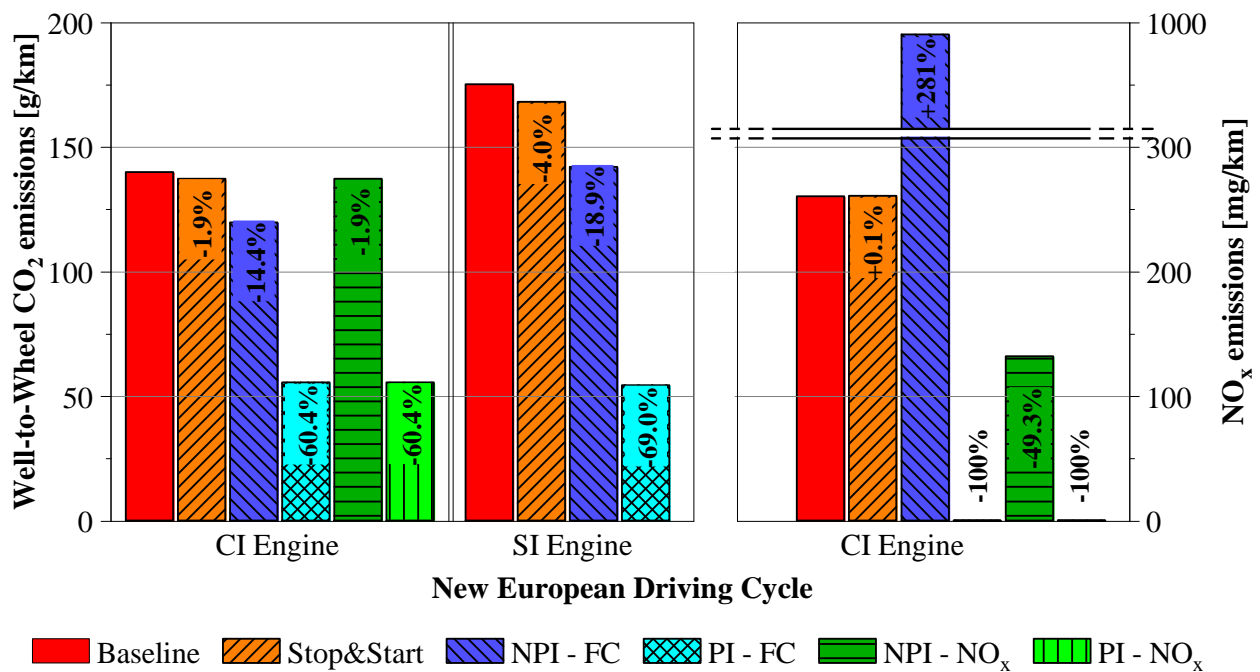
Figure 4.27 - SHEV Benchmark Optimizer: Well-to-Wheel CO₂ emissions and NOₓ emissions (NEDC)

Figure 4.27 reports an overview of the performance in term of well-to-wheel CO_2 emissions [g/km] (left diagram) and NO_x emissions [mg/km] (right diagram) along the NEDC for all the considered SHEV configurations. The baseline and the Stop&Start feature refers to the same conditions already mentioned in the analysis of the PHEV.

As far as the CO_2 emissions are concerned, the hybridization has a stronger impact in case of the SI engine, with a reduction of the CO_2 emissions, for the not plug-in, close to 20 %. This is a consequence of the high variation of the BSFC in the SI engine map (Fig.s 2.3). However, the not plug-in SHEV featured with the CI engine, due to the higher engine efficiency, performs lower CO_2 emissions (about 120 g_{CO2}/km).
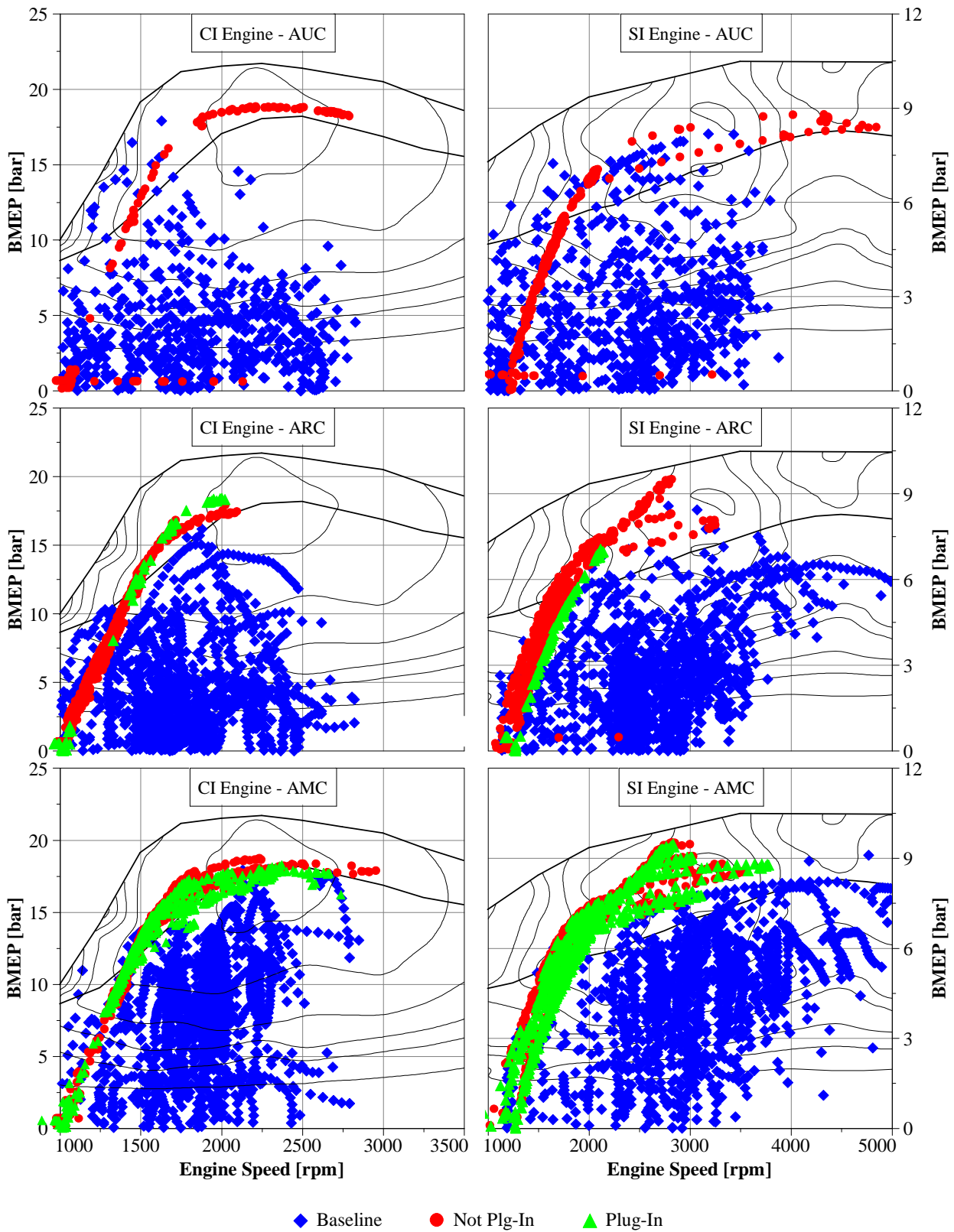
Figure 4.28 - SHEV Benchmark Optimizer: ICE operating points for the not plug-in and plug-in PHEVs compared to the baseline (Artemis Driving Cycles)

If the NO_x minimization is the target of the operating strategy, the fuel consumption is strongly compromised and about 2 % reduction in terms of CO_2 emissions is achieved. In the plug-in SHEVs, the battery energy content and the electric motor maximum power allow the vehicle to be driven completely in electric mode and the engine is never switched-on. As a consequence, the CO_2 emissions come only from the electric energy absorbed by the electric grid and no (local) NO_x emissions are released.

The SHEV was also simulated along the Artemis (Urban, Road and Motorway) driving cycles. Figure 4.28 compares the operating points of the baseline (conventional vehicle without Stop&Start feature) with respect to the plug-in and not plug-in SHEVs. The series hybridization allows a complete decoupling of the engine operating points with respect to the driving conditions. Therefore, low load - high speed conditions are completely avoided and the system (ICE+GEN) is forced to work on its best efficiency operating lines (please, refer to Eq. 3.14a).

Moreover, the operating point of the Series Hybrid Electric Vehicle are completely different with respect to the ones of the conventional vehicle. In the case of the Artemis Urban Cycle, the plug-in SHEV is able to drive the driving pattern in all electric mode and the engine is never switched-on.
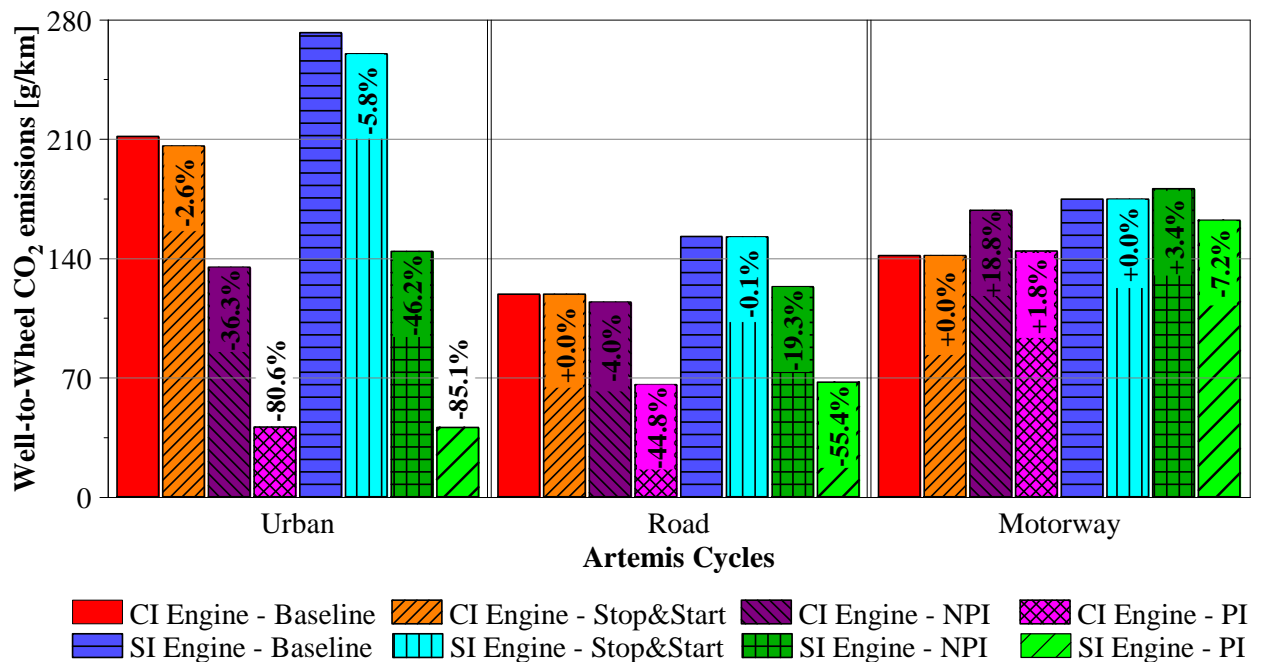
Figure 4.29 - SHEV Benchmark Optimizer: Well-to-Wheel CO₂ emissions (Artemis Driving Cycles)

Finally, Fig. 4.29 shows the wheel-to-well CO_2 emissions along the three Artemis Driving Cycles for all the SHEVs compared to the baseline (with and without Stop&Start feature). The baseline w/o S&S is considered as reference for the percentage reductions in the diagram: red bar for the CI engine and dark-blue bar with horizontal-line hatch for the SI engine. The higher is the average speed and the longer are the constant load time intervals (i.e. in the ARC, and even more, in

the AMC), the less impacting is the hybridization. Only a weak load point shift strategy is actuated and the only electric mode is not interesting.

The not plug-in SHEV ensures good performance in the case of the AUC, with a fuel consumption reduction of about 36 % and 46 % for respectively the CI and the SI engine. The improvements along the ARC are partially compromised and only in the case of the SI engine significant reductions are achieved. As far as the Motorway pattern is concerned, the SHEV shows even an increase in the fuel consumption with respect to the conventional vehicle. This is a result of the considered powertrain components and cannot be a general rule, however it underlines a main drawback of the SHEV architecture (Fig. 4.30). *The introduction of the electric transmissions, on one hand, decouples the engine operation from the driving conditions allowing improved performance in the low speed and low load cycle. On the other hand, it generally implies more losses in the transmission, that can exceed the improvements of the engine efficiency* (especially in motorway conditions).

CONVENTIONAL VEHICLES   SERIES HYBRID ELECTRIC VEHICLES

$\varepsilon_{Gb} \approx 80\text{-}95\ \%$

$\varepsilon_{EM2} \approx 85\text{-}97\ \%$ $\varepsilon_{EM1} \approx 85\text{-}97\ \%$

ICE → Gearbox →

ICE → EM2 — Inverter — EM1 →

$\varepsilon_{INV} \approx 97\ x\ 97\ \%$

Battery

Mechanical path   Electrical path
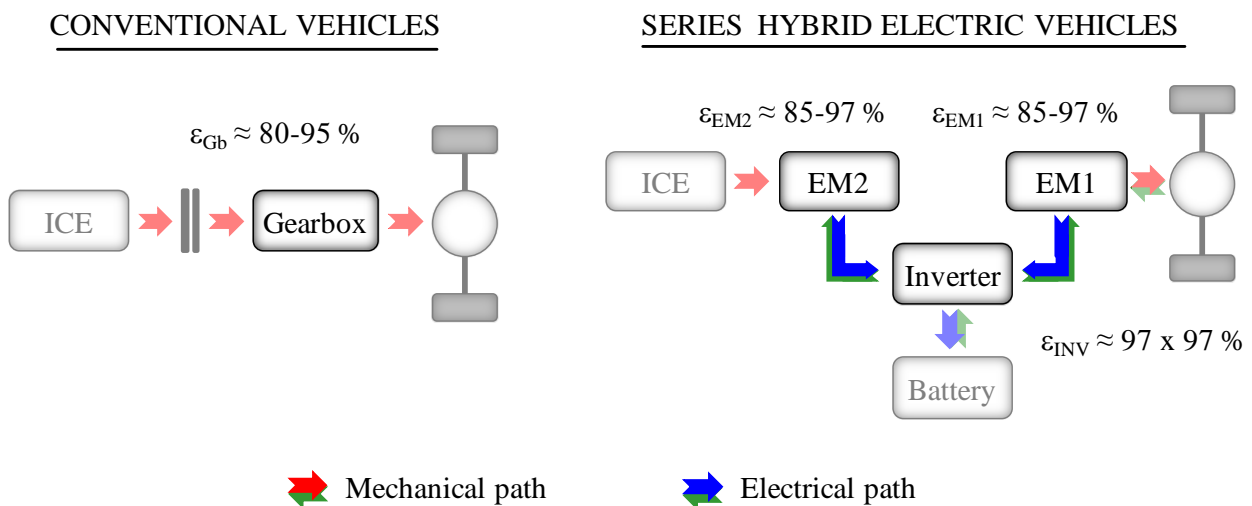
Figure 4.30 – Comparison of the SHEV electric transmission and a conventional vehicle mechanical transmission

Concerning the plug-in feature, it is more effective in the case of the AUC whereas its benefits are compromised for the highway route. As in the case of the NEDC, the CI engine performs the lowest CO_2 emissions even if its hybridization and the plug-in feature guarantee lower improvements.

4..2   Real-time optimizers

Figures 4.31-4.33 show the time histories of the battery electric power of the both real-time optimizers and benchmark optimizer (respectively blue solid line and dashed red line) and the battery SOC of the real-time optimizers (green dash-dot line) along the New European Driving Cycle for the not plug-in series hybrid vehicles. All the three Real-time operating strategies are considered.
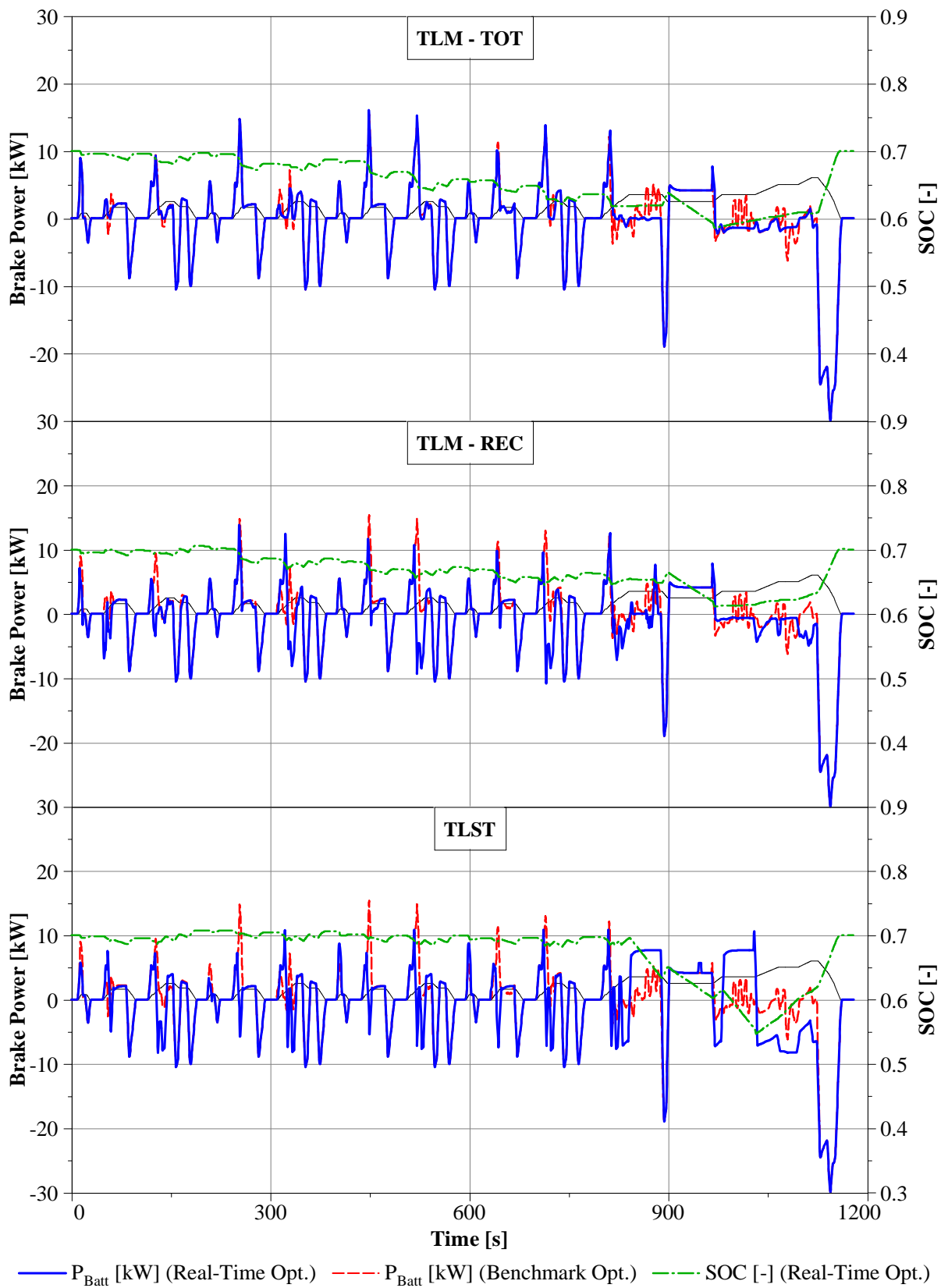
Figure 4.31 – SHEV Real-Time Optimizers: battery electric power profiles and battery State Of Charge for the CI engine with M$_{fuel}$ as target (NEDC)
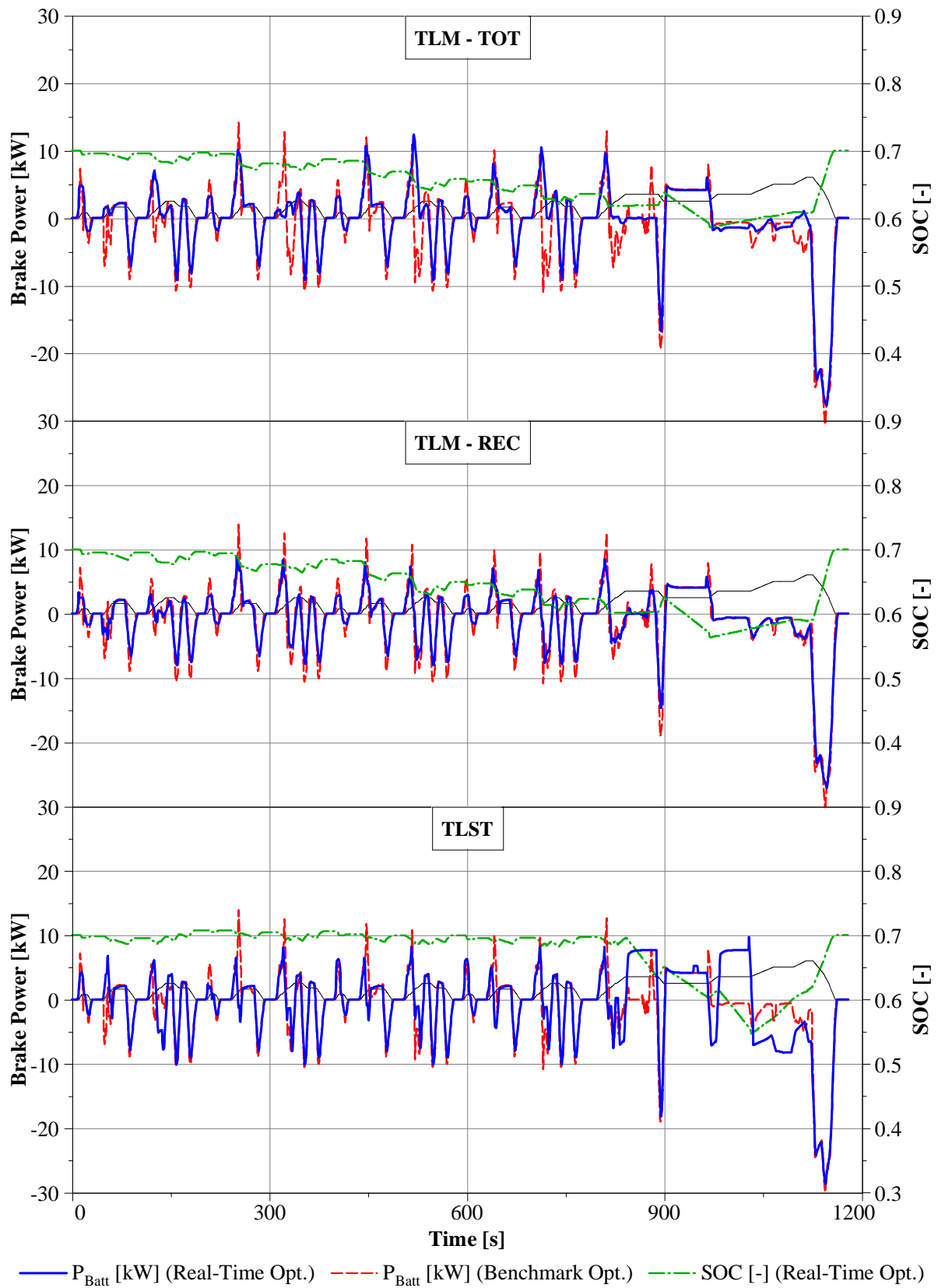
Figure 4.32 – SHEV Real-Time Optimizers: battery electric power profiles and battery State Of Charge for the SI engine with M$_{fuel}$ as target (NEDC)
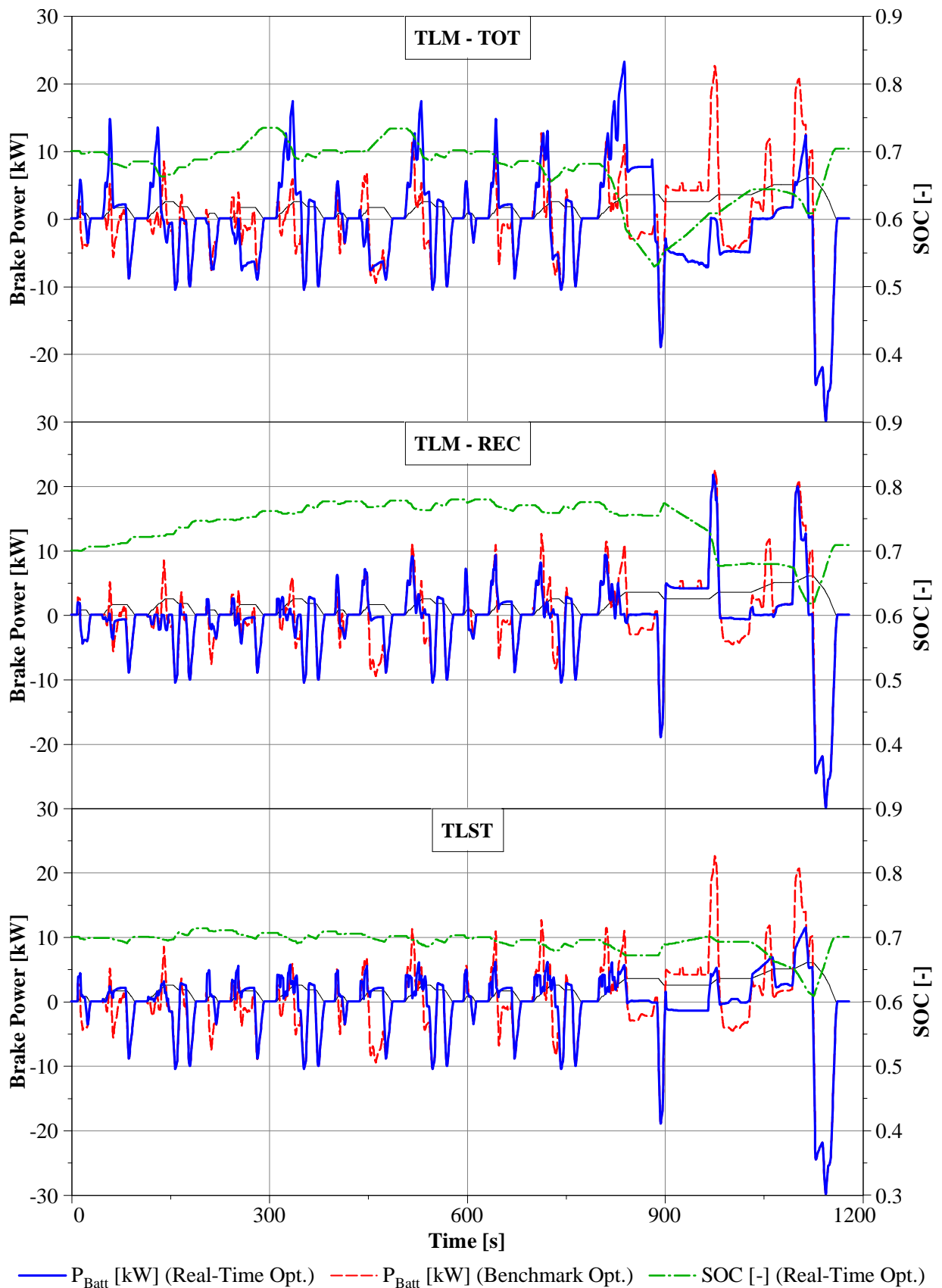
Figure 4.33 – PHEV Real-Time Optimizers: battery electric power profiles and battery State Of Charge for the CI engine with M$_{NOx}$ as target (NEDC)

In the case of the CI engine with M_{fuel} as target (Fig. 4.31), the three operating strategies have a comparable behavior: low load driving conditions are driven in pure electric mode and, in general, only a reduced load point shift strategy is implemented (negative load point shift in the extra-urban phase). The TLM TOT is the operating strategy that is more close to the BO, whereas the TLST shows many divergences, proving its more simplified approach. Accordingly, result the Well-to-Wheel CO_2 emissions reported in Fig. 4.34: the TLM TOT and the TLM REC feature a close reduction of the fuel consumption with respect to the baseline (respectively -11.8 % and -11.0 %) as the benchmark (-14.4 %), whereas the TLST guarantees more limited improvements (-7.5 %).

The SI engine without plug-in feature (Fig. 4.32) shows a similar behavior to the CI engine, with a more intense load-point shift strategy during the EUDC. The TLM REC (-26.4 %) is the real-time operating strategy that performs more closely to the benchmark (-27.5 %), the TLM TOT is slightly higher (-22.4 %), whereas the TLST have a worse behavior (-11.2 %).

Concerning the CI engine with NO_x as target (Fig. 4.31), the three real time optimizers show the same trend: the electric energy is generally stored during low load and constant speed phases to be used during the vehicle transients. However, the battery power time histories are completely different depending on the real time optimizer and the TLM REC operates most similarly to the BO. The results in terms of NO_x emissions (Fig. 4.34) shows that the TLM REC and the TLM TOT (respectively -44.3 % and -43.6 % NO_x emissions respect to the conventional vehicle) perform closely to the benchmark (-49.3 %), whereas the TLST guarantees poorer improvements (-36.7 %).
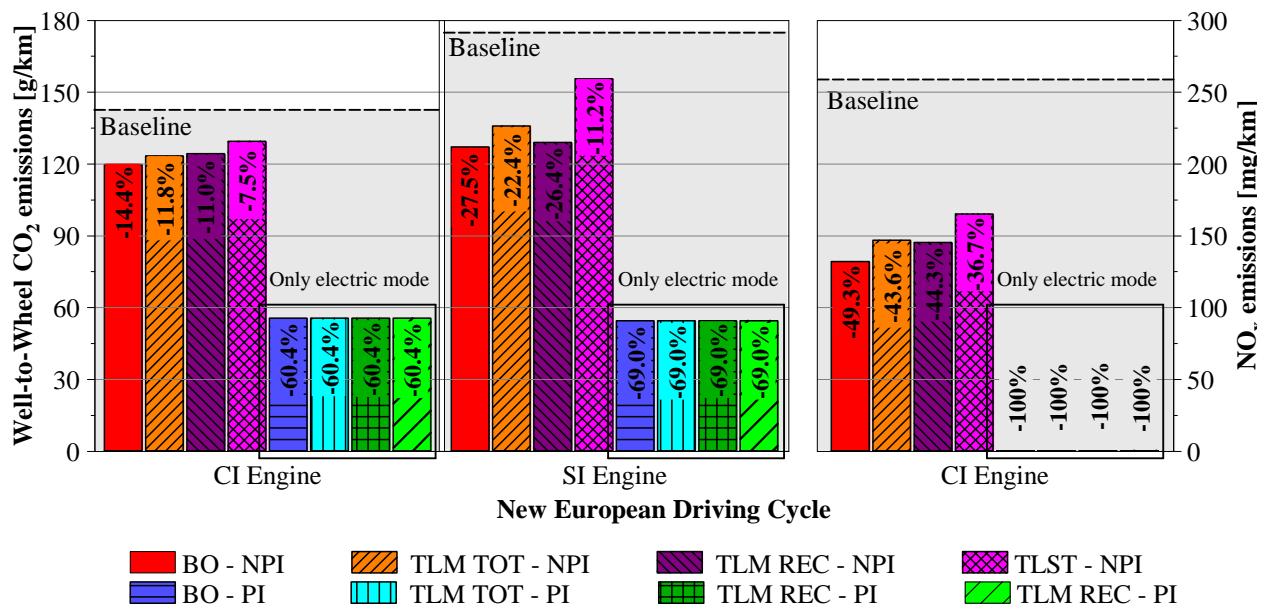
Figure 4.34 – SHEV Real-Time Optimizers: Well-to-Wheel CO_2 emissions and NO_x emissions (NEDC)

As mentioned, Fig. 4.34 shows an overview of the well-to-wheel CO_2 emissions and NO_x emissions along the NEDC, adopting the real-time optimizers. The gray background represents the baseline condition of the conventional vehicle without Stop&Start feature and the bars in red and blue (with horizontal lines hatch) quantify the benchmark optimization (see Fig. 4.27). The not

plug-in SHEVs have been already analyzed. Concerning the plug-in SHEVs, all the real-time optimizers converge to the same solution of the benchmark: only electric mode for the whole NEDC. As a consequence, the same well-to-wheel CO_2 emissions are produced for all the four optimizers (from the net electric energy usage) and no (local) NO_x emissions are released.

Figure 4.35 shows an overview of the well-to-wheel CO_2 emissions for the Artemis Driving Cycles, using the real-time optimizers. As in the case of Fig. 4.34, the gray background represents the baseline condition of the conventional vehicle and the bars in red and blue (with horizontal lines hatch) illustrate the benchmark optimization (see Fig. 4.29)
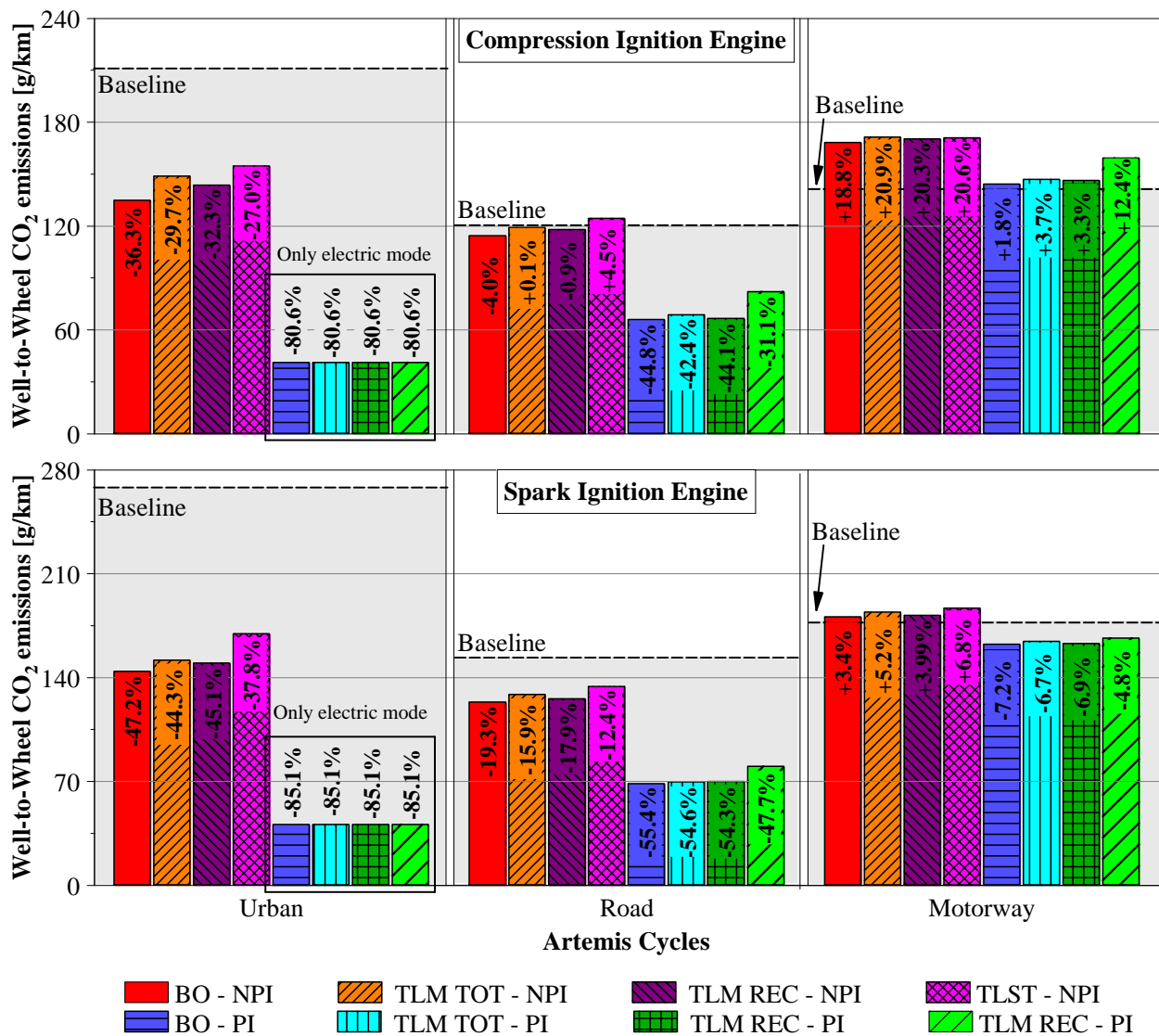
Figure 4.35 – SHEV Real-Time Optimizers: Well-to-Wheel CO_2 emissions (Artemis Driving Cycles)

The evaluation of the real-time optimizer and the benchmark is comparable to what examined for the NEDC. In general the TLM-REC is the best real time optimizer, even if the TLM-TOT guarantees only slightly lower performance. The difference between the three optimizers is

mainly shown in the case of the urban cycle, during which the hybridization is effectively employed. Only negligible differences can be noticed for the Artemis Motorway Cycle, during which the effect of the electrification is compromised.

4.3 Application to a case study: "Belt Alternator Starter with CI engine"

Within a research project in collaboration with GMPT-E (Torino), a parallel-hybrid diesel powertrain featuring a high-voltage Belt Alternator Starter (BAS) (Fig. 4.36) has been investigated ([23, 31, 32]). This mild-hybrid system is relatively simple and economic, and it enables regenerative braking, Stop&Start, ICE load point shift and electric power assistance. The optimization approaches have been performed over the New European Driving Cycle (NEDC) and Artemis Cycles (for the only fuel consumption), in order to reduce the total fuel consumption and NO_x emissions as well as to diminish the local Combustion Noise (CN) peaks. Due to intellectual property reasons, all the results are expressed in non-dimensional terms.
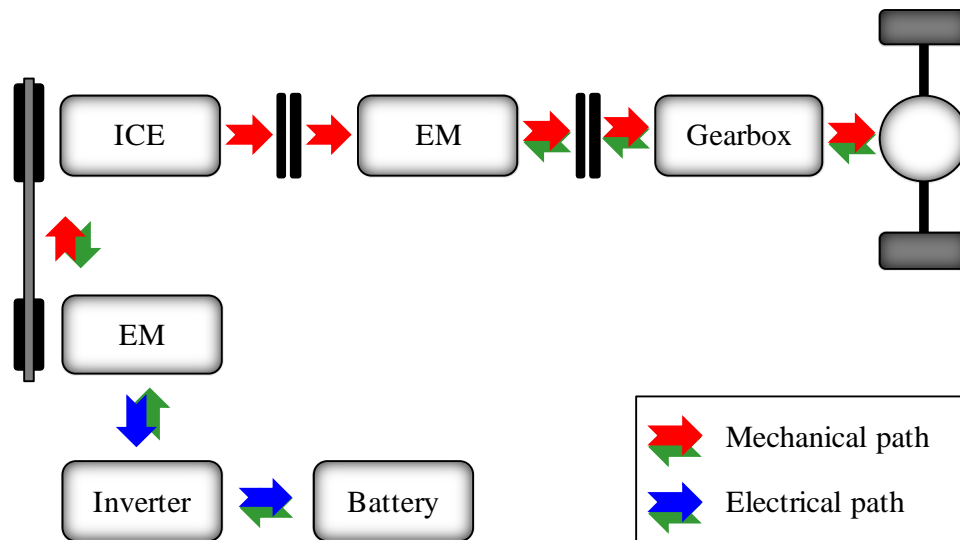
Figure 4.36 - BAS: drivetrain layout

As far as the regenerative braking is concerned, due to the position of the electric machine (upstream with respect to the ICE), dedicated model settings were required. In particular, only in the case of engaged clutch, regenerative braking is possible: in this case, the braking torque is split between the EM (P_{EM}) and the mechanical brakes (P_{brakes}), according to the following equation:

$$P_{req,cs}=P_{ICE}-I_{ICE}\omega_{ICE}\dot{\omega}_{ICE}+\varepsilon_{belt}\left(P_{EM}-I_{EM}\omega_{EM}\dot{\omega}_{EM}\right)+\varepsilon_{dl}\left(P_{brakes}-I_{dl}\omega_{wheel}\dot{\omega}_{wheel}\right) \qquad (4.8)$$

where ε_{dl}, I_{dl} represent respectively the efficiency and the inertia of the driveline from the clutch to the wheels; P_{brakes} is the mechanical power of the traditional brakes.

Regenerative braking is actuated when the accelerator pedal is released and/or when the driver presses the brake pedal. When the accelerator pedal is released, braking power is pushed up to the so-called driveability limit, which is a function of the gear number (left diagram in Fig. 4.37). When the enhanced motor brake is not capable of achieving the required braking power, the virtual driver actuates the braking pedal. The EM contribution to the total braking power (right diagram in Fig. 4.37) is a function of the Brake Pedal Position (BPP) and of the vehicle speed. Aggressive braking, significantly reduces the recoverable amount of kinetic energy due to the need to prioritize electronic stability and anti-lock braking system operations (both mechanically actuated). The

mechanical-to-electrical braking share has been implemented according to the safety and comfort requirements of the vehicle and has not been considered a free optimization parameter.
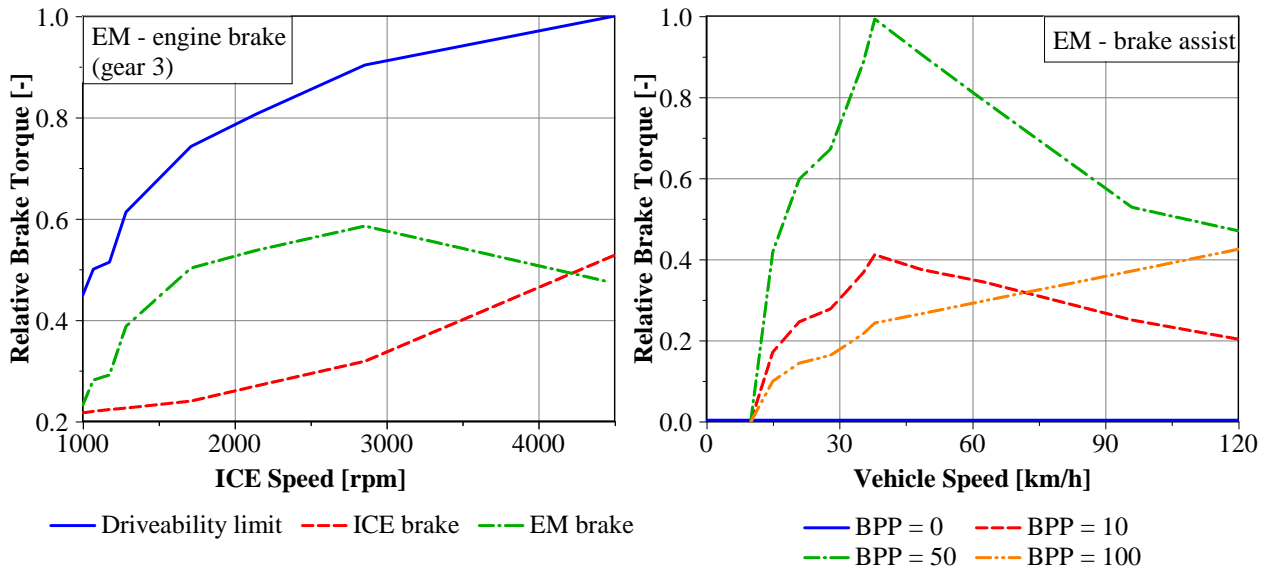
Figure 4.37 - BAS: braking torque with EM only (gear number 3) and EM assistance to mechanical braking torque

Figure 4.38 shows the $BSNO_x$ and BSFC maps with respect to the engine operating points during the NEDC for the normal production vehicle. The color scale indicates the total time the ICE operates at a specific point of the diagram. The minimum BSFC operating line results to be significantly above the minimum BSNOx one. Accordingly, a minimization of the NO_x and FC will lead to completely different operating strategies.
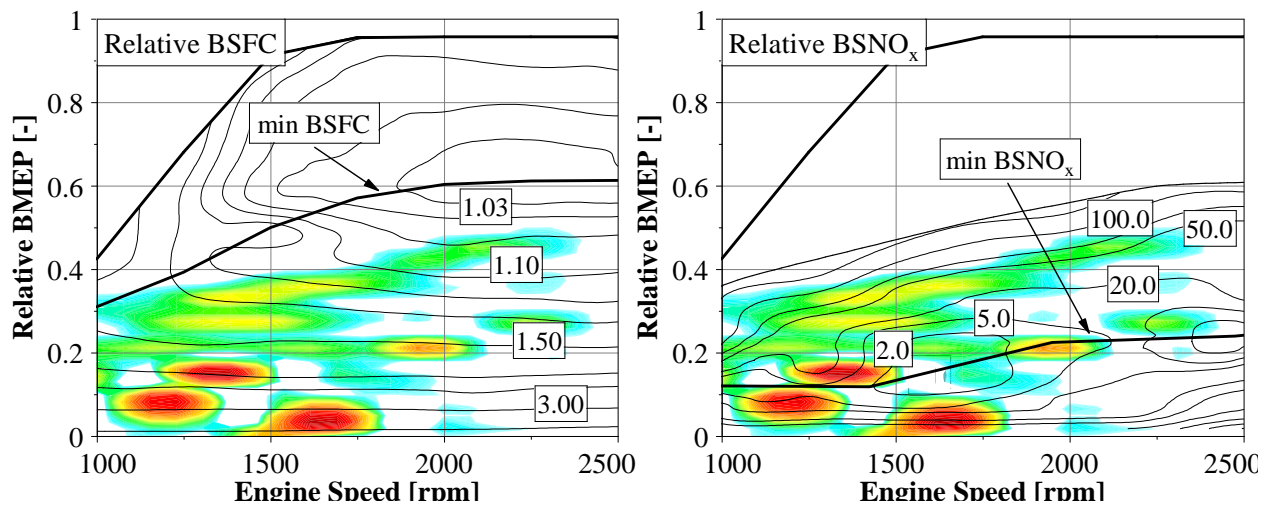
Figure 4.38 - BAS: time distribution of the ICE operating points during the NEDC for the normal production vehicle-

Both the Benchmark Optimizer (BO) and the real-time optimizer based on the Minimization of the Total Losses (TLM) were applied for the optimization of the BAS hybrid operating strategy. The only difference with respect to the methodology above illustrated, is the introduction, in the

equation of the real-time optimizer (Eq. 3.17a), of a term that considers the combustion noise. The resulting equation is:

$$P_{tot,l} = c_1 \cdot P_{ICE,l} + c_2 \cdot P_{T(ICE),l} + c_3 \cdot P_{EM\&Batt,l} + c_4 \cdot P_{SOC,l} + c_5 \cdot P_{NOx,l} + c_6 \cdot P_{CN,l}$$

$$\text{with: } P_{l,CN} < \frac{k_6}{b} \rightarrow P_{l,CN} = 0; \tag{4.9}$$

where b coefficient is applied to scale $P_{l,CN}$ and makes it comparable to the other losses, whereas c_6 represents the threshold below which combustion noise losses are no longer considered in the operating strategy.

$P_{CN,l}$ is characterized by a different structure than the other losses, since the target no longer represents the best reduction in the total consumption or total emissions. $P_{CN,l}$ has to guarantee a combustion noise as close as possible to the target, i.e. to minimize the difference between the target and the actual combustion noise multiplied by a scale factor and expressed in power law (Fig. 4.39):

$$P_{CN,l}^* = 10^{0.1 \cdot \left(CN_{Actuated}[dB] - CN_{Target}[dB] \right)} \tag{4.10}$$

The target combustion noise is defined according to the specific vehicle application, as a balance between driving comfort and the fuel economy. In Fig. 4.39 it is underlined how the operating points in a Diesel engine that are more difficult to calibrate from a CN point of view, are characterized by intermediate loads and low speeds. These operating points exhibit a large premixed fraction, due to the combination of high EGR rates, quite high fuel injected quantities and high residence time ([32, 34]).
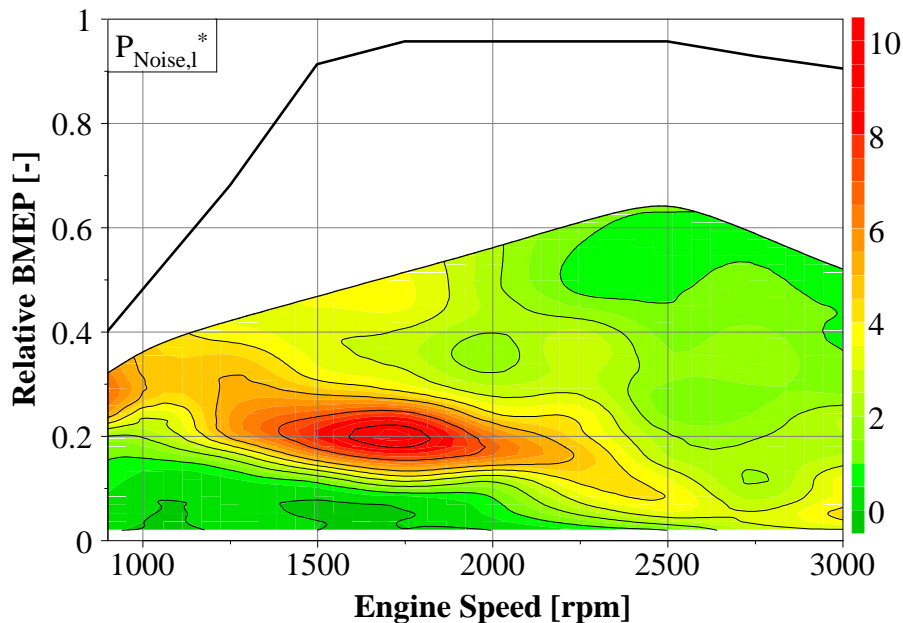
Figure 4.39 - BAS: $P_{Noise,l}^*$ map

Moreover, combustion noise is perceived in a different way depending on the vehicle speed: aerodynamic drag and tire rolling are irrelevant at low speeds and combustion noise has a stronger

impact. Eq. 4.10 considers a relationship of the CN loss with respect to the vehicle speed through an exponential coefficient a, in order to stress the low vehicle speed conditions. It is assumed that the combination of tire rolling and aerodynamic noises are dominant over combustion noise above a limit speed $v_{car,max}$ ([32]), therefore no optimization of the combustion noise is actuated for velocities higher of this threshold.

if $v_{car} \leq v_{car,limit}$

$$P_{CN,l} = \left(1 - \frac{v_{car}}{v_{car,limit}}\right)^a P_{CN,l}^* \tag{4.11}$$

else

$$P_{CN,l} = 0$$

As for the fuel consumption and the NO_x emissions also the CN has been experimentally assessed at the ICEAL of the "Dipartimento Energia" of Politecnico di Torino. The combustion noise was estimated by means of the AVL Indicom software, on the basis of the output of KISTLER 6058A41 piezoelectric transducers installed at the glow-plug seats ([36]). *The average difference between the experimental and calculated data resulted to be less than 0.2 dB.*

4.3.1 Fuel Oriented Optimization

One of the main advantages of introducing a Belt Alternator Starter in a conventional powertrain, is the possibility of downsizing the Internal Combustion Engine. In this way, more favorable operating conditions are guaranteed for the ICE during most everyday driving missions, including type-approval procedures. In a separate research program, 20% reduction in the engine displacement was selected, leading to a fuel consumption improvement of about 4.0 % along the New European Driving Cycle ([23]).

Even though the downsized engine does not cause any particular driveability or comfort concern under steady operating conditions and slow acceleration transients, a certain level of torque lag may occur under aggressive accelerations from low engine speed. The introduction of a Belt Alternator Starter results to be very attractive.

Figure 4.40 shows that the combined ICE+BAS output torque for the downsized engine (green dashed line with triangles) significantly exceeds the required target (red dashed line with diamonds). Therefore, further potential decontenting of the turbocharger, including the adoption of a fixed geometry turbine, could be considered.

As far as the benchmark optimizer is concerned, Fig. 4.41 shows the time histories of the relative electric machine brake power (i.e., the actual EM power normalized with respect to the EM rated power; solid blue line) and battery SOC (dashed red line) along the NEDC.
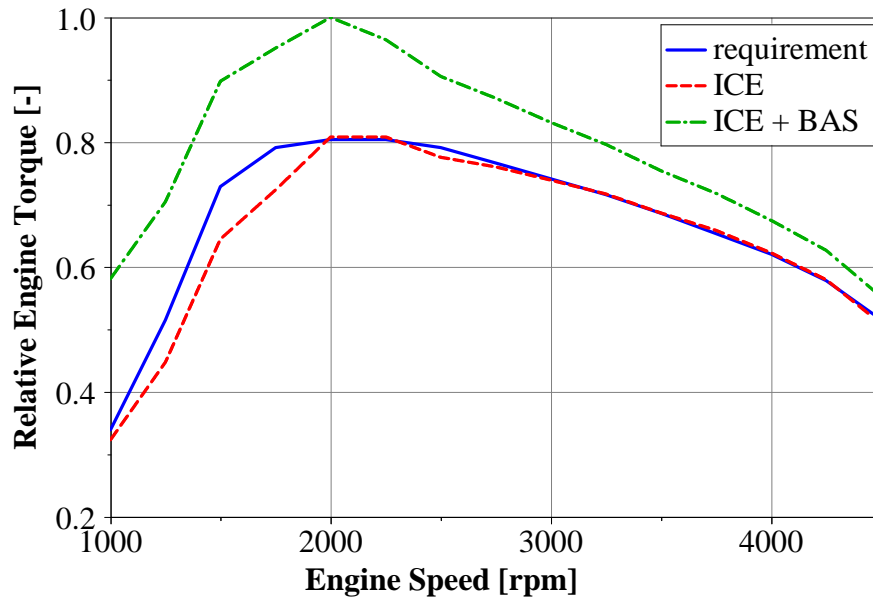
Figure 4.40 – BAS: Performance comparison

The electric machine works as generator during deceleration phases only (regenerative braking). The energy stored in the battery pack is used to run the EM as a motor mainly at low speed and at low/medium load, whereas the share of electric assist is negligible during the extra-urban phases. It is worth recalling that the NEDC is characterized by low load conditions, therefore the ICE would always operate below the minimum BSFC line (Fig. 4.38) in case of a conventional vehicle architecture. Therefore, when the negative LPS mode is actuated, the ICE load is reduced even further, and this leads to a decrease in the FC, even though the ICE efficiency deteriorates.
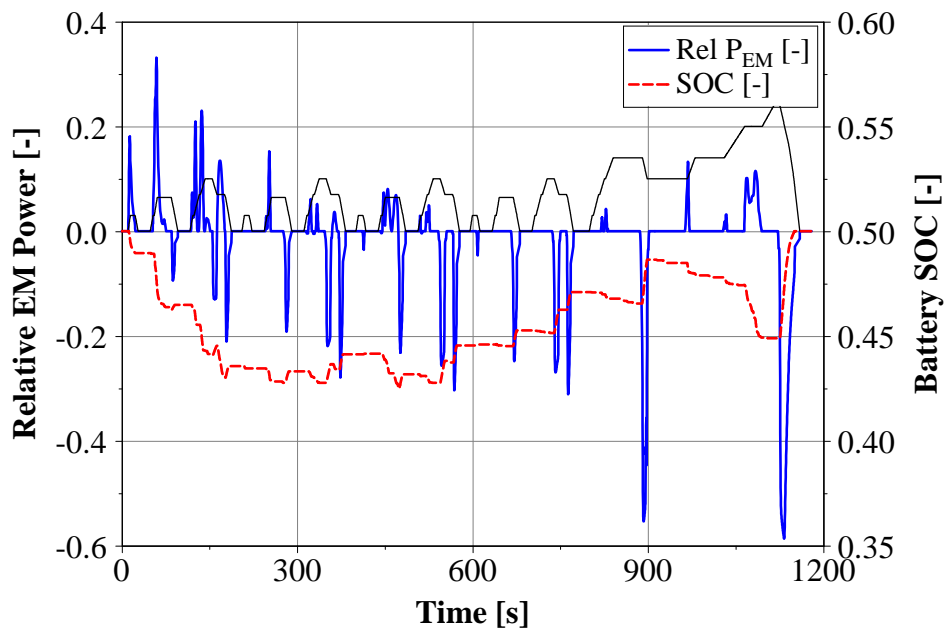
Figure 4.41 – BAS (FC target): EM power profile and battery SOC of the benchmark optimizer (NEDC)

The vehicle performance has also been estimated along the Artemis cycles (Urban, Road and Motorway, Fig. 3.8). With reference to Tab. 3.2, the AUC is characterized by longer standstill periods and by higher peak and mean vehicle acceleration values. As a consequence, the Stop&Start feature is very effective (5.5% of fuel saving with respect to the conventional vehicle) and the optimizer successfully exploits the electrically assisted propulsion (about 10% reduction of FC due to only the hybrid mode).
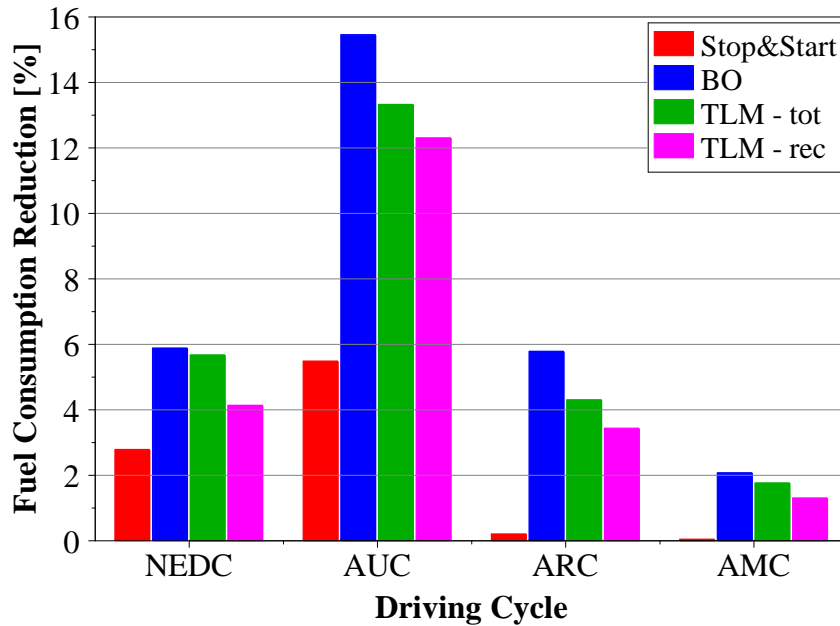
Figure 4.42 – BAS (FC target): M_{fuel} reduction for the considered driving cycles and operating strategies (with TLM- tot: total ICE losses; TLM- rec: recoverable ICE losses)

Figure 4.42 shows the comparison of the fuel consumption reduction in the case of the four driving cycles analyzed and the three hybrid operating strategies adopted: the benchmark optimizer, the TLM with total ICE losses (Eq. 3.18a) and the TLM with recoverable ICE losses (Eq. 3.18b). For the BAS configuration, the total ICE losses are the ones that guarantee the closer fuel consumption reduction to the benchmark optimizer.

4.3.2   NO$_x$ Oriented Optimization

The benchmark optimizer time-histories of the relative electric machine brake power and SOC are plotted in Fig. 4.43 for the NEDC. The electric machine works as a generator over the speed plateaus, in order to shift the ICE load up, towards the minimum brake specific NO$_x$ line (positive load point shift). It has been found that the energy stored in the battery during the positive LPS is approximately three times the energy recovered during regenerative braking.

The energy saved in the battery is used mainly to support the vehicle performance at low speed during the first urban cyle. Regenerative braking and positive LPS are then applied to increase the SOC. However, the upper limit of SOC is already reached during the last ECE, showing that the storage capacity of the battery is a limiting factor and should be incremented to allow further improvements in terms of NO$_x$ emissions.
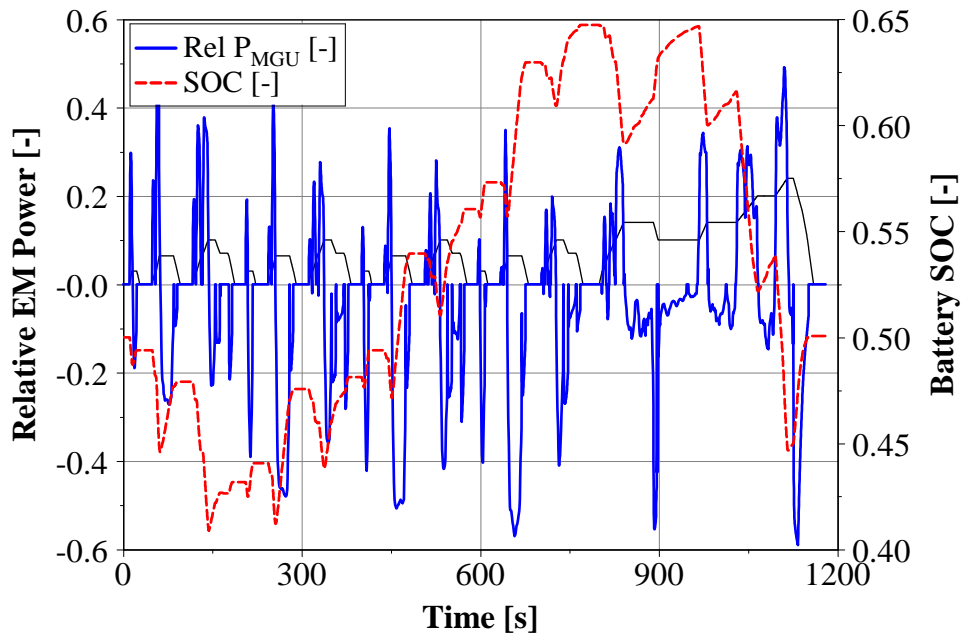
Figure 4.43 – BAS (NO$_x$ target): EM power profile and battery SOC of the benchmark optimizer (NEDC)

In the EUDC part, the MGU works mainly in motor mode to shift the ICE load downwards. The benchmark optimizer indicates an overall NO$_x$ reduction of 54% (Fig. 4.44) with respect to the conventional vehicle and a slight penalty in terms of fuel consumption.
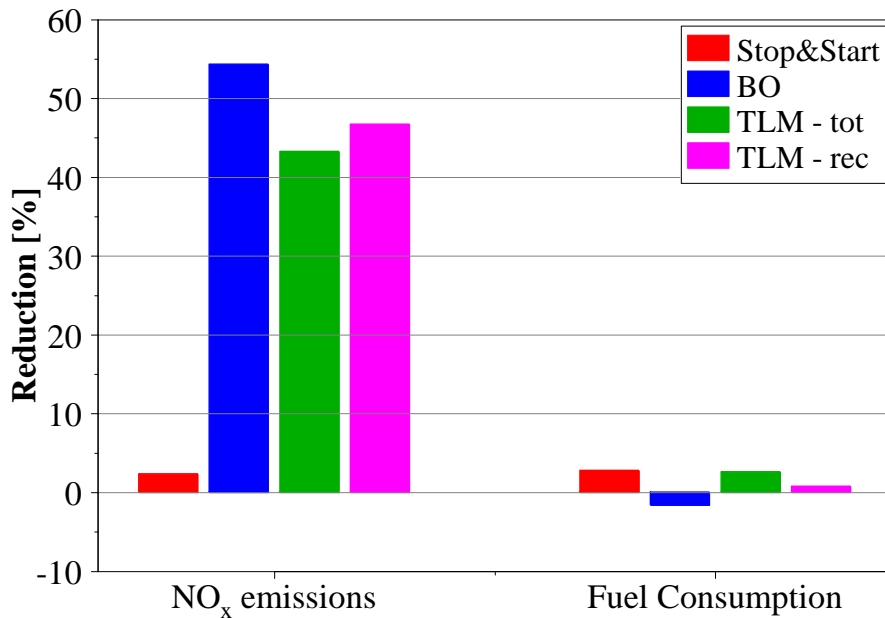
Figure 4.44 – BAS (NO$_x$ target): M$_{fuel}$ and M$_{NOx}$ reduction for the NEDC and the considered operating strategies (with TLM- tot: total ICE losses; TLM- rec: recoverable ICE losses)

During this project a less evolved approach for defining the NO$_x$ losses was taken into consideration:

$$P_{l,NO_x,tot} = \dot{m}_{NO_x} \tag{4.12}$$

This equation was missing the information of output brake power, essential in order to distinguish between operating points characterized by the same NO$_x$ emissions but different brake powers. Therefore, the recoverable formulation of the NO$_x$ losses (Eq. 3.22b) resulted to be more effective than the total NO$_x$ loss expression (Eq. 3.22a), allowing the shift of the ICE operating point toward the minimum BSNO$_x$ line and to making the EM to work as a generator in a more aggressive way (Fig. 4.44).

4.3.3 CN Oriented Optimization

A combustion noise oriented optimization has been carried out to reduce the peak values of the CN at low vehicle speeds (1st and 2nd gear) during the NEDC. Since the integral approach of the benchmark optimizer is not suitable to reduce the CN peaks locally, only the TLM optimizer has been applied.

Figure 4.45 reports the ΔCN time-histories for the baseline case and for three cases of CN optimization varying parameter v$_{max}$ and a in Eq. 4.11. It can be seen that the normal production vehicle features a maximum value of ΔCN ≈ 7.6 dB (first peak of the blue line in Fig. 4.45 and Tab. 4.3).
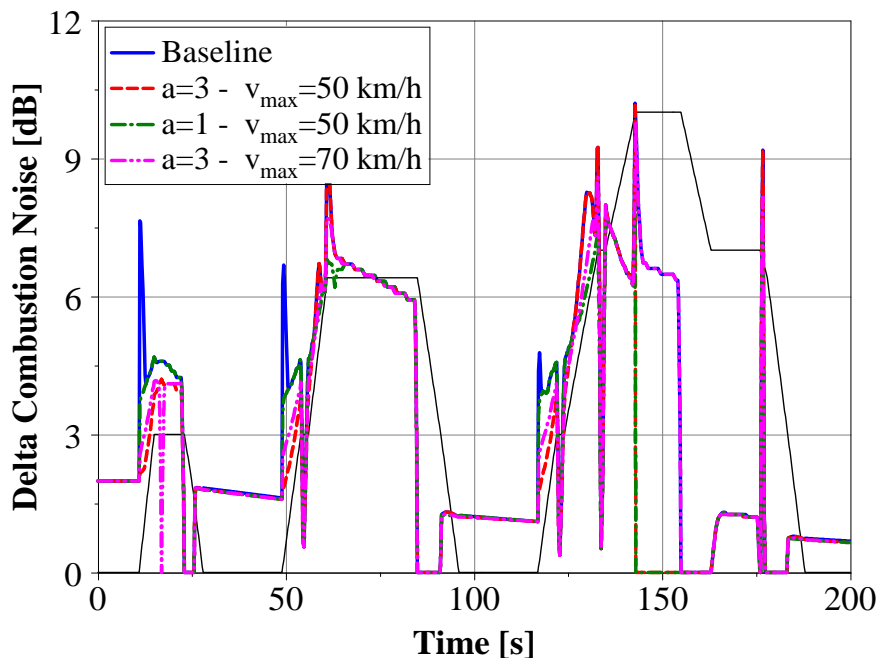
Figure 4.45 – BAS (CN target): reduction in the combustion noise (first ECE)

The first optimization case (a=3, v$_{max}$=50 km/h; dashed red line) allows a 3.4 dB reduction of the ΔCN peak (Tab. 4.3). However, the subsequent ΔCN peaks, which occur at higher speeds, result

to be greater than the baseline. By reducing the value of a, the reduction in the first ΔCN peak is less apparent, but the subsequent ΔCN peaks, which occur at higher speeds, are significantly reduced compared to the case with a=3.

The best compromise appears to be the case with a=3 and v_{max}=70, as it leads to the highest reductions in NO$_x$ levels without penalizing the CN improvement (Tab. 4.3). The different chooses of a and $v_{car,max}$ have a reduced impact on the fuel consumption reduction.

Table 4.3 - BAS (CN target): performance of the TLM (NEDC – $v_{car,max}$ in [km/h])

Optimization	FC [%]	NO$_x$ [%]	ΔCN$_{peak}$ [dB]
a=3, $v_{car,max}$=50	5.17	14.48	4.2
a=1, $v_{car,max}$=50	4.93	16.4	4.7
a=3, $v_{car,max}$=70	5.07	17.37	4.2
Stop&Start	2.77	2.31	7.6
Baseline	-	-	7.6

4.3.4   Combined Optimization

After single-target optimizations, a combined calibration is proposed in order to show a possible integration of the analyzed benefits. Figure 4.46 show the fuel consumption (left plot) and NO$_x$ emission (right plot) reductions in the case of a triple calibration for the NEDC (targeting M$_{fuel}$, M$_{NOx}$ and CN).
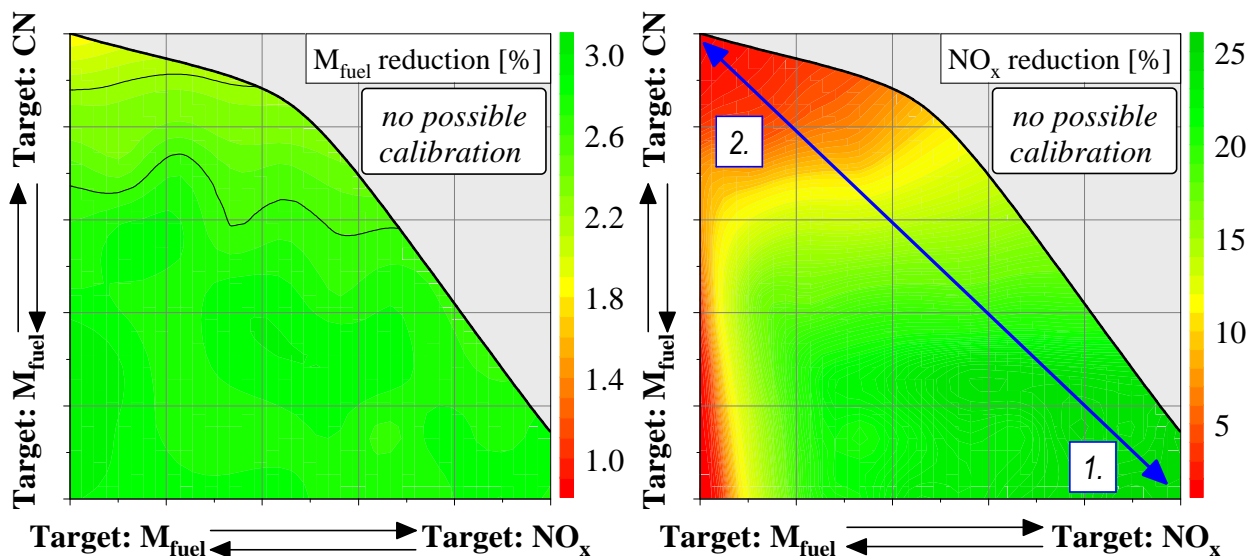
Figure 4.46 – BAS (combined optimization): fuel consumption and NO$_x$ emissions reduction [%] (NEDC)

The fuel consumption reduction is almost independent, moreover the NO_x emissions are remarkably reduced at the beginning of the increase in the dedicated calibration coefficient. Therefore, there is the possibility of introducing a third information (i.e. the combustion noise) without significantly compromising the fuel consumption or NO_x emission improvements.

Referring to Fig. 4.46, two main optimization criteria can be adopted:

1. to pursue an NO_x emission optimization. In this case, the resulting NO_x reduction can be used in various ways, for example in order to decontent the aftertreatment hardware, to reduce the penalties associated with the de-NO_x phase, to allow a less restrictive calibration of the EGR that offers further benefits for the fuel economy further, or as a combination of the previous factors (Point 1. in Fig. 4.46 – right)

2. to pursue a combustion noise optimization, in order to obtain a more balanced approach (Point 2. in Fig. 4.46 – left)

The final chosen strategy is of course dependent on the specific project targets and they cannot be decided on the basis of the simulation alone. A detailed experimental validation is needed, and the developed strategy should be based on the on-vehicle assessment of the various options in order to evaluate the most proper compromise.

All the results achieved so far suggest that the analyzed BAS architecture has significant potential for NVH and emission-oriented optimizations. On the other hand, FC reduction can mainly be achieved through downsizing and downspeeding, operations that are enabled by the BAS ([23]).

5. CONCLUSIONS

The partial electrification of passengers cars can be a suitable method to reduce the fuel consumption, NO_x emissions and combustion noise, but its success is strongly dependent on the implementation of a proper Hybrid Operating Strategy.

A Parallel Hybrid Electric Vehicle and a Series Hybrid Electric Vehicle were modeled in Matlab environment. The fuel consumption was analyzed along the New European Driving Cycle and Real World representative driving patterns (the Artemis cycles). Moreover, the minimization of the NO_x emissions was considered for the CI engine along the only NEDC. Both a novel benchmark and two real-time optimizations of the hybrid operating strategy (based respectively on the Minimization of the Total Losses and Total Load Switch Thresholds) were analyzed.

The benchmark operating strategy features the following reductions in terms of Well-to-Wheel CO_2 emissions and NO_x emissions along the NEDC:

Table 5.1- Benchmark Operating Strategy: Well-to-Wheel CO_2 and NO_x emissions (NEDC)

Case	Well-to-Wheel CO_2 emissions [g/km]		NO_x emissions [mg/km]	
CI engine				
Conventional (no S&S)	139.7	-	260.0	-
PHEV - not plug-in	120.4	-13.8%	108.5	-58.3%
PHEV - plug-in	79.4	-43.2%	13.6	-94.8%
SHEV - not plug-in	119.6	-14.4%	131.7	-49.3%
SHEV - plug-in	55.3	-60.4%	0.0	-100%
SI engine				
Conventional (no S&S)	174.9	-		
PHEV - not plug-in	142.7	-18.4%		
PHEV - plug-in	76.8	-56.1%		
SHEV - not plug-in	126.8	-27.5%		
SHEV - plug-in	54.2	-69.0%		

The better performance of the plug-in configurations is achieved with a net consumption of the battery energy content (E_{batt}=7.2 [kWh] and available SOC range of [0.2 - 0.75]). The hybridization of the CI engine, on one hand, obtains the best CO_2 emissions, but, on the other hand, accomplishes lower improvements with respect to the conventional vehicle, than in the case of the SI engine. This is due to its higher and flatter efficiency. In case of the CI engine a very interesting approach seems to be the minimization of the NO_x emissions, through an intensive engine load point shift toward the minimum $BSNO_x$ operating point. It should be reminded that no quantitative comparison is feasible between the PHEV and SHEV, because no optimization of the powertrain components was performed.

The HEVs achieve along the Artemis Urban Cycle (AUC) similar performance to the NEDC (generally slightly superior). The hybridization and the plug-in feature for both the engines is less and less impacting if an extra-urban (Artemis Road Cycle - ARC) or, even more, a highway mission profile (Artemis Motorway Cycle - AMC) is considered. In the case of the SHEV, even an increase in the fuel economy is achieved with respect to the conventional powertrain along the AMC, due to the electric transmission losses.

Table 5.2- Real-Time Operating Strategies: Well-to-Wheel CO_2 and NO_x emissions (not plug-in and NEDC)

Case	Well-to-Wheel CO_2 emissions [g/km]		NO_x emissions [mg/km]	
CI engine				
Conventional (no S&S)	139.7	-	260.0	-
PHEV - BO	120.4	-13.8%	108.5	-58.3%
PHEV - TLM TOT	120.5	-13.7%	110.5	-57.5%
PHEV - TLM REC	121.3	-13.2%	149.3	-42.6%
PHEV - TLST	122.4	-12.4%	253.2	-2.6%
SHEV - BO	119.6	-14.4%	131.7	-49.3%
SHEV - TLM TOT	123.2	-11.8%	146.6	-43.6%
SHEV - TLM REC	124.3	-11.0%	144.8	-44.3%
SHEV - TLST	129.2	-7.5%	164.6	-36.7%
SI engine				
Conventional (no S&S)	174.9	-		
PHEV - BO	142.7	-18.4%		
PHEV - TLM TOT	143.1	-18.2%		
PHEV - TLM REC	146.2	-16.4%		
PHEV - TLST	148.0	-15.4%		
SHEV - BO	126.8	-27.5%		
SHEV - TLM TOT	135.7	-22.4%		
SHEV - TLM REC	128.7	-26.4%		
SHEV - TLST	155.3	-11.2%		

The real-time operating strategies were then tested within the same boundary conditions of the benchmark (please refer to Tab. 5.2, for the only not plug-in HEVs). In the case of the PHEVs with FC as target, the real-time HOSs have a comparable behavior and close performance. This is

due to the very simple implemented control: or electric mode, in case of low load conditions, or pure thermal mode, with only a negligible engine load point shift. In case of the NO_x emission minimization, they show higher differences and the TOT TLM achieve the best result. TLM REC reaches a close performance, whereas the TLST proves to be not suitable. In the case of the plug-in PHEVs the real-time HOSs obtain a larger difference with respect to the benchmark. Good improvements were achieved by implementing a two phase optimization strategy: a first charge depleting mode and a successive charge sustaining mode.

Regarding the SHEV, the fuel consumption optimization shows a close behavior with respect to the parallel architecture even if a more intense load-point shift strategy is employed. The TLM REC is the real-time operating strategy that performs more closely to the benchmark, the TLM TOT features slightly higher fuel consumptions, whereas the TLST shows worse performance. Concerning the NO_x emissions, the three real-time optimizers implement the same behavior: the battery is mainly charged during low load and constant speed phases by means of the positive load point shift of the engine (up to its minimum $BSNO_x$ point). Afterwards, the energy saved in the battery is used during the vehicle transients to implement engine negative load point shift. The results in terms of total NO_x emissions (Fig. 4.34) shows that the TLM REC and the TLM TOT performs closely to the benchmark, whereas the TLST guarantees lower improvements. In general, the TLM with recoverable losses can have better performance than the TLM TOT, but its calibration is more challenging. In the case of the plug-in HEVs, the only electric mode of the SHEV is more efficient than in the case of the parallel architecture (due to the absence of the gearbox). Therefore, the NEDC can be driven in only electric mode.

Comparable performance to the NEDC are achieved for both the parallel and the series architecture along the Artemis Urban Cycle (AUC). The hybridization and the plug-in feature is less and less impacting in extra-urban (Artemis Road Cycle - ARC) and even more in highway mission profiles (Artemis Motorway Cycle - AMC). The real time operating strategy maintain the same trend: the TLM TOT is the best for the PHEV and the TLM REC is the best for the SHEV. The TLST always achieves the worst fuel consumption improvements.

Finally, a case study of a parallel-hybrid diesel powertrain with a high-voltage belt alternator starter was accomplished within a research project in collaboration with GMPT-E (Torino). For this architecture, a dedicated algorithm was implemented in order to consider also the optimization of the engine combustion noise. The results suggest that the BAS architecture coupled with a CI engine has significant potentials for NVH and emission-oriented optimizations. On the other hand, FC reduction can mainly be achieved through downsizing and downspeeding, operations that are enabled by the BAS.

Further developments to the actual methodology are on-going regarding the following main topics:

➤ validation of the novel benchmark optimizer based on Genetic Algorithm methods through comparison with existing optimizers (i.e. dynamic programming, ...) ([37])

➤ implementation of the proposed technique for other Hybrid Electric Vehicle architectures, like the Mixed Hybrid Electric Vehicle ([11]) and the Power Split Hybrid Electric Vehicle ([38])

➤ implementation of a combined optimization strategy, in order to co-optimize the design of the hybrid powertrain architecture ([11])

6. DEFINITIONS AND ABBREVIATIONS

AC	Alternating Current	
A_{car}	Vehicle frontal area	[m²]
APP	Accelerator Pedal Position	[%]
AMC	Artemis Motorway Cycle	
ARC	Artemis Road Cycle	
ASM	Asynchronous electric machine	
AUC	Artemis Urban Cycle	
Baseline	Conventional vehicle featured with the same engine of the HEVs	
BEV	Battery Electric Vehicle	
BMEP	Brake Mean Effective Pressure	[bar]
BO	Benchmark Optimizer	
BPP	Brake Pedal Position	[%]
BSFC	Brake Specific Fuel Consumption	[g/kWh]
$BSFC_{min}$	minimum BSFC	[g/kWh]
$BSNO_x$	Brake Specific NO_x emissions	[mg/kWh]
$BSNO_{x,min}$	minimum $BSNO_x$	[mg/kWh]
CD	Charge Depleting mode (plug-in HEV)	[%]
C_{dl}	diffusion layer capacitance	[F]
C_{drag}	vehicle drag coefficient	[-]
CI	Compression Ignition	
CN	Combustion Noise	[dB]
CO	Carbon Monoxide emissions	[mg/km]
CO_2	CO_2 emissions	[g/km]
$CO_{2,Batt}$	Well-to-Wheel CO_2 emissions from the battery energy consumption	[g/km]
$CO_{2,ICE}$	CO_2 emissions from the fuel combustion	[g/km]
$c_{p,batt}$	battery specific heat capacity	[kJ/kg]
CPP	Clutch Pedal Position	[%]
CS	Charge Sustaining mode (plug-in HEV)	[%]
$C_{SOC,l}$	parameter for the definition of $P_{SOC,l}$	[-]
CVVT	Continuous Variable Valve Timing	

$E_{batt,chem}$	battery chemical energy content	[kJ]
E_{batt}	battery electric energy content	[kJ]
ECE	NEDC urban driving cycle	
EM	Electric Machine	
EM1	Traction Electric Motor (SHEV)	
EM2	Generator (SHEV)	
EUDC	Extra Urban Driving Cycle	
EU	European Union	
EV	Electric Vehicle	
FC	Total Fuel Consumption	[g]
GA	Genetic Algorithm	
GHG	Green-House Gas	
H	battery total heat transfer coefficient	[W/K]
HEV	Hybrid Electric Vehicle	
HOS	Hybrid Optimization Strategy	
i	battery current	[A]
i_{ct}	battery circuit current through R_{ct}	[A]
ICE	Internal Combustion Engine	
ICEAL	Internal Combustion Engine Advanced Lab.	
$I_{gb,in}$	inlet gearbox inertia	[kg/m^2]
$I_{gb,out}$	outlet gearbox inertia	[kg/m^2]
I_{ICE}	ICE inertia	[kg/m^2]
I_{EM}	Electric Machine inertia (PHEV)	[kg/m^2]
I_{EM2}	Generator inertia (SHEV)	[kg/m^2]
LPS	Load Point Shift strategy	
M_{batt}	battery mass	[kg]
M_{car}	vehicle mass	[kg]
M_{fuel}	total fuel consumption	[g]
M_{NOx}	total NO_x emissions	[mg]
$\dot{m}_{fuel}$	fuel consumption rate	[g/s]
$\dot{m}_{NOx}$	NO_x emission mass flow rate	[mg/s]
NEDC	New European Driving Cycle	
MGU	Motor Generator Unit	
NMHC	Not-Methane Hydro-Carbon emissions	[mg/km]
NO_x	Nitrogen Oxides emissions	
NPI	Not plug-in feature	
OOC	Optimal Operating Condition	
OOP	Optimal Operating Point	
OOL	Optimal Operating Line	
P_{Batt}	battery electric power	[kW]
$P_{Batt,chem}$	battery chemical power	[kW]
$P_{Batt,shift}$	parameter for the definition of $P_{SOC,l}$	[kW]
P_{Brakes}	traditional brake braking power	[kW]
P_{EM}	EM brake power	[kW]
$P_{EM2,el}$	Generator electric power (SHEV)	[kW]

$P_{EM\&batt,l}$	EM and battery power losses (PHEV)	[kW]
$P_{gb,out}$	outlet gearbox power	[kW]
$P_{gb,l}$	gearbox power losses	[kW]
PHEV	Parallel Hybrid Electric Vehicle	
PI	Plug-In feature	
P_{ICE}	ICE brake power	[kW]
$P_{ICE,fr}$	ICE friction losses	[kW]
$P_{ICE,l}$	ICE power losses (TLM, PHEV)	[kW]
$P_{ICE,rec,l}$	recoverable ICE power losses (TLM, PHEV)	[kW]
$P_{ICE,tot,l}$	total ICE power losses (TLM, PHEV)	[kW]
$P_{ICE\&EM,l}$	ICE and EM2 power losses (TLM, SHEV)	[kW]
$P_{ICE\&EM,rec,l}$	recoverable ICE and EM2 power losses (TLM, SHEV)	[kW]
$P_{ICE\&EM,tot,l}$	total ICE and EM2 power losses (TLM, SHEV)	[kW]
PM	Particulate Matter emissions	
P_{NOx}	NO_x emissions equivalent power	[kW]
$P_{NOx,l}$	NO_x emissions power losses (TLM, PHEV)	[kW]
$P_{NOx,rec,l}$	recoverable NO_x emissions power losses (TLM, PHEV)	[kW]
$P_{NOx,tot,l}$	total NO_x emissions and EM2 power losses (TLM, SHEV)	[kW]
$P_{NOx\&EM,l}$	NO_x emissions power and EM2 losses (TLM, SHEV)	[kW]
$P_{NOx\&EM,rec,l}$	recoverable NO_x emissions and EM2 power losses (TLM, SHEV)	[kW]
$P_{NOx\&EM,tot,l}$	total NO_x emissions power losses (TLM, PHEV)	[kW]
P_{req}	required traction power at wheels shaft	[kW]
$P_{req,cs}$	required traction power at the ICE crankshaft (PHEV)	[kW]
$P_{req,el}$	electric power required by the EM1 (SHEV)	[kW]
PSM	Permanent magnet Synchronous electric Machine	
$P_{SOC,l}$	battery SOC control power losses	[kW]
$P_{T(ICE),l}$	ICE temperature power losses (TLM)	[kW]
$P_{tot,l}$	total power losses for S-HOS	[kW]
Q_0	initial capacity of the battery	[Ah]
Q	total capacity of the battery	[Ah]
Q_{HV}	fuel lower heating value	[MJ/kg]
Q_{NOx}	NO_x emissions equivalent lower heating value	[MJ/kg]
Range	Driving cycle range	[km]
R_{ct}	charge transfer resistance	[Ω]
RLDC	Real Life Driving Cycle	
RTO	Real Time Optimizer	
r_{gb}	gearbox transmission ratio	[-]
R_{ohm}	Ohmnic resistance	[Ω]
r_{roll}	Rolling resistance coefficient	[1/s]
SHEV	Series Hybrid Electric Vehicle	
SI	Spark Ignition	
SOC	State of Charge	[-]
SOC_{End}	Final State of Charge	[-]
$SOC_{Start,CS}$	initial State of Charge for the charge sustaining mode	[-]

SOC_{Start}	initial State of Charge	[-]
SOC_{target}	target State of Charge of the operating strategy	[-]
SPHEV	Series-Parallel Hybrid Electric Vehicle	
Stop&Start	Stop and Start feature	
t	Time	[s]
$T_{EM,fr}$	EM friction torque	[Nm]
$T_{gb,in}$	inlet gearbox torque	[Nm]
TLM	Total Losses Minimizer	
THC	Total Hydro-Carbon Emissions	[mg/km]
TLST	Total Load Switch-Thresholds	
v_{car}	vehicle speed	[km/h]
V_{oc}	open circuit voltage	[V]
$x_{CO2,fuel}$	CO_2 emitted per unit of burned fuel	[g/l]
ΔE_{req}	Difference between required and supplied total traction energy	[%]
ΔSOC	Difference between final and target SOC	[%]
$\varepsilon_{ch,el,net}$	recharging efficiency form the electric net (plug-in HEVs)	[%]
$\varepsilon_{el,mec}$	EM electro-mechanical conversion efficiency	[%]
ε_{EM}	total efficiency of the MGU	[%]
ε_{EL}	electric line efficiency efficiency	[%]
ε_{gb}	gearbox transmission efficiency	[%]
ε_{ICE}	ICE fuel conversion efficiency	[%]
ε_{NOx}	NO_x equivalent efficiency	[%]
$\varepsilon_{reg,br}$	regenerative braking global efficiency (TLST)	[%]
θ_{air}	external air temperature	[K]
θ_{Batt}	battery temperature	[K]
θ_{gb}	gearbox equivalent temperature	[K]
θ_{ICE}	ICE equivalent temperature	[K]
$\theta_{ICE,cold}$	ICE temperature at cold condition	[K]
$\theta_{ICE,warm}$	ICE temperature at warm condition	[K]
ω_{ICE}	ICE speed	[rad/s]
ρ_{Fuel}	fuel density	[kg/m^3]
ρ_{air}	external air density	[kg/m^3]
ω_{EM}	EM speed	[rad/s]
$\omega_{gb,in}$	inlet gearbox speed	[rad/s]
$\omega_{gb,out}$	outlet gearbox speed	[rad/s]

7. REFERENCES

[1] http://www.worldometers.info/cars/

[2] International Energy Agency, *World Energy Outlook*, 2010

[3] European Environment Agency, *Greenhouse gas emission trends and projections in Europe*, 2008

[4] Chamon *et al.*, *Mass car ownership in the emerging market giants*. IMF/University of Virginia, 2008

[5] J.-P. Rodrigue, C. Comtois, *The geography of transport systems*, Hofstra University,2009

[6] Direttiva del consiglio, del 20 marzo 1970, *concernente il ravvicinamento delle legislazioni degli Stati membri relative alle misure da adottarecontro l'inquinamento atmosferico con le emissioni dei veicoli a motore* (70/220/CEE)

[7] S. Pischinger, *Internal Combustion Engines*, Lecture notes of the VKA, RWTH Aachen, 2006

[8] M. Ehsani, Y. Gao, A. Emadi, *Modern Electric, Hybrid Electric and Fuel Cell Vehicles - 2nd Edition*, 2010

[9] D. Ambühl, *Energy management strategies for Hybrid Electric Vehicles*, Dissertation, ETH Zurich, 2009

[10] J. Seibel, *Optimierte Auslegung von Ottomotoren in Hybrid-Antriebsträngen*, Dissertation, Institute for Combustion Engines, RWTH Aachen University, 2008

7. References

[11] A. Balazs, E. Morra, S. Pischinger, *Optimization of electrified powertrains for city cars*, SAE Journal 2012, Paper No. 2011-01-2451

[12] International Energy Agency, *IEA Statistics - CO_2 emissions from fuel combustion*, 2010

[13] H. Hong, *Review and analysis of variable valve timing strategies - eight ways to approach.* Journal of Automobile Engineering, 218(10), 1179-1200, 2008

[14] S. Park, et al., *Effects of design and operating parameters on the static and dynamic performance of an electromagnetic valve actuator*, Journal of Automobile Engineering, 217(3), 193-201, 2003

[15] D. Naunin, *Innovative Drive Systems For Electric And Hybrid Vehicles – World-wide Developments and Tendencies Institute of Energy and automation Technology*, TU Berlin, 2004

[16] T. Miyamoto, E. Oogami, M. Origuchi, T. Tsuji, N. Hirata, T. Horiba, *Development of a lithium-ion battery system for HEVs*, SAE Journal, Paper No. 2000-01-1057, 2000

[17] J. Kümpers, C. Schmitz, *Nickel-Metallhydrid-Batterien für Hybridfahrzeuganwendungen*, Haus der Technik Fachbuch "Hybridfahrzeuge", 2005

[18] C. Samhaber, A. Wimmer, E. Loibner, *Modeling of engine warm-up with integration of vehicle and engine cycle simulation*, SAE, Paper No. 2001-01-1697, 2001

[19] L. Jarrier, J. C. Champoussin, R. Yu, D. Gentile, *Warm-up of a D.I. diesel engine: experiment and modeling,* SAE, Paper No. 2000-01-0299, 2000

[20] A. Walker, M. Lamperth, *Electric motors and generators in hybrid-electric powertrains*, SAE, Paper No., 2003-01-2313, 2003

[21] Z. Rahman, M. Ehsani, K. L. Butler, *An investigation of electric motor drive characteristics for EV and HEV propulsion systems,* SAE, Paper No. 2000-01-3062, 2000

[22] S. J. Heo, G. Kang, H. Kim, *Available power and energy prediction using a simplified circuit model of HEV Li-ion battery*, SAE, Paper No. 2010-01-1074

[23] A. Ferrari, E. Morra, E. Spessa, C. Ciaravino, A. Vassallo, *Analysis of energy-efficient management of a light-duty parallel-hybrid diesel powertrain with a belt alternator starter*, SAE Capri Conference 2011, Paper No. 2011-24-0080

[24] J. J. Greenbaum, M. A. Kluger, B. E. Westmoreland, *Manual transmission efficiency trends and characteristics*, SAE, Paper No. 942274, 1994

7. References

[25] MathWorks, *MATLAB - The Language Of Technical Computing*, www.mathworks.com/products/matlab

[26] M. Montazeri-Gh, A. Pourasmad, B. Ghalichi, *Application of genetic algorithm for optimization of control strategy in parallel hybrid electric vehicles*, Elsevier, Journal of the Franklin Institute 343 (2006), pp 420-435

[27] K. F. Man, K. S. Tang, S. Kwong, *Genetic algorithms: concepts and applications*, IEEE Trans. Ind. Electron., 43 (5), 1996

[28] Z. Michalewicz, *Genetic Algorithms + Data Structures = Evolution Programs*, AI Series, Springer-Velag, New York, 1994.

[29] K. F. Man, K. S. Tang, S. Kwong, *Genetic algorithms: concepts and applications*, IEEE Trans. Ind. Electron., 43 (5), 1996

[30] J. A. Joines, C. R. Houck, *On the use of non-stationary penalty functions to solve nonlinear constrained optimization problems with GA's*, Proceedings of the Fifth International Conference on Genetic Algorithm 467-173

[31] E. Morra, E. Spessa, M. Venditti, *Optimization of the operating strategy of a BAS hybrid diesel powertrain on type-approval and real-world representative driving cycles*, ASME Conference, Torino 2012, Paper No. ICES2012-81093

[32] E. Morra, E. Spessa, C. Ciaravino, A. Vassallo, *Analysis of various operating strategies for a parallel-hybrid diesel powertrain with a belt alternator starter*, SAE World congress and exhibition 2012, Paper No. 2012-01-1008

[33] F. Millo, et al., *Different Hybrid Powertrain Solutions for European Diesel passenger cars*, SAE, Paper No. 2009-24-0064

[34] J. Seibel, S. Pischinger, P. von Dincklage, "Optimized Layout of Gasoline Engines for Hybrid Powertrains", SAE, Paper No. 2008-28-0024

[35] S. Pischinger, *Internal Combustion Engines*, Lecture Notes of the VKA, RWTH Aachen

[36] A.E. Catania, R. Finesso, E. Spessa, Predictive *Zero-Dimensional Combustion Model for DI Diesel Engine Feed-Forward Control*, Energy Conversion and Management Vol. 52(10), Sept. 2011, pp. 3159–3175, Elsevier, ISSN: 0196-8904

7. References

[37] D. Bianchi, L. Rolando, L. Serrao, S. Onori, G. Rizzoni, N. Al-Khayat, T. Hsieh, P. Kang, *A rule-based strategies for a series-parallel hybrid electric vehicle: an approach based on Dynamic Programming. In: ASME Dynamic Systems and Control Conference*, Cambridge, September 13-15, 2010

[38] J.P. Arata, M.J. Leamy, J. Meisel, K. Cunefare, D.G. Taylor, 2011, *Backward-Looking Simulation of the Toyota Prius and General Motors Two-Mode Power-Split HEV Powertrains*, SAE International Journal of Engines, 120 (1): pp. 1281-1297

8. CURRICULUM VITAE

Personal Data

Name	*Edoardo Pietro Morra*
Date and place of Birth	*15th March 1984, Cuneo (Italy)*
Nationality	*Italian*

Education

1998-2003	*Scientific diploma at Liceo Scientifico Peano, Cuneo (grade: 100/100)*
2003-2008	*Master Degree in Energy and Nuclear Engineering at Politecnico di Torino, Torino (grade: 110/110 cum laude)*
2009-2011	*Doctoral student at Dip. di Energetica of Politecnico di Torino, Italy*

"Optime Prize" as the best graduate of the Energy Engineering at Politecnico di Torino (2007, 2009) and selected in the short list for the award "Best young master graduate for the 2007/2008 academic year" of the Politecnico di Torino

Publications

1. A. Ferrari, E. Morra, E. Spessa, C. Ciaravino, A. Vassallo, "Analysis of energy-efficient management of a light-duty parallel-hybrid diesel powertrain with a belt alternator starter", SAE Capri Conference 2011, Paper No. 2011-24-0080

2. A. Balazs, E. Morra, S. Pischinger, "Optimization of electrified powertrains for city cars", SAE Journal 2012, Paper No. 2011-01-2451

3. E. Morra, E. Spessa, C. Ciaravino, A. Vassallo, "Analysis of various operating strategies for a parallel-hybrid diesel powertrain with a belt alternator starter", SAE World congress and exhibition 2012, Paper No. 2012-01-1008

4. E. Morra, E. Spessa, M. Venditti, "Optimization of the operating strategy of a BAS hybrid diesel powertrain on type-approval and real-world representative driving cycles", ASME Conference, Torino 2012, Paper No. ICES2012-81093

Work Experience

2011	*internship on the optimization of Hybrid Electric Vehicles featured with gasoline engines – FEV, Aachen – Germany (5 months)*
2012 →	*senior simulation engineer of Hybrid Electric Vehicles and transmission at AVL, Graz - Austria*

125